Deposit & Copying of Dissertation Declaration

UNIVERSITY OF CAMBRIDGE

Board of Graduate Studies

Please note that you will also need to bind a copy of this Declaration into your final, hardbound copy of thesis - this has to be the very first page of the hardbound thesis.

1 Surname (Family Name)	Forenames(s)	Title
Hodgson	Andrew Christopher	Mr

2 Title of Dissertation as approved by the Degree Committee

Microfluidic Devices for the Investigation of Pluripotency in Embryonic Stem Cells

In accordance with the University Regulations in *Statutes and Ordinances* for the PhD, MSc and MLitt Degrees, I agree to deposit one print copy of my dissertation entitled above and one print copy of the summary with the Secretary of the Board of Graduate Studies who shall deposit the dissertation and summary in the University Library under the following terms and conditions:

1. Dissertation Author Declaration

I am the author of this dissertation and hereby give the University the right to make my dissertation available in print form as described in 2. below.

My dissertation is my original work and a product of my own research endeavours and includes nothing which is the outcome of work done in collaboration with others except as declared in the Preface and specified in the text. I hereby assert my moral right to be identified as the author of the dissertation.

The deposit and dissemination of my dissertation by the University does not constitute a breach of any other agreement, publishing or otherwise, including any confidentiality or publication restriction provisions in sponsorship or collaboration agreements governing my research or work at the University or elsewhere.

2. Access to Dissertation

I understand that one print copy of my dissertation will be deposited in the University Library for archival and preservation purposes, and that, unless upon my application restricted access to my dissertation for a specified period of time has been granted by the Board of Graduate Studies prior to this deposit, the dissertation will be made available by the University Library for consultation by readers in accordance with University Library Regulations and copies of my dissertation may be provided to readers in accordance with applicable legislation.

3 Signature	Date
	19/10/17

Corresponding Regulation

Before being admitted to a degree, a student shall deposit with the Secretary of the Board one copy of his or her hard-bound dissertation and one copy of the summary (bearing student's name and thesis title), both the dissertation and the summary in a form approved by the Board. The Secretary shall deposit the copy of the dissertation together with the copy of the summary in the University Library where, subject to restricted access to the dissertation for a specified period of time having been granted by the Board of Graduate Studies, they shall be made available for consultation by readers in accordance with University Library Regulations and copies of the dissertation provided to readers in accordance with applicable legislation.

Microfluidic Devices for the Investigation of Pluripotency in Embryonic Stem Cells

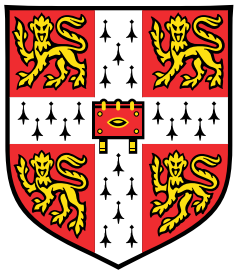

Andrew C. Hodgson

Supervisor: Dr. Kevin J. Chalut

Department of Physics
University of Cambridge

This dissertation is submitted for the degree of
Doctor of Philosophy

Fitzwilliam College

January 2017

Microfluidic Devices for the Investigation of Pluripotency in Embryonic Stem Cells

Andrew C. Hodgson

Abstract

This thesis presents the development of microfluidic devices designed to facilitate research into mouse embryonic stem cells (ESCs). ESCs are a well-studied cell, largely due to their pluripotent nature, meaning they are able to differentiate into all cell types of the body and may self-renew indefinitely in appropriate culture conditions. ESCs, along with many other lines of biological enquiry, are increasingly studied with the use of microfluidic technology which enables fine tuning of physical and chemical environments unachievable on the macro scale. Two varieties of microfluidic technology are presented in this thesis, one for high-resolution mechanical phenotyping of ESCs and the second as a novel in-chip culturing platform to study cellular transitions.

Chapter 1 presents a broad introduction to ESCs and biological enquiry with microfluidics, aimed to underpin the following Chapters. Chapters 2 and 3 present self-contained projects, thus each include a motivation and introduction section more specific than that presented in Chapter 1. These Chapters also contain their own methods, results and conclusion sections. Finally, Chapter 4 presents a summary of the work performed along with an outlook of upcoming investigations.

In Chapter 2, I present a microfluidic device developed and utilised in collaboration with Christophe Verstreken (Department of Physics, University of Cambridge), which has been used to apply a mechanical stress to live cells enabling measurement of their nuclear deformability. The device facilitates detection of both nucleus and cytoplasm which can then be analysed with a custom-written MATLAB code. Quantitative measurements of nuclear sizes and strains of ESCs indicated a negative Poisson ratio for nuclei of cells cultured in specific medium conditions. Furthermore, we demonstrate that the device can be used to physically phenotype at high-throughput by detecting changes in the nuclear response after treatment with actin depolymerising and chromatin decondensing agents. Finally, we show the device can be used for biologically relevant high-resolution confocal imaging of cells under compression. The work from this chapter is presented in Hodgson *et al.* [1].

In Chapter 3, I present a novel microfluidic platform developed in collaboration with Prof. Austin Smith and Dr Carla Mulas (Centre for Stem Cell Research, Cambridge). The developed platform enables individual ESCs to be cultured under continued observation as

they exit their pluripotent stem cell state. Each cell within the device may be extracted from the chip at any time for further investigation without disturbing other cells. Assessing the transition from the stem cell state in individual cells is paramount if we are to understand the mechanisms of pluripotency.

For Mam, Dad

&

Helen

Declaration

I hereby declare that except where specific reference is made to the work of others, the contents of this dissertation are original and have not been submitted in whole or in part for consideration for any other degree or qualification in this, or any other university. This dissertation is my own work and contains nothing which is the outcome of work done in collaboration with others, except as specified in the text and Acknowledgements. This dissertation contains fewer than 60,000 words including appendices, bibliography, footnotes, tables and equations and has fewer than 150 figures.

Andrew C. Hodgson
January 2017

Acknowledgements

I would like to begin by thanking my supervisor, Dr. Kevin Chalut. Kevin has been an excellent mentor and guide throughout my M.Phil, Ph.D and into postdoc. Kevin welcomed me into his group, despite having only basic biological and cleanroom training and enabled me to transition into a competent biophysicist. I am extremely grateful for his belief and trust in me.

I would like to give special thanks to my collaborators throughout the project:

Christophe Verstreken for both his work towards our first published paper and for his generosity in proof reading my thesis.

Carla Mulas and Austin Smith for their collaboration in the second half of this project, which I have thoroughly enjoyed and will be continuing into postdoc. Carla has been a pleasure to work with and always available to guide me through the biological background to our work.

Stefano Pagliara has been an excellent teacher, taking the time to educate me on the intricacies of photolithography and microfluidics.

Ulrich Keyser, for his steadfast support into all of the work contained within.

Caterina Lani, without whom I may not have transitioned from coasting rugby player into a, somewhat, diligent student and physicist.

My examiners, Florian Hollfelder and Oliver Otto, for their careful, thoughtful and constructive assessment of my thesis.

Completing this Ph.D has been somewhat bitter-sweet. It was the loss of my Dad, Chris Hodgson, to cancer which directed my studies following M.Phys Astrophysics to M.Phil Nanotechnology and beyond. I know that there would be no one prouder of where I am now and I will always be grateful for the opportunities his hard work, sacrifice and example have afforded me.

Since my Dad's passing I have been supported through my studies by my incredible Mam, whose strength and support have been vital and without whom, I would not have this Ph.D and so much more.

Finally, I would like to thank my wonderful fiancée, Helen, for supporting and sticking with me through the last 7 of my 12 years as a student, patiently waiting for me to '*finish that bloody Ph.D*'.

Table of contents

List of figures

Chapter 1

Introduction

The PhD project presented in this thesis is centred around the development of microfluidic devices to be used in furthering our understanding of embryonic stem cells (ESCs). ESCs are certain cells extracted from an embryo at a specific stage of development. ESCs are pluripotent, which means they are able to self-renew and are competent to generate all somatic cells, making them a popular focus of investigation. Investigations into ESCs are increasingly performed with microfluidic chips [2][3], which enable fine tuning of the spatial and chemical environment thereby allowing researchers to recreate traditional assays with less reagents and greater precision [4]. Advanced microfluidic technologies have yielded unprecedented access to novel methods of investigation. As part of this project, we have developed new microfluidic tools to investigate the physical and biological properties of ESCs and in particular, how pluripotency is maintained and lost.

What are the mechanisms involved in the maintenance of pluripotency? How is pluripotency lost at the beginning of lineage specification? Answering these questions will close critical gaps in our understanding of embryogenesis and will strongly have an impact in scientific and medical research. Importantly, directing the differentiation of stem cells will allow the growth of specific cells and tissues for use in research in cases where these are currently extremely difficult, costly, or potentially unethical to obtain directly (for example, from human embryos in the case of ESCs). In addition, a thorough understanding of the pluripotency of ESCs will ultimately enable the reprogramming of adult stem cells for personalised regenerative medical therapies.

The physical nature of the cell and its surroundings, influences biological properties. The physical environment of ESCs, for example, can play a role in directing cellular differentiation [5], whilst the physical properties of the cell itself have been shown to correlate with certain stages of pluripotency [6]. Microfluidics-based technologies have revolutionised our ability to probe the physical nature of cells while tightly controlling their environment.

This thesis describes my development of microfluidic devices that aim to provide new insights into the maintenance and exit from pluripotency of mouse ESCs. The practical work has been split into two parts. In Chapter 2, I present a device for physically phenotyping ESCs in a high-throughput fashion, enabling detection and measurement of both the nucleus and cytoplasm. In Chapter 3, I describe the development and application of a novel microfluidic cell-culture system which yields unmatched time resolution and cell specificity in investigations of the exit from pluripotency. Together I envisage that the technologies and analyses reported here consist of an important contribution to the furthering of our understanding of pluripotency.

1.1 Mouse Embryonic Stem Cells

During this thesis project, each element of the microfluidic device was designed to facilitate novel investigations of ESCs, both through mechanical phenotyping of cells at specific stages of development, as well as a single-cell culturing system to enable precise control and imaging of ESCs. The culturing and biological characterisations of the cells used were performed in collaboration with researchers at the Cambridge Centre for Stem Cell Research: Christophe Verstreken (Chapter 2; development and characterisation of a mechanical phenotyping device) and Dr. Carla Mulas (Chapter 3; development of a cell-culture device that overcomes a fundamental problem when analysing developing ESCs).

In 1981, Evans and Kaufman were the first to successfully extract and establish cultures of pluripotent mouse ESCs *in vitro* [7]. They identified several conditions, including that ESCs must be extracted at approximately 4.5 days (denoted E4.5) during the process of embryogenesis in order to efficiently obtain viable *in vitro* cultures. At E4.5 the mouse embryo contains three cell types: the embryonic epiblast, the primitive endoderm, and the trophectoderm.

The extracted epiblast cells are known as ESCs *in vitro* and contain a clearly defined nucleus surrounded by a cytoplasm. Within the nucleus, DNA stores the hereditary information of the organism: the blueprint to produce both replicas of itself and the proteins which give the cells their function. Two elements affecting the production of proteins by the cell are the expression of transcription factors and their access to DNA, which in turn depends on DNA packing and conformation [8].

Transcription within ESCs is regulated through a variety of mechanisms. First, proteins called transcription factors can recognise and bind specific sequences of double stranded DNA. Conditional on additional layers of control in the form of transcriptional promoters, these transcription factors can then induce RNA production and its subsequent translation into proteins. As such, gene regulation is the primary determinant of the cellular phenotype. Nevertheless, the expression of genes is also influenced by other elements, including the local accessibility of chromatin, which refers to the higher levels of DNA organisation, with more tightly packed chromatin in a specific region resulting in reduced levels of the transcription of genes in this region.

Mechanical forces from the external cellular environment can affect gene expression and the cell phenotype in a number of ways, a process which is referred to as mechanotransduction [9][10]. On one hand, force sensors in the plasma membrane of the cell can detect tension and induce a cascade of proteins to be activated, which can result in the cell reorganising itself to adapt to these external biophysical signals, and activating specific transcription [11]. On the other hand, these forces can be propagated through the cytoskeleton, which

is directly connected to the nucleus, possibly leading to a force-induced reorganisation of chromatin [12]. Both of these pathways thus influence gene expression, either through direct biophysical and 'mechanical' means, or through the activation of biochemical pathways [13].

1.1.1 Pluripotency in Culture

ESCs are pluripotent, thus have the ability to differentiate into any embryonic lineage which can further differentiate into any cell types in the organism [14]. They also form chimeras: ESCs may be implanted into a blastocyst which can continue normal development, the result of which is an adult organism containing cells from two sources [15]. Whilst the potential of the pluripotent cell is well defined and understood, its complex transcriptional, molecular and physical journey as its pluripotent state is lost requires further elucidation.

A common protocol for maintaining naive ESCs in pluripotent culture is to include leukaemia inhibitory factor (LIF) and fetal bovine serum, the chemical composition of which is ill-defined, in the growth medium. Although this protocol induces inhibitor-of-differentiation proteins, ESCs cultured in this way display transcriptional heterogeneity [16]. A particularly challenging problem for investigating the exit from pluripotency arises due to the serum/LIF cells ability to express factors characteristic of cells at various stages of development [17].

In 2008, Ying *et al.* [18] developed a culture system as a replacement for serum in an effort to overcome some of the shortcomings in maintaining pluripotency. Within this paper two inhibition factors (known as 2i) along with LIF to the base culture medium (N2B27) which is now a well-established protocol for maintaining pluripotency in culture (referred to herein as 2i/LIF). Each of these two inhibition factors has a distinct yet complementary effect on the pluripotency network of ESCs. CHIRON99021 is an inhibitor of GSK3, while PD0325901 blocks the FGF-MAPK signalling cascade, together preventing ESCs from differentiating or even down-regulating naive pluripotency factors. In contrast to the serum/LIF system, the 2i/LIF system allows us to indefinitely culture ESCs in a state of naive pluripotency with a high degree of transcriptional homogeneity [16].

Following the removal of 2i from culture conditions, ESCs transition through various phases marked by expression of certain transcription factors and changes in physical characteristics [19][20]. Initially, cells are in a state of 'naive' pluripotency, a ground state of pluripotency characterised by the expression of naive pluripotency markers [21]. Only 4 h after the removal of the 2i factors from the base culture medium, the transcriptional profile of ESCs dramatically differs from the stable naive transcriptional profile [20]. By 24 h after removal of inhibitors, cells have lost their naive pluripotent state as cells down-regulate naive factors.

The cells then enter into a formative phase, in which the expression of naive transcription factors is extinguished but the expression of specification factors has not yet begun. The formative phase, recently hypothesised by Prof. Austin Smith, assumes that the period between naive pluripotency and primed for differentiation is necessary to acquire competence for multi-lineage commitment. An initial aim of the device produced in Chapter 3 will be the testing of this hypothesis. Within the formative window, cells are thought to alter their genomic and epigenomic landscapes from the blank canvas of the naive state in order to increase cellular susceptibility to the cues of lineage commitment, accompanied by restructuring of the nucleus. This formative phase establishes competence for somatic and germline lineage commitment to the epiblast fate and is characterised by a selection of post-implantation epiblast factors. Approximately 48 hours after removal of inhibitors, ESCs express priming transcription factors which primes the cells for commitment to a certain lineage.

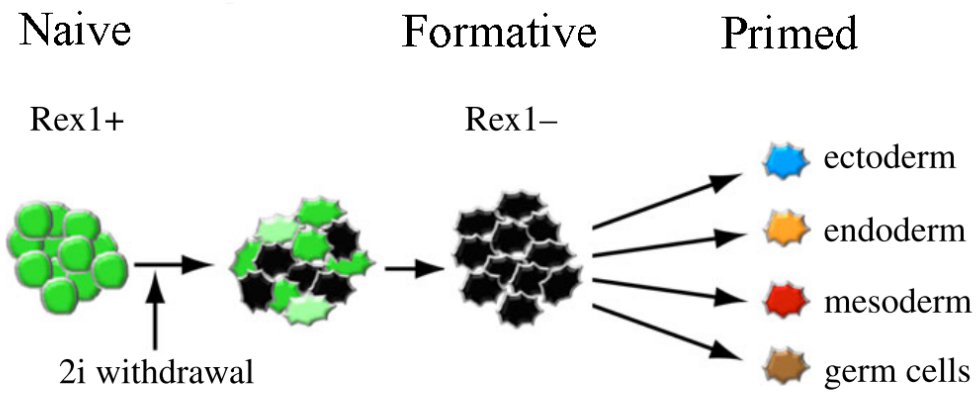

Figure 1.1: **Progression from Naive to Primed Pluripotency**
From the naive state of pluripotency, Rex1 downregulates following the removal of 2i. After approx. 24 hours, most cells have lost the capacity to self-renew and have entered the formative phase. After approx. 72 hours after 2i withdrawal, the cells enter the primed state. *Figure adapted from Kalkan and Smith (2014) [20].*

We are able to visually observe the release from the ground state of pluripotency due to the naive marker Rex1, which down-regulates at exit from naive pluripotency[20]. It is possible to engineer cells to express a fluorescent protein (GFP) when Rex1 is expressed (Rex1:GFPd2) [17], allowing quantitative visualisation of Rex1 expression. The use of the Rex1:GFPd2 cells plays a vital role in the work presented in Chapter 3. Such cells enable a visual output of exit from naive pluripotency in real-time. Combined with a microfluidic platform to take advantage of this information, we aim to assay cells at precisely timed steps

through their transition from naive pluripotency to lineage commitment. Using this approach we hope to further elucidate the mechanisms guiding the first steps of cellular specialisation.

1.2 Microfluidics

The aim of this project has been to develop and use microfluidic technology to further our understanding of pluripotency in ESCs. The use of microfluidics for biological enquiry has expanded rapidly in recent years due to the a range of advantages over traditional macro-scale methods [22]. For instance, the nano- and pico-litre volumes of microfludic devices offer greater control of spacial and chemical environments whilst also requiring lower quantities of reagents [23].

With the advent of soft-photolithography techniques, microfluidic devices may be designed and fabricated on relatively short timescales [24][25]. Devices have been used for a myriad of purposes including on-chip cell culture [26] and phenotyping [6][27], two applications of particular relevance to this thesis.

This section introduces some of these advantages and devices along with the underlying concepts of microfluidics. I present a review of the devices pertinent to the investigations presented in the following chapters, including Quake valves, mechanical phenotyping and on-chip cell culture followed by a description of the fabrication techniques used as part of this thesis.

Whilst the following chapters present two distinct types of devices, viscous forces dominate over inertial forces in both devices due to their length scale and flow rate. The viscous and inertial forces are related by Reynolds number, Re, defined as

$$Re = \frac{\rho v L}{\mu} \tag{1.1}$$

where ρ is fluid density, v is velocity of the fluid with respect to the object, L is a characteristic linear dimension and μ is the dynamic viscocity of the fluid. For many microfuidic devices the Reynolds number is typically less than 10 thus small enough to be neglected, whilst laminar flow is observed for Reynolds numbers of less than 2000 [28]. The effect of a negligible Reynolds number on the fluid dynamics within a microfluidic channel can be described by the Navier-Stokes equations for the velocity field of an incompressible Newtonian fluid, given by

$$\rho\left(\frac{\delta \mathbf{v}}{\delta t} + \mathbf{v}\cdot\nabla\mathbf{v}\right) = -\nabla p + \mu\nabla^2\mathbf{v} \tag{1.2}$$

where ρ is the fluid density, $\mathbf{v}$ is the flow velocity, p is the pressure and the term $\mu\nabla^2\mathbf{v}$ represents the viscosity where μ is the dynamic viscosity. When viscous forces dominate inertial, the inertial terms of Equation 1.2 can be removed to leave the Stokes equation:

$$\nabla p - \mu \nabla^2 \mathbf{v} = \mathbf{0} \tag{1.3}$$

Using this equation, we are able to model the velocity profile of the flow within our channels. If we dictate that the fluid moves along the x-axes of the channel, Equation 1.3 becomes

$$\frac{\mathbf{dp}}{\mathbf{dx}} = \mu \frac{\delta^2 v}{\delta y^2} \tag{1.4}$$

Integrating this twice with respect to y to solve for v:

$$v = \frac{1}{2\mu} \frac{\mathbf{dp}}{\mathbf{dz}} y^2 + c_1 y + c_2, \tag{1.5}$$

where c_1 and c_2 are constants from the integration. To solve for both constants, the distance between the channel h and $-h$ are used as boundary conditions. Considering that the velocity is zero at these points, Equation 1.5 becomes,

$$v = -\frac{1}{2\mu} \frac{\mathbf{dp}}{\mathbf{dz}} (h^2 - y^2). \tag{1.6}$$

Therefore fluid flow is fastest at $y = 0$, the midpoint of the channel walls, decreasing to zero at the walls, producing laminar flow. This means that there is a gradient of velocity in the y direction.

The simple predictability of laminar flow enables microfluidic chips a level of control unattainable in the often turbulent regimes of their macro-scale counterparts. As the flow patterns within microfluidics are easier to model, chemical gradients, object positioning, focusing and shear stresses can be used directly as tools of enquiry [29], exemplified by the devices of the following review. Modelling of the flows within the devices of Chapter 3 has been computed using laminar flow dynamics within the low Re number regime using finite element modelling and computational fluid dynamics software (COMSOL 4.4). This enables us to visualise how the flows are effected by obstacles within the channels.

Before discussing such devices, I first introduce the Quake valve [30]; an element of microfluidic technology which has had considerable impact on the field and is integral to the device presented in Chapter 3.

1.2.1 Microfluidic Valves

The microfluidic valve, developed in 2000 by the Quake group (Stanford University) [30] [31] [32], uses multilayer soft lithography to produce devices with multiple layers. Whilst there are many variations for the fabrication and actuation of valves [33][34][35][36], the underlying principle of layers separated by membranes remains constant. In its most simple form, two microfluidic channels can cross one another, separated by a membrane. Pressure applied into one channel forces a deformation of the membrane into the second channel, thereby closing it as shown in Figure 1.2

Figure 1.2 depicts a single 'flow channel' crossed by a single 'valve channel', similar to the original design by the Quake group. Indeed, throughout this report, 'flow channel' refers to the channels in the layer which fluids, media, cells *etc* are directed and investigated while 'valve channel' refers to the channels in the layer above and separated by a membrane which expand to close the flow channels below.

The dimensions and profile of the valve and flow channels have a profound effect on the closure of a channel for a given actuation pressure [37][38][39]. One of the most significant features of the valve is the cross-section of the flow layer. For the valve to achieve complete closure of the flow channel beneath, the flow channel must have a rounded profile (Figure 1.2). For rectagular profiled flow channels, the actuation of the valve only leads to a partial closure, an example known a sieve valve [40]. This discussion is developed further in Chapter 3.2.4.

A particularly powerful application of the Quake valve is multiplexing, in which many channels can be controlled by a low number of inputs [32][41]. The non-latched multiplexing valve, whereby pressurising a combination of valve channels affects the flow in a single or multiple flow channels [31], is of particular importance to the applications presented in this thesis. In such devices, control of N flow channels requires $2\log_2 N$ valve channels, thus with only 20 valve inputs we can control 1024 flow channels. This dramatically reduces device size and simplifies experimental procedure. An example of this scaling in practice is shown in Figure 1.3. It relies upon combinations of valves being actuated in tandem to isolate a particular flow channel. If there are 2 flow channels, 2 valves are needed to control which individual channel opens and closes. If the flow channel number was doubled to 4, 2 more valves would be required for single flow channel control. Beyond this number of flow channels, multiplexing becomes a powerful application. To transition from 4 flow channels to 8 channels, we can simply duplicate the existing array of valves and channels. If we label one block of 4 'A' and the duplicated block of 4 'B', then to regain single channel control only two more valves are required for the 4 extra channels, one to close off block 'A' and one to close off block 'B'. Duplicating again, takes the number of channels to 16 and adding just

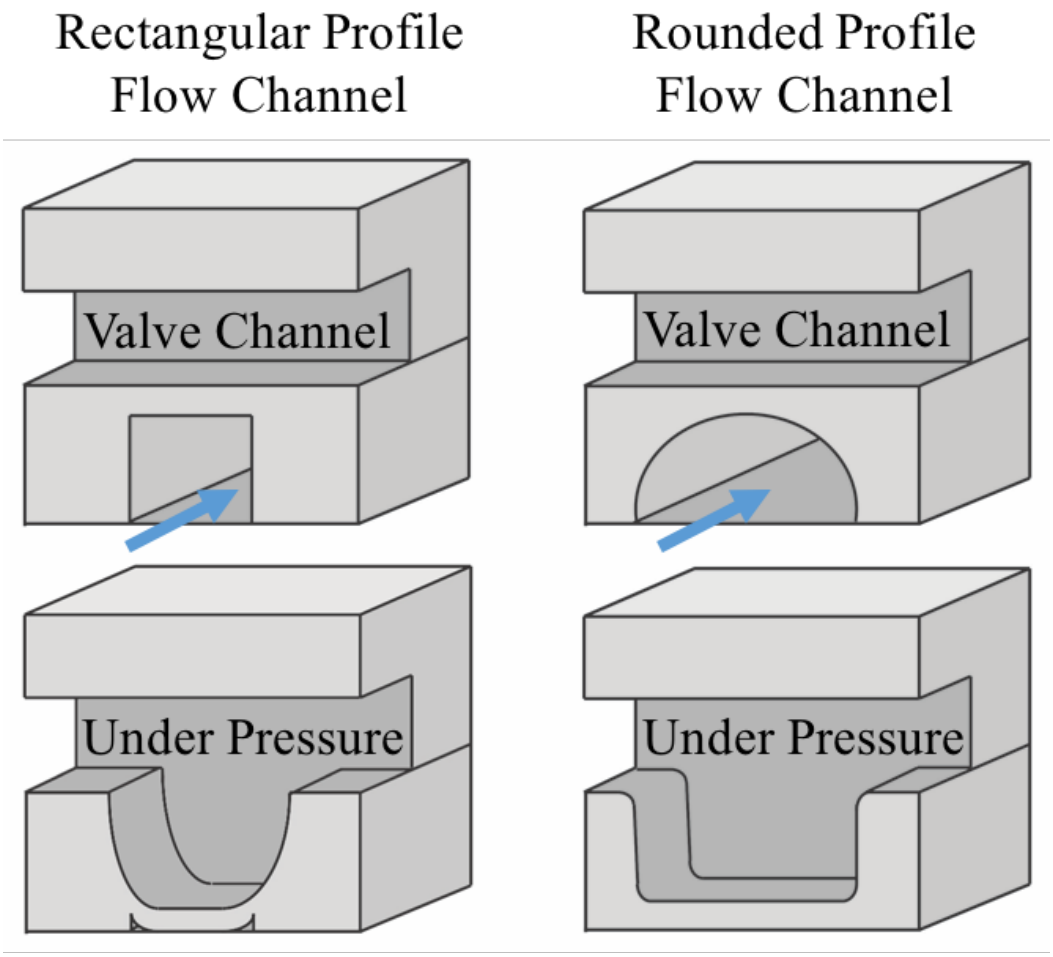

Figure 1.2: **Microfluidic Quake Valves**
Diagram illustrating the difference between rounded and rectangular flow channels. The flow channels are separated by a thin membrane from the valve channels. When the valve layer is pressurised, the membrane expands into the flow channel below. The rounded flow channels close completely while the rectangular form a sieve valve in which the lower corners remain open.

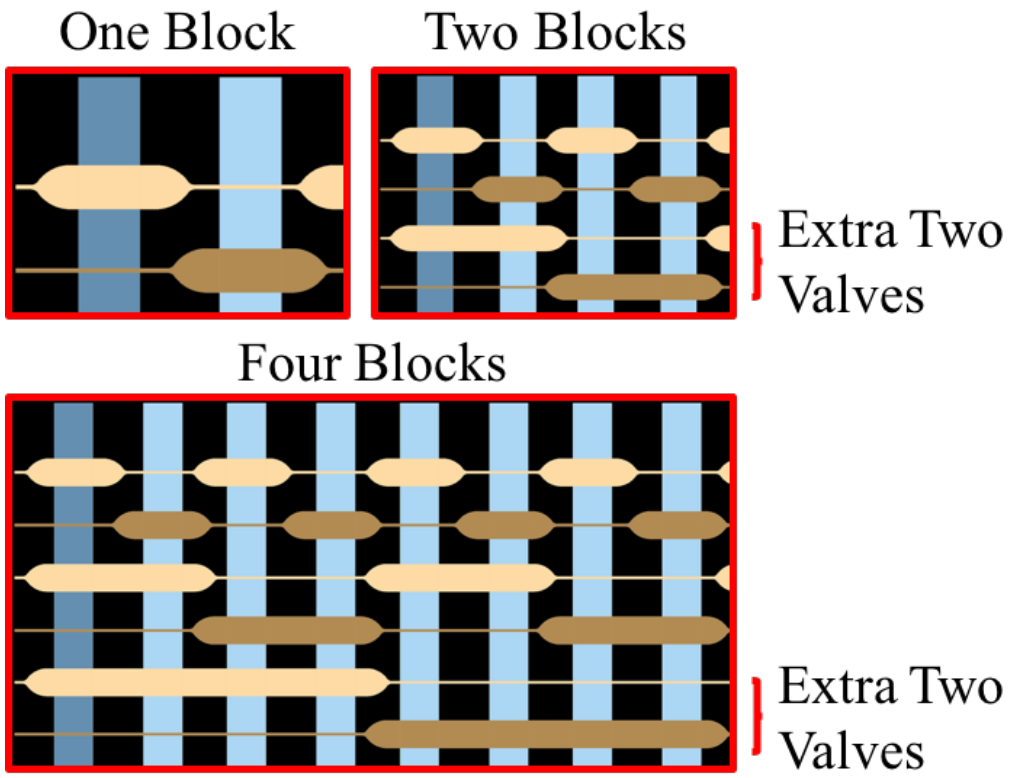

Figure 1.3: **Multiplexing Valves**
Depiction of flow channel up-scaling with valve multiplexing. Dark blue represents open channel and light blue closed. Light yellow represents unactuated valve channel and dark yellow actuated valve. For one block of two channels, two valves are required to isolate a single flow channel. Doubling the channel number requires two new valves as shown in 'Two Blocks' section. Doubling the flow channel number again to 8 still only requires two extra valves, as shown in 'Four Blocks'.

two more valves to control the old and new duplicated blocks means single channel control can be achieved with 8 valves.

1.2.2 Microfluidic Devices for Mechanical Phenotyping

The precision the microfluidic environment enables phenotyping of cells based on their mechanical properties. As discussed in Section 1.1, the mechanical properties of cells correlate with their biological function and in ESCs, their stage of differentiation. Using techniques such as hydrodynamic stretching [42] [43] [29], the deformability of cells have been used to mechanically phenotype cells in a high-throughput manner. The principle of applying deformation to mechanically phenotype has been applied as part of the work presented in Chapter 2.

In 2012, Gossett *et al.* [42] developed a technique for large population mechanical phenotyping on a microfluidic chip, capable of assessing single-cell deformability at a rate of up to 2000 cells/s. Cells are inertially focused to the channel centreline and are deformed on contact with a flow approaching from the opposite direction, meeting at a cross junction. At the centre of the junction, cells deform in the stretching extensional flow and are directed towards one of two outlets. Image analysis of cells under deformation is used to produce a scatter density plot of deformability against initial diameter. Measurements of various cell types reveals the characteristic size/deformability profile for particular cells which can be used to identify multiple cell types present within a population. The deformability cytometry (DC) technique was developed further in 2013 by Tse *et al.* [43] in which the device was used to diagnose malignant plural effusions, presenting this technology as a promising label free diagnostic device.

An alternative to previous deformability cytometry methods has recently been developed by Otto *et al.* (2015) [29] as a method of on-the-fly mechanical phenotyping of up to 100 cells/s. The device enables hydrodynamic deformation of cells by focusing the flow through a channel with a smaller cross section than the approach. Whilst performed at a lower throughput than Tse *et al.*, real-time characterisation resulted in many more cells being analysed. Because of the high number of cells which can be analysed in real time, scatter plots of deformability and cell size can be used to identify sub-populations in the cells passing through the channels more quickly, building on the potential of the diagnostic tools of DC.

An alternative to hydrodynamically applying deformations to cells is using microfabricated channels smaller than the characteristic cell size. Microfluidic channels have been fabricated to mimic narrow spaces certain cells pass through within an organism, particularly cells related with disease or immune response. In 2013, Rowatt *et al.* [44] observed the passage of human promyelocytic leukemia (HL-60) cells though 5μm channels as a model system for assessing the impact of nuclear shape on cell deformability. They found that the ability of an HL-60 cell to pass though a constriction was connected to its expression levels of lamin A where over-expression decreases the cells ability to compress.

Microfabricated constrictions have recently been used by Thiam *et al.* (2016) [45] to observe the migration of cells though regions between 1 and 5 μm wide. The ability of certain cells to constrict through regions much smaller than themselves is particularly important for immune response cells but also plays a key role in the formation of metastatic cancer cells. Studies have shown that a limiting factor of a cells ability to deform through narrow pores is the nucleus, due in part to the structural rigidity of the nuclear lamina [46]. The mechanism by which cells possessing a rigid nuclear structure migrate through narrow pores was investigated by Thiam *et al.* using dendritic cells, which are part of mammalian immune response. They found that to migrate though the constriction channels, the cells generated a dense actin network which enabled the nucleus to deform, possibly by rupturing the nuclear lamina. The results of their study highlight both the ability of microfabricated channels to probe the mechanics of cells, particularly nuclear mechanics and the importance of the physical nature of cells in performing their biological functions.

As exemplified by the microchannels above, microfluidics enables fine tuning of the cellular micro-environment [47][48]. As discussed in Section 2.1.1, the environment of a cell can play a significant role in its development and its biological properties [49]. Within the field of microfluidics, environmental effects have been assessed using micron-scale structures to control cell shape [50] and using elastomer posts to assess the forces applied by cells on their surroundings [51] and by patterning the substrate on which cells are grown [52][53].

Patterning within a microfluidic device has recently been used by Théry *et al.* (2016) [54] to investigate the link between the rescue from microtuble depolymerisation and microtubule self-repair. The ability of damaged microtubles to incorporate new tubulin dimers to recover initial stiffness was previously demonstrated by Schaedel *et al.* (2015) [55], also using a micropatterned microfluidic device. Both devices featured micropattered lines for microtubule seeds to graft, having flowed from the chips inlet. Microtubles grow from these seeds as free tubulin dimers flow across the chip. In the initial 2015 investigation, Théry *et al.* applied a cross-flow, perpendicular to the direction the microtubles formed, thus inducing bending. Damage from bending resulted in a softening of the microtuble, however, given a sufficient amount of time and the introduction of free tubulin dimers, the microtubles were able to repair and return to their original stiffness. In 2016, they then showed that self-repair appears to actively contribute to growth of the local microtuble network, again highlighting the role microfluidics can play in investigating sub-cellular mechanics.

1.2.3 Microfluidics for Biological Control

Using multiplexed microfluidic valves as introduced above, in Chapter 3 I present a device in which ESCs can be cultured on-chip and removed individually at the users discretion, to study cellular transitions. The process of replicating macro-scale culture conditions on-chip is complex, involving the scaling down of the process to the micron-sized channels alongside investigating the effects of media and gas exchange and examining the effect of the physical environment [56]. Whilst there are still new technical challenges to overcome, the potential benefits to research of the miniaturisation are significant [57].

Perhaps the most powerful application of micro-scale cell culture is the ability to isolate single cells from a population. This leads to potentially altering chemical environments of cells in parallel, on the same chip or removing individual cells for functional studies. A form of technology for culturing individual cells in isolation has been recently commercialised by Fluidigm as the 'C1' chip. This device is capable of culturing up to 800 cells with sizes from 10 to 17 μm before performing single cell genomics such as mRNA or DNA sequencing. A crucial limitation of this technology, however, is that individual cells may not be recovered from chip. A device capable of cell culture and removal was developed by Lecault *et al.* (2011) [58] in which thousands of cells can be cultured in nano-litre sized chambers. Whilst cells within this device may be recovered, a feature necessary for the device in Chapter 3, we require the ability to remove single cells in an automated fashion, which this device does not facilitate. Furthermore, we identified during the development of our device that ECSs which have adhered to their surroundings are considerably more challenging to remove from culture than the hematopoietic stem cells used by Lecault *et al.* Due to the absence of a device satisfying all technical and biological requirements, we present here a custom-designed approach incorporating microfluidic droplet technology for encapsulating cells.

As described in Chapter 3, our solution to the problem of adhesion between ESCs and the chip was the encapsulation of cells within agarose-based droplets, provided by Dr Carla Mulas and Timo Kohler (Department of Biochemistry, University of Cambridge) using technology developed by the Hollfelder group. The technology is based on the formation of aqueous microdroplets using immiscible oils [59][60][61] which are formed on the device shown in Figure 1.4. Investigations with agarose beads proved highly effective for supporting ESCs under self-renewal conditions (Kleine-Brüggeney *et al., In Revision*). In agarose alone ESCs could exit the naive state, yet they could not then differentiate towards specific lineages. This may be due to agarose being inert and without any form of matrix, bypassing the interaction between naive ESCs and the extra cellular matrix (ECM). ESCs were able to proliferate for days within the agarose beads and were capable of transitioning from the naive phase. Due to the lack of interaction with matrix scaffold, the cells were not then

able to transition to the primed phase. As part of work in progress, we are optimising the matrix conditions within the beads by co-polymerising agarose with fibrinogen, which following incubation with thrombin becomes agarose-fibrin. The encapsulated cells interact and remodel the fibrin, leading to increased survival and the ability to differentiate.

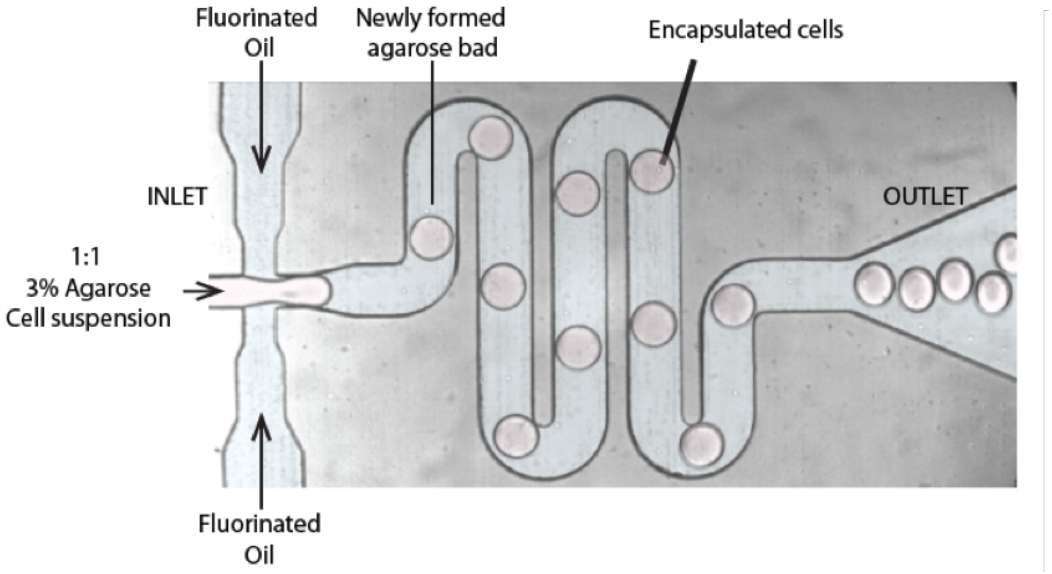

Figure 1.4: **ESC Encapsulation**
False coloured image of the device used to encapsulate ESCs in agarose droplets. The flow of agarose cell suspension is pinched by a cross flow of fluorinated oil to form beads which flow to the outlet for collection. Image courtesy of Hollfelder group and Dr Carla Mulas.

Droplet-based microfluidics provides a convenient method of isolating single cells in defined conditions, such as the encapsulation and culture of human cells on chip by Clausell-Tormos *et al.* (2008) [60]. In their study, single cells were encapsulated at a rate of roughly 300 cells per second and could be maintained in culture for several days. This device indicates the potential of encapsulated cell culture with singularly confined cells. The culture was performed off-chip before being reintroduced to assess viability, showing that after 14 days there was no degradation or coalescence of the beads. They also identified the importance of both the biocompatibility of the encapsulation substrate and gas exchange on long term culture. The biocompatibility in terms of the substrate for culturing ESCs means not only maintaining cells in pluripotent conditions, but also facilitating differentiation along all lineages upon exit of the stem cell state. This requires precise tuning of the chemical and physical nature of the beads using a combination of agarose and fibrin as described above.

When encapsulating cells within microdroplets, it is commonly required that the drops contain a specific number of cells. A method for producing beads with a high proportion

containing single cells was developed by Edd *et al.* (2008) [62] which used flow-focusing to organise cells into evenly spaced streams. The focusing relies on the high-aspect ratio of the flow channel combined with high flow-rate guides cells into two separate lines along the channel walls with enough separation so as to produce single cell containing drops.

Having developed beads which both support ESC differentiation and do not adhere to the interior surfaces of the device, the beads of our device must be manoeuvred and stored on-chip. There have been a broad range of devices designed to store microbeads for cell culture. A simple version of such a device was presented by Schmitz *et al.* (2009) [63] who encapsulated yeast cells in a water-in-flurocarbon emulsion then trapped 8000 beads in 'dropspot' traps. The dropspot trap works by forcing beads into a series of circular traps connected by a thin reservoir. More recently, in 2014 Khorshidi *et al.* [64] presented a device capable of storing singularly encapsulated human embryonic kidney cells in individual micro-wells on chip. Beads are forced along a channel slightly narrower than themselves and micro-wells placed along the length of the channel act as traps when beads uncompress and move into them. All 6000 traps could then be imaged automatically using image analysis software based on circular Hough transform to detect beads.

Whilst the traps of the devices introduced above effectively maintain a large number of isolated single cells on chip in a capacity suitable for continued imaging, individual cells may not be removed in isolation, nor can the conditions be altered for specific beads. Furthermore, the beads are required to undergo a compression in order to be stored, which may introduce stress on the cells within. As an alternative to using force applied directly by the walls of the device in order to manoeuvre the cells into traps, a similar function can be performed by manipulation of the hydrodynamic flow profile within the chip. An example of such an approach is the device presented by Chung *et al.* (2011) [65], in which a serpentine channel lined with micro-well traps cells which migrate to the channel walls. This technique enables the filling of 95% of the traps which have a density of 860 per mm^2 with low shear stress. This and the devices described above, exemplify the variety and potential of microfluidic devices for on-chip culturing and mechanical phenotyping. Our application of some of these techniques is presented in the following chapters, whilst the next section provides an overview of the microfluidic device fabrication process.

1.3 Design and Fabrication of Microfluidic Devices

The following methods section describes this process of producing a microfluidic chip, including computer aided design (CAD), production of photomask for photolithography, creation of a mould and fabrication of a device from polydimethylsiloxane (PDMS). These techniques form the basis of the protocols used in the following chapters.

1.3.1 Computer Aided Design and Photolithography

All of the devices developed during this PhD project feature micro-scale channels, in which cell suspensions or objects may flow, that require a mould to produce usable chips. The mould is formed of a silicon wafer substrate with photoresist features adhered to the surface. 'Photoresist' refers to a broad range of light sensitive materials whose material properties change with exposure to UV radiation. There are two main groups of photoresist: positive and negative. The former becomes soluble to its own developer following the appropriate exposure while the latter becomes insoluble. Selectively exposing regions of photoresists coated on a substrate is the foundation of photolithography.

To selectively expose specific areas to UV, a photomask is designed using CAD software and printed by a specialist company. In the case of negative resists, the mask is transparent where the features will remain, and opaque everywhere else. For chip features smaller than 20μm, an opaque layer for the mask formed of low reflective chrome oxide deposited onto a quartz or lime glass substrate is used. While being excellent for accuracy of design replication, durable and easy to clean, they are more expensive than the alternative when such precision is not required. For features larger than 20μm, or for cheap and rapid prototyping, emulsion film masks were used. These use a soft photographic emulsion gel to block light from the photoresist but must be first adhered to a glass support.

After design and photomask production, the silicon substrate of the mould is coated with the appropriate photoresist. While a range of materials can be used as a substrate we opted for silicon for all devices in this report, due to its excellent adhesion with photoresists. Furthermore, silicon can be polished to a highly smooth and clean surface which eliminates distortions caused by scratches and surface contamination in the resulting devices.

The channels within a microfluidic chip are three dimensional. Two of the dimensions, feature width and length, are set by the photomask. The third, feature height, is set by the thickness of the photoresist layer coated over the silicon wafer base. To achieve a precise and even finish, a spin-coater is used to spread photoresist over the wafer surface to the required thickness. Negative photoresists used as part of my work are all part of the SU-8 (Microchem, Massachussetts, USA). These resists have a range of viscosities; more viscous

resists are used to produce thicker coatings and therefore higher features. The SU-8 2000 series contains resists capable of film thicknesses from 0.5 to 200μm. Only one variety of positive photoresist is used in my work, AZ 40XT, which is capable of producing films up to 120μm over two applications.

The protocols and timings for the negative and positive photoresists and the varieties within are varied, however all resists used here require a baking step (soft bake) before UV exposure. The effect of the soft bake is to remove the solvent required for resist spreading. The total bake time, temperature and time taken to reach that temperature varies between resists. It is important not to heat too quickly as doing so may cause cracks in the surface whilst insufficient bake times leave too much solvent in the resist leading to erosion, leaving the features poorly defined in the later stages of fabrication. Excessive bake times, however, can thermally decompose the photoactive compound of the resist, thus requiring a longer development process which can introduce erosion.

As with the spinning and baking protocols, the exposure is dependent on the type of resist used. The manufacturer provides technical data for the total exposure energy required to activate the photoactive compound. All devices were exposed to UV using an MJB-4 contact mask aligner (Karl Suss, Munich, Germany). Exposure time corresponded to the total energy needed divided by the power output of the UV lamp. For SU-8 resists, the effect of exposure is the crosslinking of exposed regions making them insoluble to developer. Crosslinking means these resists are thermally stable (up to approximately 300°C) and extremely difficult to wet-chemically remove. Following exposure of SU-8 resists, the wafer is baked again in a post exposure bake (PEB) step to complete the crosslinking. For positive AZ resists, the area to be removed by developers is exposed. In this instance, the exposure has the effect of forming a carboxylic acid which renders them soluble in aqueous alkaline solutions. Due to the lack of cross-linking, further heating of AZ resists can cause a re-flow of material. This properly is vital for the work performed as part of Chapter 3.

To reveal the features on the silicon surface, the wafers are placed in the appropriate developer. For the SU-8 features, this is propylene-glycol-mono-methyl-ether-acetate (PGMEA) which removes all unexposed regions. Developing time depends upon the film thickness, which can be obtained from tables provided by the manufacturer. Small variations on this time will derive from the length of the baking and exposure. For AZ resists, an aqueous alkaline developer is used given the high alkaline solubility of the exposed resist. Development times are again dependent on film thickness, although AZ has a greater risk of over developing features than SU-8 due to the absence of crosslinking. Isopropanol is used to clean the surface of developer residue once developing is complete. For the SU-8 features,

a final bake at a temperature of up to 200°C can harden the features and may smooth over small cracks.

1.3.2 PDMS Microfludic Chips

After production of the mould, a PDMS replica is produced. Whitesides *et al.* (2000) list a number of reasons for the suitability of PDMS [66]:

- Accurate reproducibility of micron-scale features; optical transparency
- Low curing temperature
- Non-toxic and compatible with cell culture
- It can be reversibly deformed
- Forms an irreversible seal following exposure to air plasma
- Controllable surface chemistry
- It can be removed from delicate moulds without causing damage.

To prepare PDMS, a siloxane oligomer (base) is mixed with siloxane cross-linkers (curing agent). The ratio of base:curing agent allows some control over the material properties of the final device; increasing the amount of curing agent in the mixture increases the device stiffness. The mixture must be degassed under vacuum to remove air which may create imperfections in the device. Following this, PDMS may then be poured over the mould up to the height required for the final device. For my devices this is approximately 1cm. The chips are cured in an oven at 60°C before being cut from the mould with a scalpel.

As introduced above, when exposed to air plasma, PDMS can form an irreversible seal [24]. For the devices presented as part of my work, the seal is formed with a glass slide or cover-slip. Placing the two exposed surfaces together creates a covalent bond between the two. In addition, the surface chemistry is temporarily altered to make the usually hydrophobic PDMS surface hydrophilic.

Chapter 2

A Microfluidic Device for Characterising Nuclear Deformations

This chapter presents one of the two separate lines of investigation undertaken during my thesis research. As I started my first project, the investigations of Pagliara *et al.* (2014) [6] were coming to completion. Much of the work performed by Pagliara *et al.* in this paper involved the use of a microfluidic device capable of applying a small compressive force to ESCs. This design allowed imaging of a fluorescently labelled nucleus, before and during compression through a constriction channel in a microfluidic device. Measurements of the transverse and axial dimensions of the nucleus were used to calculate the strain in response to the compression [6].

As discussed in Section 1.1, cell mechanics plays a vital role in cell function. This relationship is also true for nuclear mechanics, which are affected by various biological processes, from cancer formation to stem cell development [67]. Few tools, however are available in stem cell research that allow the investigation of the mechanical and physical characteristics of the cell and its nucleus.

With the aim of facilitating the quantitative study of nuclear and cell mechanics, I contributed to the development of a new microfluidic tool for applying small nuclear deformations to ESCs, critically augmenting the technique used by Pagliara *et al* (2014). Below I describe the characteristics of this device, reporting the results of an investigation into the mechanical and structural response of ESCs to compressive stress alongside the dependence of these responses on their biological state.

2.1 Motivation

As discussed in Section 1.1, the relationship between ESCs and their external environment plays a vital role in cellular development and function. The mechanics of ESCs also change in tandem with development [68]. Microfluidic devices are an ideal tool to probe the physical properties of cells whilst tightly controlling their environment [58][69][2][29]. This section provides an overview of the development of a microfluidic device which allows investigation of the mechanical properties of ESCs and their nuclei in a high-throughput fashion.

2.1.1 Cellular Mechanics and Pluripotency

The establishment, maintenance and exit from pluripotency of ESCs is controlled by a complex network of both biological and physical factors. It is currently still not well understood how these factors are controlled and connected. Pertinent physical effects can be categorised as external or internal; the former refers to the cell's interaction with its environment, how that environment affects cellular development and how external forces can impact on fate decisions [49][70]. For instance, physical properties of a cell's local environment can affect the lineage to which it commits after a fate decision [49]. This effect can be mediated through cell-cell adhesions [71] and through substrate stiffness, which has previously been shown to direct the differentiation of mesenchymal stem cells by altering the elasticity of the matrix microenvironment [5].

The response to external physical forces is dependent on the internal biophysical properties of the cell. For example, the cellular response to mechanical forces is influenced by cellular stiffness: softer cells are more sensitive to external forces than stiffer cells [72]. Within this context, it is interesting to note that ESCs exhibit specific mechanical differences which distinguish them from their differentiated progeny. In a previous study, ESCs were approximately seven times softer and more sensitive to stress than differentiated cells, as demonstrated by their greater increase in cell area in response to stress [72].

Beyond cell stiffness, the physical properties of the nucleus have been shown to vary with cell function and development. Pajerowski *et al.* (2007) [73] demonstrated a correlation between developmental plasticity and the physical plasticity of the nucleus; human ESCs which were more able to modulate gene expression had more physically malleable nuclei. Investigation using human ESCs revealed a 6-fold stiffening in the nuclei of fully differentiated cells. The developmental plasticity may correlate with physical plasticity due to alterations in transcription factor access to DNA. Using the transcription factor Nanog as a reporter for pluripotency, chromatin has been found to decondense as Nanog expression was

down-regulated in mice ESCs [19]. Thus, as ESCs moves toward lineage commitment, their nuclei become softer.

In 2014, Pagliara *et al.* assessed the physical characteristics of ESC nuclei in the naive, primed and what they described as the "metastable transition state" (the formative phase). Using a combination of microfluidic technology and atomic force microscopy (AFM), they discovered that transition state nuclei displayed a displayed a negative Poisson's ratio. This rare physical property, known as auxeticity, implies that the material undergoes an elongation along the perpendicular axis as it is elongated along one axis (Figure 2.1). This property results in a total increase in nuclear volume in the presence of uniaxial elongating stress.

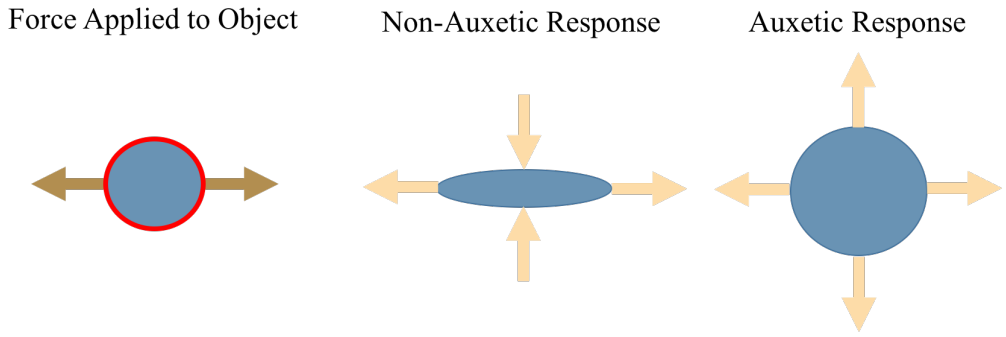

Figure 2.1: **Auxetic Response to Stress**. Auxetic materials react to uniaxial extensional stress with an overall increase in volume, depicted here as an extension in both the direction of and perpendicular to the applied force.

In summary, there are clear and compelling links between cellular mechanics and the developmental state of an ESC. External forces influence differentiation, whilst nuclear and cellular mechanics play a role in the effect exerted by external forces. Nonetheless, there remains few tools at our disposal to probe the underlying physics both internal and external to a cell. Microfluidics provides an ideal platform for such investigations due to the precise control over the physical environment which applies stress to the cell, combined with the ability to image responses to that stress in single nuclei. Using the microfluidic device used by Pagliara *et al.* 2014 as a starting point, I set out to achieve an improved array of devices to probe both the cellular and the nuclear mechanics of ESCs.

2.2 Microfluidic Devices for High-throughput Cell Investigations

One of the most challenging aspects of developing microfluidic tools for stem cell research is managing the often troublesome characteristics and requirements of stem cells themselves. ESCs are naturally adherent cells for example, a property which complicates single cell high throughput phenotyping. A second consideration is that for such devices to be efficient in acquiring data from cells, their experimental set-up must be simple enough to perform in tandem with preparation of the cell samples. Given the delicate nature of ESC culture and the need to perform experiments at specific times (for example at a certain number of hours post 2i removal), device handling must be as convenient as possible. This section presents the range of devices developed in an attempt to produce a high-throughput, easy to handle device for applying small constrictions to ESCs.

2.2.1 Multi-height Device Fabrication

The underlying principles and core fabrication methods used for the devices in this section are presented in Section 1.3.1. An element of the fabrication process which was not discussed, however, is the process required to produce devices of multiple internal heights. For multi-height devices, the channel in which the cells flow can vary in height along its length. This is vital if we are to achieve a two-dimensional compression.

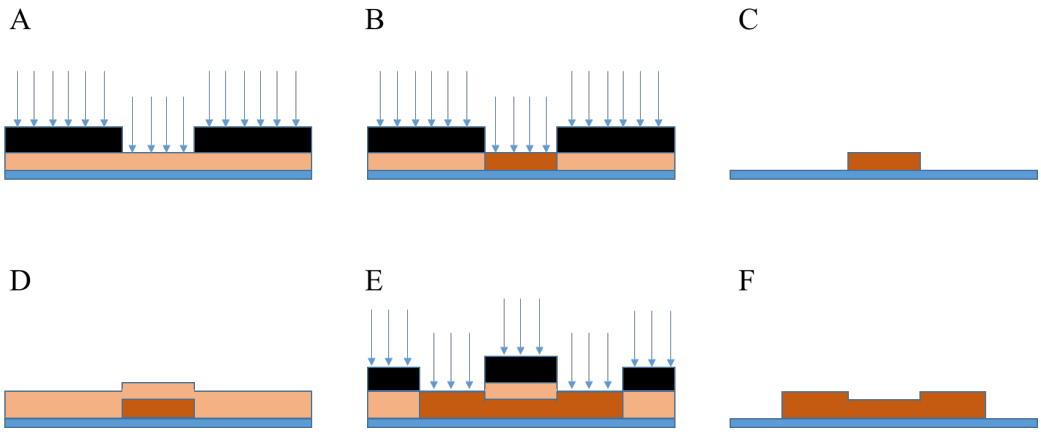

Figure 2.2: **Fabrication protocol for multi-height devices**
(A) A mask enables selective exposure of photoresist on a silicon wafer. (B) to (C), exposed region becomes insoluble to developer, leaving a raised feature on the wafer. (D) A second layer of photoresist is spun over the wafer and features. (E) to (F), exposing an overlapping region around the existing features joins the reservoirs and creates a step in feature height.

As previously explained, the height of the channels and features in the microfluidic chip is determined by the thickness of the spin-coated layer of photoresist. For a device to have two heights, for example a 20μm high reservoir channel with a 12μm high constriction region, the photolithography and coating is performed in two steps. Firstly, a 12μm layer of photoresist is coated over the silicon wafer and after the relevant bakes, exposure and development, 12μm high features remain. Following this process, a 20 micron layer of photoresist is coated over both the silicon wafer and the 12μm features. The microscope is then used on a mask aligner allowing the 12μm features to be identified as protrusions in the surface of the 20μm layer (as shown in Figure 2.2(E)). The fine stage controls of the mask aligner are used to align the constriction channels to the edges of the entry channels and are exposed and developed once more. This leaves the 20μm entry channels connected by the 12μm constriction channels.

2.2.2 Devices to Improve Efficiency and Throughput

The device used in Pagliara *et al.* (2014) consisted of 4 constriction channels 10μm in height. Two channels were 10μm wide and two were 12μm wide. The inlet reservoir was 20μm high so as to not impede the flow of ESCs. Using a pressure source to flow cells along the constriction channels, they imaged the cells before, during and after constriction. A significant hindrance to their data acquisition came from blockages in the constriction channels as cells inevitably form aggregates in suspension [74]. Each of the designs presented in this section have been fabricated and then tested using ESCs. Weaknesses and advantages of each design were assessed in developing the next generation of devices. The first round of designs aimed to improve on throughput by reducing this damage caused by blockage or reducing the likelihood of blockage.

Increasing Channel Number and Length

The first design was a simple expansion of the channel number. Given that a blockage would render a constriction channel unusable, more channels were thought to increase the time available to capture and image before all the channels are blocked. Further consideration was given to the difficulty of imaging a cell whilst under constriction due to their increase in speed though the smaller volume, therefore the channels were also increased in length.

Figure 2.3 shows the three variations we began to test. The first (Figure 2.3 (A)) is a simple increase in channel number, length and includes an escape channel. The escape channel is wider than the constriction channels and exists to allow agglomerates of cells to pass though without causing a blockage. The second, (Figure 2.3 (B)) addresses the issue

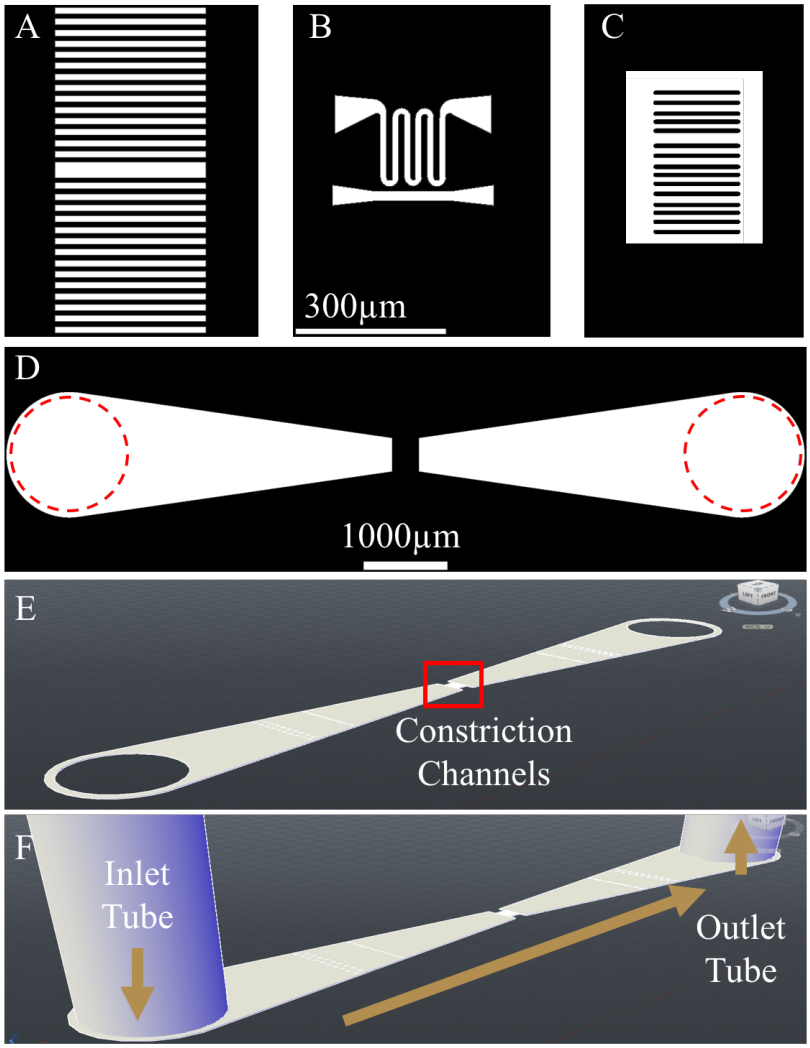

Figure 2.3: **Two-Height Chip Schematics**
(A), (B) and (C) display designs for the constriction channels of the two height devices. The white area represents transparent sections of the mask where features will be post development. (D) depicts the inlet reservoirs which align over the constriction channels. The dashed line displays the area where inlet holes are punched. (A) shows 12μm constriction channel with a 20μm escape channel. (B) is a single 12μm wide and appox. 1.5mm long serpentine constriction channel with a single escape channel. (C) is a large channel which spans the inlet reservoir. Compression of the cells is between the features within. This method enables the entrance of the compression section to be more rounded than (D). (E) shows a full view of three-dimensional projection of a two height device with straight central constriction channels. Holes are punched with a 1.5mm biopsy punch though the PDMS chip to provide fluidic control within the reservoirs and across the channels. (F) columns represent the FEP tubing connecting the chip with the pressure source. One side is filled with cells suspended in culture medium forced across the constriction channels by the pressure of syringe pump.

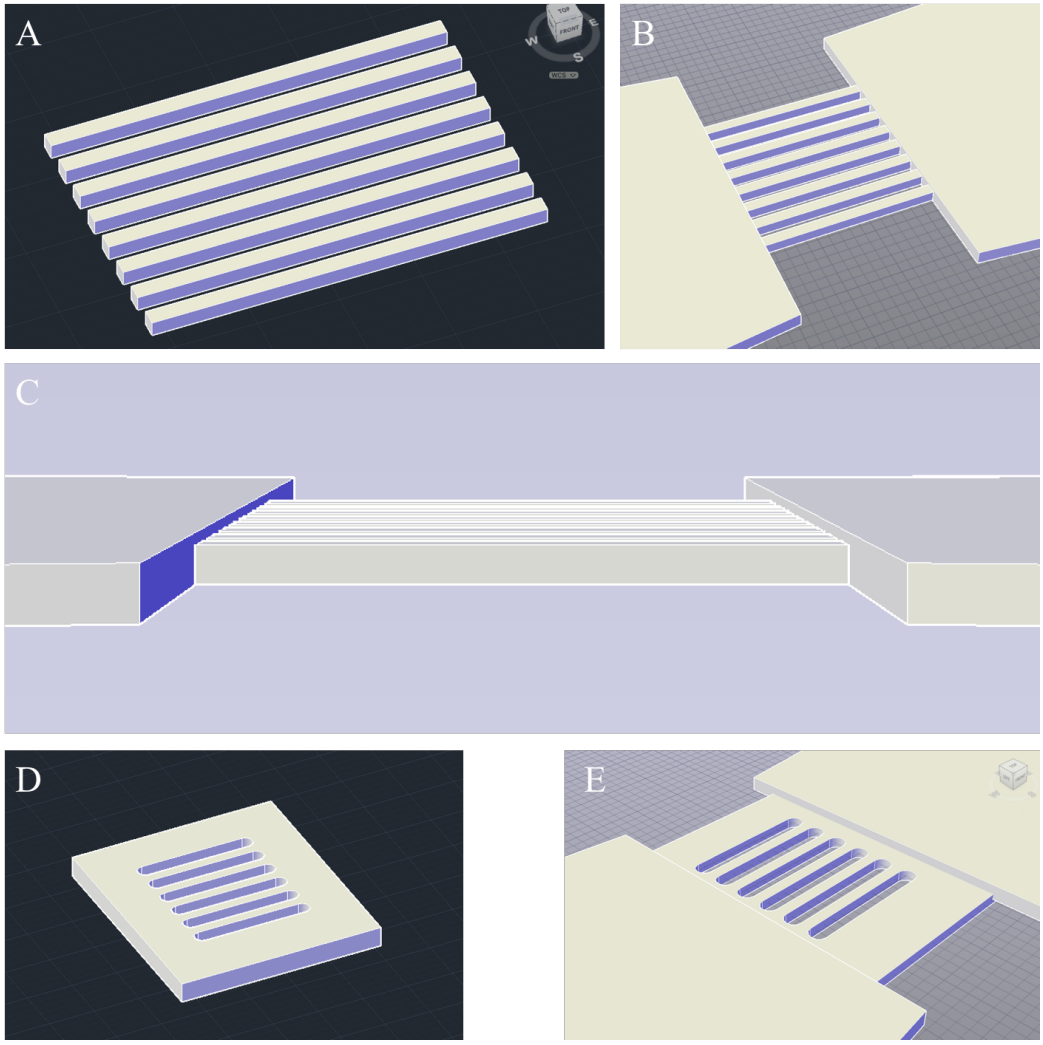

Figure 2.4: **Projection of Two-Height Chip**
(A) shows a three-dimensional schematic of constriction channels on a wafer before the inlet reservoirs are laid over the top. (B) shows the same channels with the inlet reservoirs now added to the wafer. (C) is a side on view displaying the change in height between the inlet reservoir and constriction channels. (F) easy entry for the cells into the constriction channels, obstacles within a large channel can be rounded at the initial point of contact with a cell. (D) displays a channel with such obstructions within on a wafer before the addition of the inlet reservoir. (E) shows the added reservoir and the step in height between the two layers.

of channel length by aiming to maximise the time a cell is imaged under compression. We observed that cells could be damaged by unforgiving angular entrances to the constriction channels. This damage can leave debris or even DNA which causes the subsequent cells to become stuck. Figure 2.3 (B) includes a gradual entry aimed to ease the cells into the channel, reducing damage and blockages. Figure 2.3 (C) was designed to address the issue of channel entry and increased channel number simultaneously. This design acted as one large channel which contained rounded features within. The space between the features emulated the constriction channels of the previous chips. Three dimensional diagrams of versions of of Figure 2.3 (A) and (C) are displayed in Figure 2.4. Running experiments with cells using these designs, we found that there were still some flaws. Whilst increasing the channel length did improve our ability to image cells under constriction, the serpentine design of Figure 2.3 (B) was not sufficiently high-throughput given its single channel. We further identified that despite the rounded entrances to the channels of (C), the cells had a tendency to become blocked at the beginning of the 12 μm high constriction region. Design (A) possessed an improved balance of throughput and channel length, but did not benefit from the rounded channel entrance. To further diminish the chance of blockages, we next investigated constriction along a single axes using single height devices.

Single Height Constriction Channels

The single height design poses a number of advantages over the multi height counterparts. Primarily, we are able to design the shape of the channel entry to be gradual therefore reducing blockages and cell damage and second, there is no focal shift as the cell moves from the inlet reservoir into a two-dimensional constriction channel. Finally, we aim to make the chips as user friendly as possible, so the investigator is able to focus on cell culture over chip fabrication. The single height chips do not need careful alignment or challenging two-step photolithography and may be produced much more quickly and easily.

The first array of designs emulated those for the two-step devices in single step format. This iteration included many more constriction channels per chip. We found that increasing the number of constriction channels however, does not necessarily increase the effective throughput of the device. Whilst the inclusion of more channels than can occupy the imaging window can be effective in the case of blockages, too many channels across the chip reduces the number of cells per channel in a given time. This is not only time inefficient for data acquisition, but the increased experiment time may be harmful for the cells by spending extended periods within the inlet tubing. There is a trade-off between increasing channel number to reduce blockage impact and decreasing channel number to observe more cells per channel. As the number of channels increases, the number of cells passing through the device in a single observable area decreases as Figure 2.5 displays a selection of these designs. (A) is a version of Figure 2.3 (C) in which rounded obstructions form constriction channels and (C) applies the serpentine design of the two-step devices to an up-scaled single step device. Following testing of both of these designs, we found that cells became regularly lodged within the serpentine designs. The straight constriction channel device proved to have too many channels, with the throughput within the imaging window diminishing when compared to chips with fewer channels. Brightfield images of these two variations are displayed in Figure 2.5 (E) and (F). Furthermore, we found that the inclusion of the 'escape channel' for large objects was too frequently the route taken by ESCs which could have otherwise been analysed.

The next version of the device proved to be the final iteration and has been used in the experiments which follow in this chapter (Figure 2.6). The previous devices taught us that too many channels were counter-productive to useful throughput, that the smoother entrances to the constriction region reduced damage and blockages but also that we had not addressed the issue of agglomerates of cells entering the device. The final design divides the inlet reservoir into as many sections as there are constriction channels. Cells which enter the chip flow into the separated inlet reservoirs out of view of the constriction channels. This means that if a blockage were to occur in a channel, it would not cover the entrance to the adjacent

constriction channel as well, allowing the neighbour to remain open. Furthermore, blockages at the entrance to the constriction section will not effect the imaging at the entrance to the adjacent channels; with previous versions the blockages could obscure otherwise imageable cells passing into another channel. We also included columns between the cell inlet and the beginning of the reservoir to serve as a filter for large debris. The characterisation of this device is presented below as part of our experiments into ESCs mechanical response to stress.

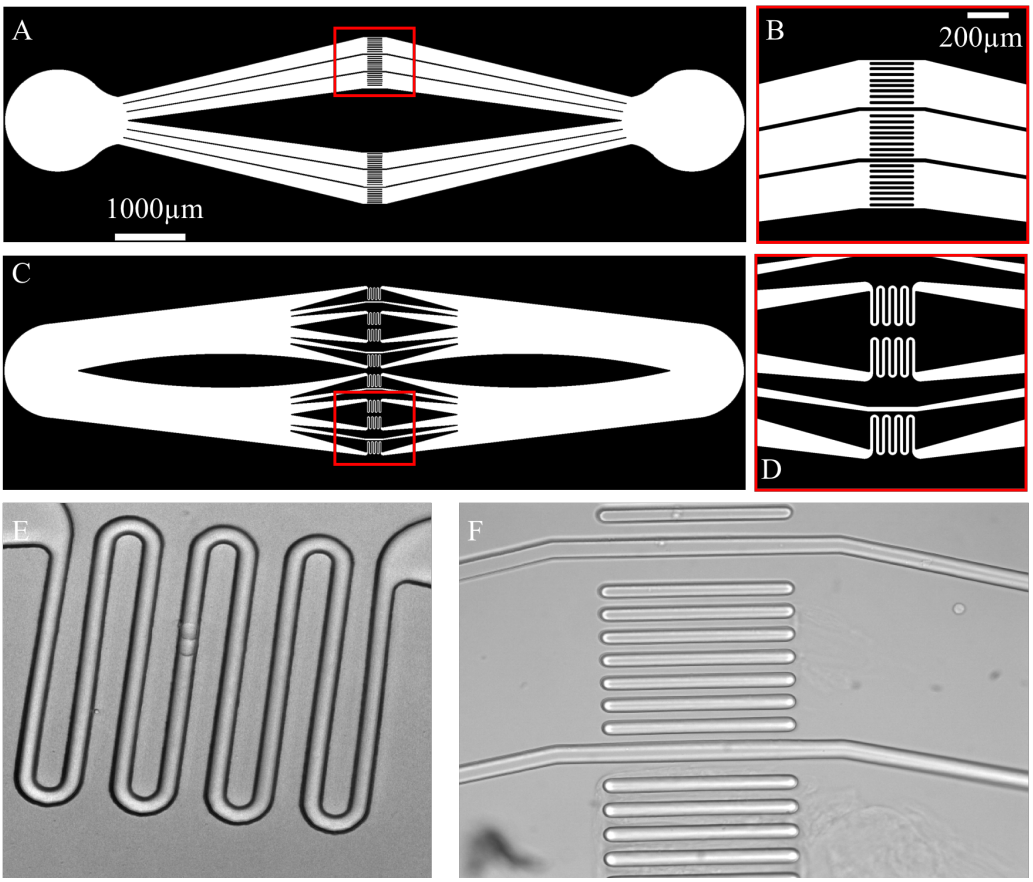

Figure 2.5: **Single Height Scaled-up Chips**
(A) and (C) are both schematics for the scaled up versions of the single height devices. (A) features 3 blocks of 9 channels, with constriction widths of 12 to 14 μm. (C) is a single height version of the serpentine chip with 8 constriction regions and 4 bypass channels. (E) and (F) Brightfield Image of Single Height Serpentine and Straight Constriction Channels. (E) two cells are captured under constriction within a single step serpentine channel. Constriction channel dimensions are 12μm wide, 20μm high and approx. 1.5cm long. (F) 12μm constriction channels with 20μm escape channel. The single height design allows the rounding of the constriction channel entrances to reduce damage and clogging.

2.3 Methods for Investigating ESC Mechanical Response to Constriction

This section will initially present the experimental method for a series of experiments which have been submitted as part of a paper to the journal Lab-on-a-Chip with co-lead author, Christophe Verstreken. The device used is the single height constriction chip (16μm high with a 12μm constriction region) displayed in Figure 2.6 and described above. I will present the graphical user interfaces (GUIs) coded to improve ease and efficiency of data handling and analysis plus those which were written to help characterise the devices.

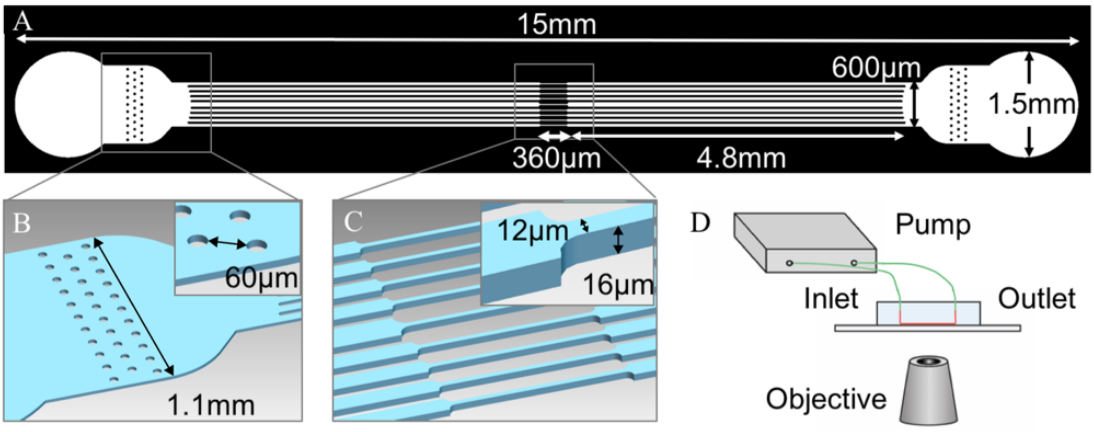

Figure 2.6: **Single Height Device Used in Characterisation Experiments**
(A) Schematic of the 16μm high chip with 12μm constriction channels. Filter columns (B) are present close to the inlets to collect large debris. The constriction channels (C) are separated by their own individual reservoir so blockages do not hinder imaging of the adjacent channels. (D) is and outline of the experimental set-up: a pressure pump drives cells across the chip which it accesses via FEP tubing.

The ESCs used in our experiments were cultured differently to those used by Pagliara *et al.*. As described in previous sections, the 2i/LIF culture system used by Pagliara *et al.* is now commonly used over the Serum/LIF culture system utilised prior to its development. A feature of Serum/LIF maintained cells is spontaneous differentiation, with cells displaying transcriptional heterogeneity [16]. This heterogeneity should present in their physical properties. We were also interested to see if the auxeticity observed in the 2i/LIF cultured cells was present in the Serum/LIF cultured cells, particularly as a large amount of research to date has been performed with Serum/LIF cells. We therefore cultured the ESCs used for the following experiments in the Serum/LIF culture system.

In order to assess the chip's ability to phenotype cells we used two additional treatments. The first was Cytochalasin D, an inhibitor of actin polymerisation [75]. It is hypothesised

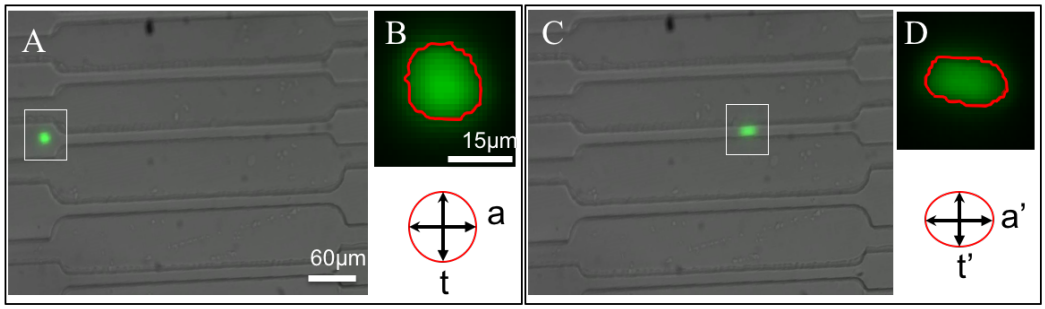

Figure 2.7: **Cell Selection and Thresholding**
Screenshot of the MATLAB GUI for cell selection and thresholding. (A) Cell approaching constriction channel. White box represents region selected by the user. (B) The cell is automatically thresholded, an ellipse is fit and measurements of axial and transverse lengths are taken. (C) The user progresses the image sequence to identify the cell from (A) under compression. (D) The cell is again thresholded and measured. (Image taken from Hodgson *et al.* (2017) [1])

that due to the lack of polymerised actin filaments, cells are more easily deformable. We thus hypothesised that cells would translocate through the constriction channels more quickly with this treatment. To test this hypothesis we performed experiments enabling us to compare the translocation times of cells with and without treatment though the constriction channels. We then tested whether treatment of cells with Trichostatin A (TSA) would affect the relationship between compression and strain by modifying the material properties or average size of the nucleus. TSA has the effect of decondensing the chromatin structure of the nucleus. As chromatin is a primary structural component in the nucleus of ES cells, its decondensation could have an effect on the nuclear response to compression [67]. Hence we examined whether the increase in nuclear deformability due to chromatin decondensation (as observed in both Chalut 2012 and Krause 2013) would, at least in small nuclei, increase the magnitude of the axial strain.

We have calculated the axial strain as

$$S_a = \frac{(a' - a)}{a} \tag{2.1}$$

where a' and a the compressed and uncompressed axial lengths respectively. Similarly, the transverse strain is defined as

$$S_t = \frac{(t' - t)}{t} \tag{2.2}$$

where t' and t the compressed and uncompressed transverse lengths respectively. The axes used in these equations are depicted in Figure 2.7: a and t are taken from the pre constricted thresholded image (A and B), a' and t' are taken from the constricted thresholded image (C and D).

2.3.1 Statistical Methods

We used an n-way ANOVA to analyse the data taken for translocation time of Cytochalasin D treated cells. Variables used were 'cell sample' and 'drug treatment'. Each sample of cells were divided in two, one half remaining as a control while the other half underwent Cytochalasin D treatment. 4 samples were used to create 4 treated and 4 control groups. AVOVA was performed using MATLAB and OriginPro. Where appropriate, the statistical significance of our strain measurements were assessed by ANOVA or standard error of the mean.

2.3.2 Cell Culture

The ESCs were cultured in conditions for sustaining naive pluripotency. ESCs were maintined in an icubator set to 37°C and 7% CO2. The base culture medium used was Glasgow Eagle's Minimal Essential Medium (GMEM) (Merck), supplemented with 10% HyClone Fetal Bovine Serum (GE, CT, United States), L-glutamine (Invitrogen), MEM Non-Essential Amino Acids (PAA), Sodium Pyruvate (Invitrogen), β-mercaptoethanol (Sigma) and LIF (Millipore)[76]. Cell culture was performed by Christophe Verstreken who split the cells every second day to avoid overcrowding of the cells in the culture wells. A 5 minute incubation in Accutase was sufficient to dissociate ESCs from tissue culture plastic, which is then diluted in PBS to arrest cell damage. Tissue culture plastic is the base substrate used for culturing our ESCs, but a 0.1% gelatin coating is required for survival and attachment. Following PBS dilution, the supernatant is centrifuged for 3 minutes at 1400rpm to condense the cells at the base of the tube. After aspirating the PBS and re-suspending in new medium, the cells can be re-plated onto the gelatin coated culture flask.

Prior to imaging, the cells used in the experiments were treated with 2 μM SYTO 13 (Invitrogen) for 30 min. This marker flourescently stains the nucleus at an intensity 3 to 4 times higher than the cytoplasm, allowing thresholding methods to detect nuclear and cytoplasmic boundaries [77]. Following treatment, cells were centrifuged so the SYTO 13 solution could be removed and were then re-suspended in the base culture medium. For strain analysis experiments, the cells were re-suspended at a concentration of $3\text{x}10^6$ cells/ml.

To measure the strains expressed by cells under compression following the TSA treatment, 5 μm TSA was added to the culture medium and incubated for 5 hours. Following this period, the SYTO 13 protocol from above was used to stain the cells. For the translocation time experiments, Cytochalasin D was added to the cells 10 minutes before our experiments on its effect at a concentration of 2μM [75].

2.3.3 Device Fabrication and Experimental Setup

Following the process of design, fabrication and testing in section 2.2.2, the device used for our experiments as part of Hodgson *et al.* (2017) [1] is the single height device containing separated delivery channels, 12 μm constriction regions and inlet filters, shown in Figure 2.6.

The mask for this device was designed using AutoCAD as introduced in Section 1.3.1 and printed onto an emulsion film with a resolution of 128,000 dpi. The channel height of 16μm was achieved by spinning SU-8 2015 (Microchem) at 3000 rpm for 60s on a silicon wafer to make a mould. A soft bake at 65°C for 3 minutes followed by 5 minutes at 95°C prepared the wafer for exposure. A UV lamp (365-405nm, 20mW cm^{-2}) exposed the visible regions of the wafer through the mask for 6 seconds which was followed by a 5 minute post bake at 95°C. The unexposed resist was removed with propylene glycol monomethyl ether acetate (PGMEA) (Sigma-Aldrich) and cleaned with isopropanol. Finally, the mould was verified to have a feature height of 16μm using a stylus profilometer (Dektak, Bruker, Billerica MA, USA).

To produce the chip from the mould, we placed the wafer from above in an open container slightly larger than the wafer. Degassed 9:1 (base : curing agent) PDMS was poured over up to a height of approximately 1.5cm and cured at 70°C for 60 minutes. When cured, a scalpel was used to cut the chip free from the mould. To connect the channels within the chip to the syringe pump of pressure pump used to control the flow.

We found the use of two alternative sources appropriate for different experiments. The advantage of using a syringe pump is less variation in cell flow velocity for a given requested flow rate between chips. The difference occurs due to pressure gradient variations from factors such as tubing length and volume as well as inlet and outlet hight. The pressure pump is able to give more finely tuned control over the flow velocity of the cells, however the requested pressure for a given flow rate varied between devices for the reasons given above. This means that for experiments requiring high resolution imaging, the sensitivity of the pressure pump was used, whist for the characterisation of the chip throughput, the syringe pump was used.

For fluidic access, holes were punched with a 1.5mm biopsy punch (Kai Medical). Oxygen plasma treatment at 100W for 20s (Diener Electronic GmbH and Co. KG, Germany)

was applied to the featured side of the chip and a glass slide (24x50mm, 0.13-0.16mm, Menzel-Gläser). When the two exposed surfaces were placed in contact, they formed a strong bond. We used FEP tubing (1/16 in x 0.03 in, outer and inner diameters respectively, Gilson, UK) to connect the punched inlets to a flow control system depending on the experiment. The inlet tube was filled with a cell suspension while the chip and outlet tube was filled with cell culture media pre-equilibrated to culture conditions by incubating it at 37°C and 7% CO_2.

For the strain analysis experiments, flow across the constriction channels was controlled using an MFCS-4C flow controller (MAESFLO, Fluigent). Imaging was performed on a Leica SP5 (Leica Camera AG) in epifluorescence mode, using a 20x/0.5N.A. objective and 2x2 binning.

For translocation measurements, the microfluidic chip was connected to a syringe pump (Nemesys, Cetoni) set to 100μl/hr. We used 4x4 binning on an Olympus IX73 epifluorescence microscope (Olympus) using a 20x/0.5N.A. An optiMos sCMOS camera was used to record the measurements.

2.3.4 Analysis Software

The goal of the microfluidic devices of this chapter is to facilitate detection and measurement of ESCs. To perform these tasks, a collection of MATLAB graphical user interfaces (GUIs) have been coded. The various GUIs have been developed to enable quick and efficient analysis of the images taken while using the chips. The aim in developing the software was to remove all images which could not be analysed in a fast and computationally-light way; to provide the user with instant visual and numerical feedback for each cell analysed; to enable multiple measurements for the same cell in each region to be averaged; and to automatically store and save the data in a convenient manner for further analysis.

The first GUI was developed to solve a number of issues in the analysis of the images collected while observing the effect of compression on ESC nuclei. The primary difficulty was in the number of frames in the sequence which cannot be analysed, either through an absence of cells or blocked, stationary cells.

The data analysed by Pagliara *et al.* (2014) was collected by importing an image stack of all frames taken during the experiment into ImageJ (National Institutes of Health, Bethesda, Maryland, USA). A Leica SP5 camera was used to capture the cells under compression without blurring and was left running between cell arrivals. This, alongside the necessity of a cell concentration low enough to avoid clumping and overcrowding, leads to many frames in the stack being dark or unable to be analysed. The user must therefore cycle though these unusable frames to reach useful ones and as the image stacks may be comprised of

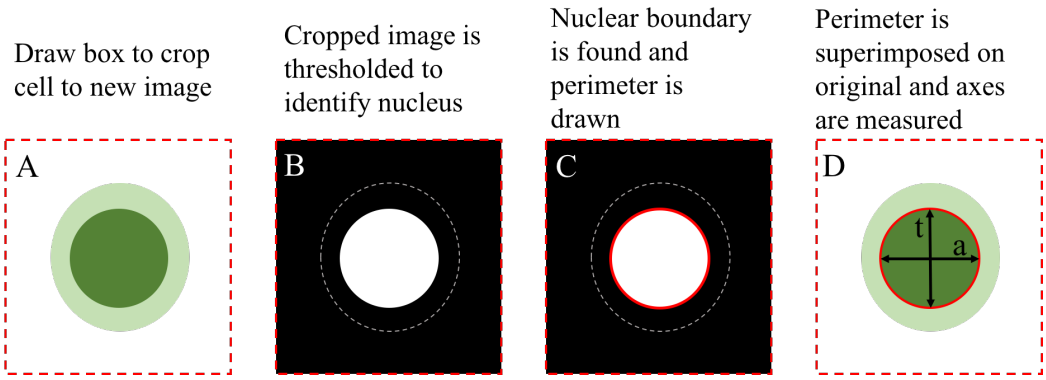

Figure 2.8: **Image Processing Steps**
(A) The user draws a box around a cell of interest. The GUI crops the area and puts the image thorough a thresholding algorithm. (B) The algorithm creates a binary image, in which the nucleus is white and all else black. (C) The boundary of the white area, and thus nucleus, is identified. (D) The boundary is then superimposed over the original cell image to clearly display the nucleus. An ellipse fit is used to measure the major and minor axes dimensions to use in the strain calculations.

thousands of images, this is a potentially time consuming and inefficient process. A further difficulty with this method is due to the images being taken with a GFP filter to observe the fluorescence of the cell. This results in the user being unaware of the cells location relevant to the constriction channels and may result in smaller cell distortions being overlooked. To measure a cell it must then be cropped into a new image which is thresholded using the ImageJ thresholding algorithms to find the boundary of the nucleus. At this stage the user must assess the image by eye to identify if the thresholding has achieved an accurate fit to the nuclear boundary. To calculate the strain, the boundary is characterised with an ellipse fit to find the length of the major and minor axes which are imported into a spreadsheet. The analysis GUI was designed to streamline this process to produce results more quickly and efficiently, the steps of the image processing used by the software are displayed in Figure 2.8.

The thresholding algorithms provided with the ImageJ software are available online in MATLAB form. These functions have been incorporated into the GUIs, each using a different method to threshold an image. The methods used for the analysis in this chapter are *MaxEntropy* and *Intermodes*. Thresholding is a technique which involves transforming a grayscale image into a binary black and white one. The algorithm determines a value, T, between 0 and 255 for pixel intensity. A pixel value in a grayscale image below T becomes 0 (thus black) while pixels over that value are made white (Figure 2.8 (B)).

Two GUIs have been coded to analyse the compression of ESCs, each with the same core structure which will be discussed before describing the specifics of each. The original aimed

to fully automate the process of cell detection, thresholding and measurement. The second version, used for the data provided in this chapter, is a semi-automated system in which the user chooses the cells to analyse.

On launching the GUI, the user is invited to specify the path to both a background image showing the chip features and the image stack taken in flourescence mode. This will automatically display the background image in the GUI image window. The user is then informed of the total number of frames in the stack and must fill in the physical size of the image in microns. The user may chose where within the image stack to begin and end before executing the analysis sequence; clicking the 'Run' button then begins the filtering function.

Early versions of the GUI read in the whole stack to be held in the memory to be accessed for analysis and display rapidly. This, however proved to be computationally over-taxing and inefficient. The final version avoids this issue by registering the location of the useful images numerically in an array. The image numbers correspond to an image location on the hard-drive which is accessed when required.

The algorithm begins by running a 'for' loop over the entire image stack. Within the loop, each image is subtracted from an image 20 frames away from it in the stack. If a cell has entered the frame, then there will be pixels with a value greater than 0 within the subtracted image. The user can specify a pixel value to count as a minimum threshold detection. If this threshold is met, the image number, and therefore location, is saved to the array containing the location of all frames which have met the required detection threshold. This produces a single column of numbers in ascending order, relating to the frame number in the original stack. Breaks in the sequence are due to dark frames or images in which cells are stationary for 20 frames for more. Using the slider bar above the image window, the user can navigate through the post-filtered frames which are automatically superimposed over the background. The GUI also informs the user of how many frames are left post filtering.

Automated GUI

In the earlier version of the GUI, the next step could be automated. Having selected a threshold method for the nuclei, the images saved in the previous step could be automatically displayed one by one as a sequence. Each image would then be run through the *centroids* command which identifies objects (cells) within the frame. The command reveals the central coordinate of each cell clearly detectable in the frame. In using this, a predetermined boundary is placed around the cell and displayed in the GUI window. The boundary extracts the section contained within, which is temporarily saved and input to a thresholding algorithm. The thresholded image is then used to measure the cell.

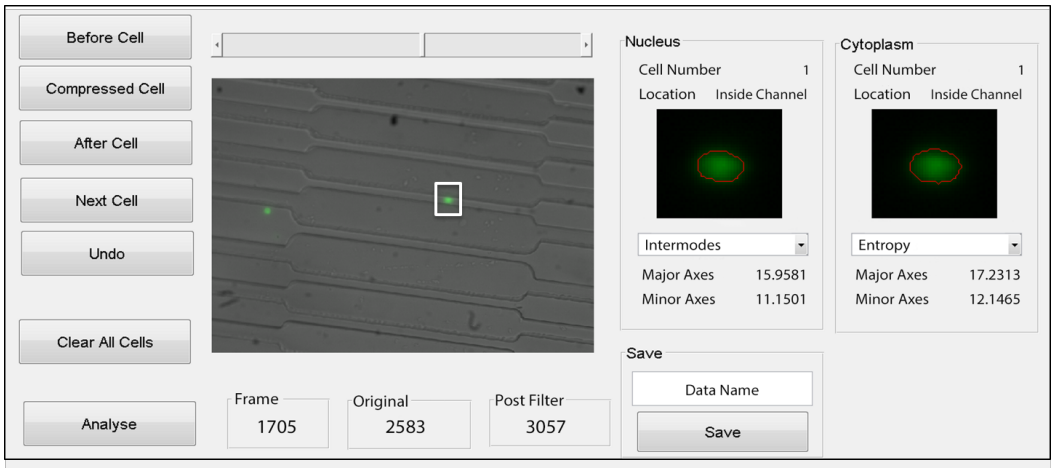

Figure 2.9: **Manual GUI**
Following the removal of dark frames, the user moves the slide bar above the main window to cycle through frames. In this frame, the user has selected the cell within the white box. Automatically, the image is cropped, thresholded then redisplayed in the 'Nucleus' and 'Cytoplasm' windows. The measurements of major and minor axes are displayed and a boundary of the nucleus or cytoplasm is superimposed upon the corresponding image. The user is able to change the thresholding using the drop down box. In this instance, *Intermodes* and *MaxEntropy* thresholding was used.

To account for more than one cell being in the frame at once, the automated GUI assigns each identified cell a coordinate. If, for example, two cells are present in frame 1, the GUI identifies and measures both cells. In the next frame, the process is repeated. To distinguish between cells as they translocate though the chip, the x-coordinate is used. The cell with the highest x value in each sequential frame is measured as the same cell until it leaves the chip and the cells are ordered from frame to frame by x position. Each time a cell is identified it is thresholded and measured automatically, therefore a mean size can be calculated for a cell over its total time in the imaged region and saved to an array. For the strain measurements to be calculated, the GUI requires the location of the transcription channels to identify when a cell is under compression or not. The user assigns the location by marking the beginning and ending of the constriction channels on the GUI window using the mouse pointer.

The identification of cells in this manor worked well, and if cells entered one by one and flowed in a predictable fashion, the automatic measurement and logging is efficient. There are, however, issues which were not solved. The first is in the instance that a cell became stuck and overtaken by the cell behind whist occupying the reservoir on approach to the constriction channel. This invalidates the logging of cells by x position. Secondly, the automated method does not allow the user to visually assess the accuracy of the thresholding, which may lead to skewed values in the average measurements if the thresholding fails. It

was decided to continue with the semi-automated manual GUI for the analysis of our data given its improved accuracy of recording.

Manual GUI

The user scrolls though the images using the slider for the manual GUI (Figure 2.9) following the filtering of redundant frames. There are three buttons for beginning cell measurement: 'Before Cell', 'Compressed Cell' and 'After Cell' referring to a cell before, during and after compression respectively. Clicking on one of these launches the region of interest function which enables the user to draw a box around the cell to be measured. The first time this is done with the 'Before Cell' button, the cell number is set to 1. The region of interest drawn around the cell is cropped, set to grayscale and input into the thresholding algorithms. The user can select a method for both the nuclear and cellular perimeter detection from the drop down menu. Returning values for T, binary images are made for both the nucleus and cytoplasm. The *regionprops* function is performed on the images to apply an ellipse fit, providing values for the minor and major axes. These values are saved to an array along with the cell number and the coordinates of the binary image boundaries are taken to superimpose an outline on the original image. This enables the user to see instantly how effective the thresholding has been.

The next step is to draw a box around the cell, which automatically changes the frame to the next in the series. If the user is unhappy with the thresholding method employed, they are able to select another from the drop-down menu; this automatically re-runs the process from above, displaying a new boundary and measurements. If the user would like to reject the measurement entirely, the *Undo* button removes the last measurement from the array. Multiple measurements of the cell may be taken as it translocates to produce mean values.

The user selects the *Compressed Cell* button to draw the region of interest when the cell enters the constriction channel. The measurements are stored in a separate section of the array to represent a second region. Similarly, when the cell exits the channel, *After Cell* is selected for the third region of interest. If the user is satisfied with the measurements, pressing *Next Cell* adds one to the cell number count so the next cell can be selected with *Before Cell*. Having measured the cells in the image stack, the user can select *Analyse* to calculate the mean dimensions of all cells for before, during and after compression. This process, along with calculations for axial and transverse strain, are written to file by pressing *Save*.

Translocation GUI

We used the device to assess the translocation time of cells though constriction channels, the details of the experiment are presented in the following section. To rapidly record the number of frames a cell was present within the constriction channels, a GUI was written. The translocation differs GUI from the manual GUI in the options presented to the user and the data taken. The translocation GUI simply requires the user to identify the frame in which a cell enters and then exits the constriction channel, it does not take any thresholding or image analysis; its aim is to record the amount of time each cell spends under constriction. The frames were filtered in a similar way to the cell measuring GUI described above. Having filtered the frames, the user scrolls though the images to the point a cell enters the channel then presses *Cell in*, subsequently when the frame in which the cell exits the channel is reached, the user presses *Cell out*. At the end of the image stack, the user can save the data of occupation time to file for further analysis.

2.4 Characterisation and Results

The single height constriction chip was initially characterised by assessing the throughput of cells at a range of concentrations and flow rates. To begin, we varied the flow rate of the syringe pump input to the chip from 10 to 80 μl/hr. There are issues concerning both flow rates too low and too high. Flow rates which are too low allow cells to become aggregated which then forms blockages. Furthermore, whilst the media used in our experiments was conditioned and warmed to incubation standards, the microfluidic environment is not as tightly controlled as the incubator itself. This means having as many cells as possible pass though the constriction channels before they begin to deteriorate is important. Caveats of high flow rates is in the imaging capability of the camera (some cells may pass too quickly for detection) and with cell damage due to collisions. The damaged cells may form agglomerates which prevent cells from reaching the channels. The data collected supported our concerns over high flow rates; the relationship between throughput and flow rate was linear however only to a point. As shown in Figure 2.10 (A), over 40 μl/hr the relationship became linear. We believe one of the causes of this relationship may be due to the 110 fps camera rate being unable to record all translocating cells at the higher flow rate.

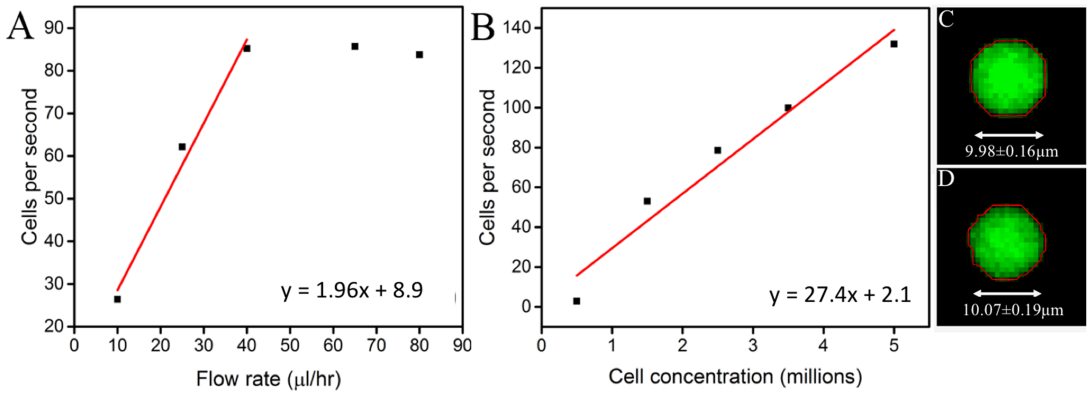

Figure 2.10: **Cell concentration and flow rate**
Cell throughput, measured as number of cells per second, as a function of (A) the flow rate and (B) the initial cell concentration. A linear fit has been applied to both plots, however just the first three points of (A) have been utilized. (C and D) Thresholding of (9.9 $\pm$ 0.12) μm fluorescently labelled beads (red outline). The mean diameter was measured to be (C) (9.98 $\pm$ 0.16) μm outside and (D) (10.07 $\pm$ 0.19) μm inside the compression channel (n = 19), illustrating the consistency of our measurement technique. *Image and caption from Hodgson et al. (2017) [1].*

Having determined the optimal flow rate, we then assessed the effect of cell concentration on throughput. Again intuitively, simply increasing cell number should lead to an increase in

the number of cells passing though the constriction channel. We were, however, concerned that too many cells may lead to increased numbers of agglomerates and thus blockages. In varying concentration from 1-5 million cells per ml (Figure 2.10 (B)) and setting flow rate to 40μl/hr, we found a linear relationship between concentration and throughput. Throughput increased at higher concentrations, yet we found that a concentration of 3.5 million cells/ml was a favourable balance between cell numbers and a consistently achievable cell culture number.

To identify any potential alteration in focal plane and to assess the accuracy of our size measurements, fluorescently labelled beads with a mean size of (9.9$\pm$0.12) μm were flowed through the compression channels. Images of the beads were taken and thresholded both outside and inside of the compression channels to provide size measurments. With n=19 beads, we measured the diameter of the beads to be (9.98$\pm$0.16) m outside and (10.07$\pm$0.19) μm inside of the compression channels (Figure 2.10 (C) and (D)).

We analysed the strain and recovery in cells both with and without TSA treatment by including regions before and after the constriction channel in our images. Using the analysis GUI described above, we found that the major axes of both the nucleus and cytoplasm significantly increased whilst in the constriction channels for both treated and untreated cells. However, we found no correlation between axial strain and cell size, and no indication that larger cells (i.e. > 16 μm, the channel height) have a different mechanical response than smaller cells (< 16 μm). The post-constriction images revealed that for both TSA treated and untreated samples, cell size returned to the pre-constriction measurement (Figure 2.11 A and B). This indicated that we were able to probe the mechanical response of the nuclei upon entering constriction channels without permanent damage.

We next chose to examine if the mechanical response to constriction remained consistent throughout the occupation of the channel or if instead the cell behaved viscoelastically, altering the mechanical properties over a longer time-scale. To achieve this, cells (n=20) were imaged at multiple points both outside and inside the constriction channels. For each recorded instance, i, of cell j, we calculated a χ^2-value of the axial strain defined as

$$\chi^2_{ij,ax} = \frac{a_{ij,ax} - \bar{a}_{j,ax}}{\bar{a}_{j,ax}} \tag{2.3}$$

where $a_{ij,ax}$ is the axial strain of the nucleus of cell j at the instance i, and $\bar{a}_{j,ax}$ is the average axial strain of all the instances of cell j. Binning the instances according to their position in the first (n=57), middle (n=65) or final (n=69) third of the channel, we found no significant differences between channel positions. If the mean χ^2-value were not close to zero for each section of the channel, this would signify that the strain of the nuclei changes with increasing time under constriction. As the χ^2-value is consistently close to zero, this

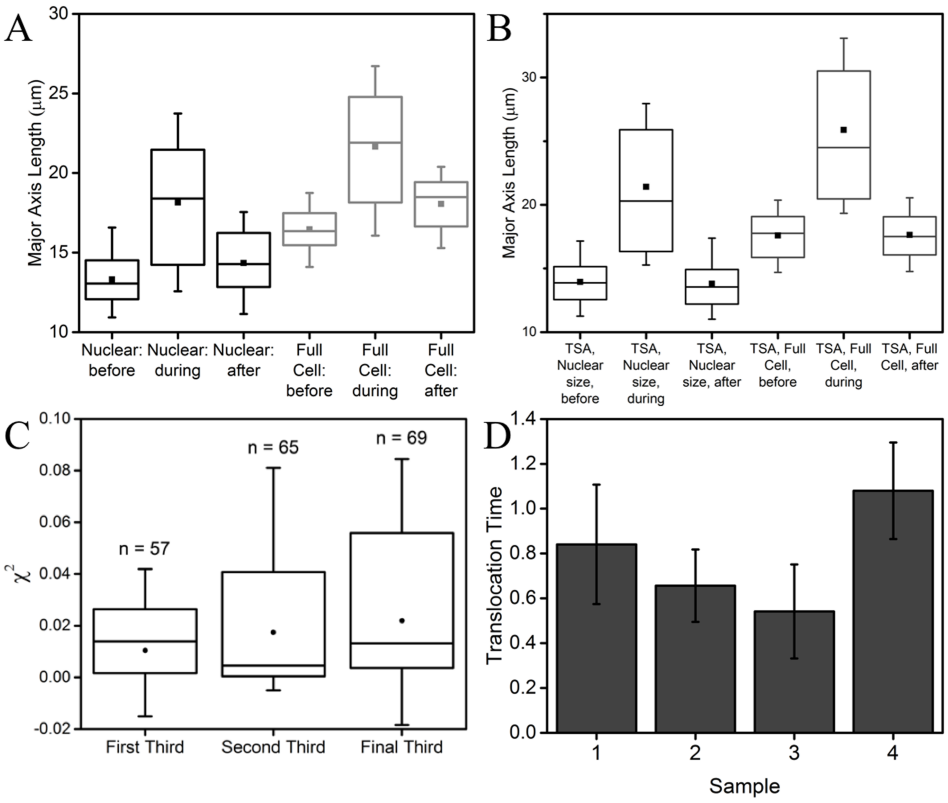

Figure 2.11: **Mechanical phenotyping of ES cells**
Length of the nuclear and cellular major axis measured before, during and after compression for (A) control cells (n = 117) and (B) cells treated with Trichostatin A (n = 162). For both the whole cell and the nucleus, the major axial length returned to its approximate original size post-compression. (C) χ^2-value of the cells along the length of the channel. The distributions of χ^2-value of nuclei in the first, middle and final third of the channel are not significantly different. (D) To characterize and display the capabilities of the microfluidic device, measurements were conducted to determine the ability of the chip to distinguish deformability of ES cells. Images were captured at 234 frames per second to record the translocation time of cells through the constriction channels. The translocation time in frames of control and cells treated with Cytochalasin D were compared. The effect of the cytochalasin D treatment on ES cells significantly decreased the translocation time ($P << 10^{-4}$, $n > 200$ cells for each dataset, due to experimental variability, there is also a significant interaction effect for experiment number, $P << 10^{-4}$). *Image and caption from Hodgson et al. (2017) [1].*

indicates that there is no influence of viscoelastic response on our measurements (Figure 2.11 (C)).

We next treated ESCs with Cytochalasin D to inhibit actin polymerisation as an assessment of our ability to phenotype cells based on translocation time. We hypothesised that the disruption of the actin filaments within the cytoskeleton [78] would lead to increased deformability, detectable though a decrease in the time taken for a treated cell to translocate the constriction channel. We performed this experiment by splitting a sample of cells in two, then applying the Cytochalasin D treatment to one of the halves. This process was repeated with four samples, finding that whilst there was a high degree of variability over the days, the translocation time was significantly shorter post-treatment (ANOVA: $P << 10^{-4}$, $n > 200$ cells for each dataset, experiment number interaction effect $P << 10^{-4}$. Figure 2.11D). The interaction effect signals that whilst there is a significant effect on translocation time from treatment, the effect is inconsistent between samples. We thus showed that this device can be used for high-throughput mechanical phenotyping.

To assess the effect of strain on the cells, the constriction channels were sized so the channels compressed the cytoplasm without directly compressing the nuclei. To do so we set the constriction channel width to 12μm, larger than the median diameter of the nucleus (11.6 ± 0.2 μm) and smaller than the median cell size ($14.3\pm0.2\mu$m). This ensured that we collected data, at least for some of the cells, corresponding to the effect a compressed cytoplasm has on a nucleus, and not just the direct effect of the channel walls on the nucleus. For cell nuclei larger than the median value (close to or larger than 12μm), the primary compression on the nucleus was directly from the channel walls. For smaller nuclei, the stress was a result of an extension in the cytoplasm. Figure 2.12 (A) depicts this effect, as a decrease in nuclear size is accompanied by a lower direct impact from the channel wall. For small cells, the elongation of the cytoplasm from the stress of the channel walls was propagated to the nucleus via the cytoskeleton. The small nuclei therefore experienced a primarily uniaxial strain as the cytoplasm extended along the channel axis. Large nuclei primarily experienced biaxial strain as the walls also compressed the nucleus across the channel axis.

Using the analysis GUI, we were able to distinguish the effects of compression on the cytoplasm and the nucleus. For the reasons discussed above, we split the sample into two subpopulations based on nuclear size. One sample contained cells with nuclei smaller than the median, the other having nuclei larger. With these samples, we calculated the strain for each group which is shown in Figure 2.12 (B) and 2.12 (C). As we would expect from the effect of direct compression leading to a biaxial strain on larger nuclei, transverse cytoplasmic (-0.021 ± 0.008) and nuclear (-0.06 ± 0.01) strain were negative. Both the

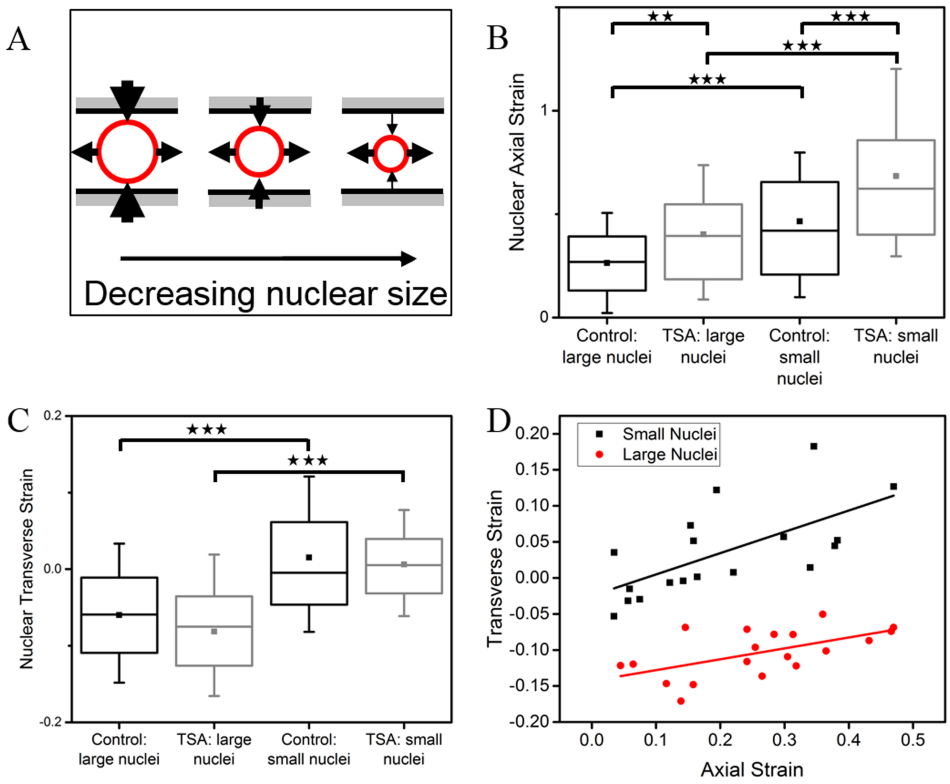

Figure 2.12: **Nuclear mechanics of ES cells**
(A) Diagram of forces on the nucleus in response to confinement of cells in the channel. Large cells experience biaxial forces in the form of a direct compression from the walls of the channel in the transverse direction, and a pulling force from the cytoskeleton in the axial direction. As the nuclear size decreases, the transverse compression decreases, and nuclei experience an increasingly uniaxial force. (B, C) Quantification of nuclear deformability in the (B) axial and (C) transverse direction for control and TSA-treated cells (n = 159 treated, n = 117 control). Cells with nuclei larger than the median (n = 81) experienced a smaller axial and transverse nuclear strain than those that are smaller than the median (n = 78). The transverse strain for small nuclei is close to zero. A positive axial strain signifies an increase in length of the nuclei along the channel during compression, while a positive transverse strain corresponds to an increase perpendicular to the channel length. The nuclei of cells treated with TSA are more deformable, as evidenced by an increase in the magnitude of the axial strains, while the transverse strains are not significantly different. (D) Axial and transverse strain of control ES cell with nuclei smaller than the median nuclear diameter; only axial strains smaller than 0.5 have been plotted, as the strain relationship is valid only for small strains. Two lines of best-fit have been plotted, one for cells with nucleus smaller than the median, and for cells with nucleus larger than the median, illustrating the effect of the channel walls described in (A). Each line has a positive linear relationship between transverse and axial strain (gradient of 0.30 ± 0.09 for cells with small nuclei and 0.15 ± 0.05 for cells with large nuclei). Both samples therefore possess a negative Poisson's ratio, suggesting that these cells are auxetic, with the effect being damped in the large cell subset. *Image and caption from Hodgson et al. (2017) [1].*

cytoplasm (0.24±0.02) and the nucleus (0.26±0.03) expanded in the axial direction during compression.

For cells with nuclei smaller than the median, we saw a significantly larger axial strain ($P < 1x10^{-4}$) with a cellular and nuclear axial strain of (0.38±0.04) and (0.46±0.04) respectively. In contrast to the large nuclei population, we found the small nuclei expressed a positive, yet very close to zero, transverse strain (0.02±0.02). This indicates that within this sample in these conditions, some of the nuclei may be auxetic as reported by Pagliara *et al.* (2014). As is discussed in section 1.1.1, culturing in Serum/LIF, as we have here, maintains cells which possess transcriptional landscapes of both naive and primed cells. Pagliara *et al.* performed their analysis on cells which were in the naive state, which is controllable using the 2i/LIF, serum free, culture protocol.

We further investigated the observation for small nuclei by comparing the relationship between axial and transverse strain for those cells, shown in Figure 2.12 (D). Poission's ratio is a method of quantifying a materials characteristics in terms of its response to stress. The ratio is between axial and transverse strain where Poission's ratio

$$\nu = -\frac{d\varepsilon_{trans}}{d\varepsilon_{axial}} \tag{2.4}$$

in which $d\varepsilon_{trans}$ and $d\varepsilon_{axial}$ are the changes in transverse and axial strains respectively for small strains. Hence we performed this analysis with cells of axial strain smaller than 0.5. We then approximated the Poisson ratio by fitting the nuclear transverse strain versus nuclear axial strain data to a linear function. In addition to this, we divided the sample into cells which had nuclei larger than the median value or smaller than the median value. This allowed us to analyse the effect of the channel wall on the strain in the resulting analysis. We found that the large nuclei cells had a line-fit gradient of 0.15±0.05 while the smaller cell nuclei exhibited the greater Poisson's ratio of 0.30±0.09 (Figure 2.12 (D)). This confirms the result found in Pagliara *et al.* (2014), which stated that ESCs exhibit auxeticity for a period after the withdrawal of inhibition factors. In contrast to that paper, we expected to see a greater level of heterogeneity given the use of Serum/LIF conditions. We thus displayed an improved method for approximations of Poisson's ratio in cell nuclei.

Treatment with TSA has the effect of decondensing chromatin and softening the nucleus [67]. We investigated the response of ESCs treated with TSA to compression in terms of their strain as previously. We hypothesised that the decondensing effect and change in size would exacerbate the deformations observed in the untreated cells. We thus aimed to identify if the decondensing of chromantin, which Chalut (2012) and Krause (2013) identified increased

nuclear deformability, leads to an increase in the magnitude of axial strain for small nuclei detectable by our device.

Our first observation was that the TSA treatment led to a small increase in the median nuclear size before compression (11.8 ± 0.2 μm). In addition, we identified the axial strain to be significantly increased ($P < 0.001$) in TSA treated cells against untreated but for cells with nuclei smaller than the median, we found little effect on the mean transverse strain (0.006 ± 0.006). The axial strain, however increased significantly to 0.68 ± 0.04 ($P < 0.001$). The increase observed in the axial strain in TSA treated cells compared to untreated cells, confirms the previous observations with improved throughput.

In considering which device to perform our investigations with as previously discussed, the single height device has the advantage of having no shift in focal plane on entering the constriction channels. This enabled us to employ high resolution microscopy to probe the effect of confinement on cellular organisation, an area not extensively studied. As an exercise to demonstrate the potential of the single height design, we imaged ESCs stably transfected with Lifeact-tagRFP to observe the effect of compression on the actin cortex. Christophe Verstreken transfected cells with a Lifeact-tagRFP plasmid. Lifeact is a commercially available protein that binds to actin, and so this Lifeact-tagRFP plasmid is a fluorescent marker of F-actin (Figure 2.13).

To obtain precise control of the flow rate and thus the position of cells within the chip, we used a MFCS-4C pressure pump controlled by the MAESFLO control software (Fluigent, France). We were able to pause the cell both outside and inside of the constriction channel which could be imaged with a spinning disk confocal microscope (Figure 2.13). Using these images, we performed a three-dimensional reconstruction of the cellular actin cortex to display the actin cytoskeleton surrounding the cell in high resolution. We then converted the images into a two-dimensional heatmap for Lifeact signal intensity along the cortex. This was performed over the whole cell both before and during compression, which highlighted this as a potential technique for studies investigating intracellular structural responses to compression in single cells.

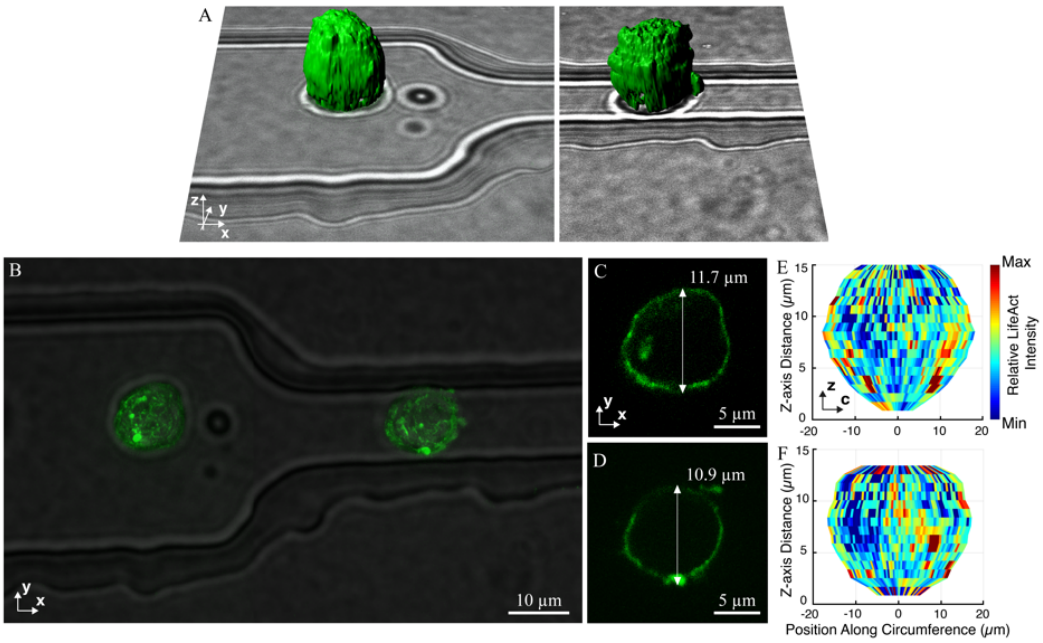

Figure 2.13: **3D reconstruction of ES cells in confinement**
The microfluidic device can be used for confocal microscopy at high numerical aperture of cells containing biological markers to study the intracellular changes that take place in response to confinement. To demonstrate the image quality and level of positional control over the cells within the chip, as well as the possibilities for further analysis, we imaged cells that were transfected with the actin-marker Lifeact within the microfluidic device before and during compression. (A) Composite of two images showing three-dimensional reconstruction of the actin cytoskeleton (green) of a cell before (left) and inside (right) the channel overlaid on the corresponding bright-field images. (B) Maximum projection of the image from the actin network. A slice in the xy-plane through the middle of the cell (C) before and (D) inside the channel. (E, F) Two-dimensional projection of the Lifeact intensity in the cortex of the cell (E) before and (F) inside the channel, with the circumference of the cortex along the horizontal direction. *Image created by Christophe Verstreken and caption from Hodgson et al. (2017) [1].*

2.5 Conclusions

The final device developed and used in our experiments has been shown to be capable of mechanically phenotyping ESCs through uniaxial compression. As per our aims, the PDMS chip is more easily produced than previous versions [6] and may be used for biological experiments by those inexperienced in microfluidics. The writing of a MATLAB GUI has enabled a more time efficient and user friendly method for quantitatively analysing the images obtained using our device. By using the thresholding methods included in the GUI, a user can visually assess the boundaries located and depicted by the code. In addition to this, the user has instant feedback on the axial and transverse dimensions of the selected cells, used to assess the strain induced by the compression.

We have demonstrated that the single height device is able to identify both nuclear and cellular deformations of ESCs treated with SYTO13. In particular, we have observed that nuclei smaller than the channel width display a negative Poisson ratio in response to a uniaxial force so are thus auxetic. This supports the findings of Pagliara *et al* (2014) in which transition state ESCs (cells 24 hours after removal of 2i) were found to be auxetic. In the Serum/LIF culture system, cells are more heterogeneous in their expression of naive, transition and primed factors so some cells may exhibit physical properties of the transition ESC.

Using Cytochalasin D, we have demonstrated the devices ability to identify alterations to the mechanical phenotype of ESCs. This treatment makes an ESC more deformable due to a lack of polymerised actin filaments. This was shown to reduce the time taken for cells to translocate through the constriction channels. The phenotyping capabilities of our device were further exemplified through TSA treatment. TSA causes a decondensation of chromatin, making the nucleus more deformable. We identified that this increase in deformability causes an increased strain response from uniaxial compression compared with untreated cells. We furthermore demonstrated the potential of the device for high resolution microscopy by using fluorescent markers to showcase the ability of the device to identify intracellular structural changes induced by constriction.

The methodology and device presented here provides a further tool for our investigations into the mechanical phenotypes of ESCs, either with high resolution or improved throughput. ESCs undergo mechanical alterations synchronously with their exit from pluripotency and lineage commitment. A complete understanding of both the chemical and mechanical phenotypes at key stages of development is vital to progress our knowledge of pluripotency. The link between mechanical and biological changes are not limited to the ESC, but other cells, such as oncogenic cell types as well [67]. This device could be used to investigate the mechanical properties of these cells, which are strongly influenced by their mechanical

environment. Furthermore, the impact of culture medium conditions on a cell's mechanical response to stress can be probed.

Chapter 3

A Novel Microfluidic Culture Platform to Observe the Exit from Pluripotency

As discussed in the previous chapters, the transition of ESCs from naive pluripotency to lineage commitment is an important developmental process that is currently not well understood. Novel microfluidic technologies could provide an inroads to advance our understanding of the biological mechanisms. The development of a microfluidic device for the task, presented in this Chapter, represents one of the major achievements of this PhD project. This emerged from a problem faced in the current research of this project's main collaborators, Professor Austin Smith and Dr Carla Mulas.

In this chapter, I first expand on the discussion provided in Chapter 1.1 to present the aims and motivation of the microfluidic device. Methods specific to this device are included, although underpinned by the principles laid out in Section 1.2. The most current device at time of writing is the result of many rounds of testing and design; an outline of its development is provided, while the main discussion focuses on the most recent iteration. The section is completed by a plan for further developments of the device along with the new avenues for ESC research they provide.

3.1 Motivation and Requirements

As introduced in Chapter 1.1, the path taken by ESCs from their naive, ground state of pluripotency to being primed for lineage commitment is complex, this section will highlight why this process requires further characterisation. We aimed with this project to combine cell encapsulation, microfluidics and live imaging to monitor the state of individual cells in real time. The specific aim of the devices presented here is to track agarose encapsulated cells on chip with the ability to recover them at any interval for functional and biochemical analyses.

3.1.1 ESC exit naive pluripotency asynchronously following 2i withdrawal

In their naive state, ESCs are capable of self-renewal and have the potential to differentiate into any somatic tissue. The process by which they lose this ability and become committed to a certain lineage is not well understood. Elucidation of this process is of fundamental biological interest and potentially pivotal in our efforts to harnessing stem cells for regenerative medicine and wider biological research.

Naive ESCs can be maintained in culture using inhibitor molecules (2i) to block differentiation and are said to be in a 'ground state' [18] of pluripotency. When cultured in 2i, the naive ESC population is relatively homogeneous [16]. Upon withdrawal of the inhibitors from the culture media, ESCs will begin to exit the stem cell state, initially down-regulating naive transcription factors. As discussed in Section 1.1, the phases of development between naive pluripotency and lineage commitment are characterised by a change in the expression of specific transcription factors. In the absence of inhibitors, the ESC population begins to downregulate naive pluripotency factors as it leaves the stem cell state. This progression to lineage commitment occurs over approximately 40 hours, with some cells losing the ability to self-renew as soon as 20 hours [79]. It is possible to observe loss of ability to self-renew via the reporter Rex1, expression of which is extinguished on exit from the ground state. Using Rex1:GFPd2 cells, in which green fluorescent protein is expressed from the Rex1 (Zfp42) locus, we are able to visualise the downregulation of Rex1 and thus the exit from naive pluripotency. Using their fluorescent output with flow cytometry 24 hours after the removal of 2i, cells were sorted into Rex1:GFPd2^{HI} and Rex1:GFPd2^{LO} populations which feature high and low levels of Rex1 respectively, then returned to 2i conditions. As discussed in Section 1.1, only naive ESCs capable of self-renewal are able to form colonies in 2i media. It was found that the Rex1:GFPd2^{HI} cells displayed unaltered colony forming efficiency whilst the Rex1:GFPd2^{LO} population had lost the capacity for self-renewal [80]. Considering the homogeneous nature of 2i cultured cells, this result implies that the exit from self-renewal is

asynchronous across cells within a given population. Furthermore, it suggests the possibility that the exit may occur relatively acutely; the resolution of current population-based assays, however, is not appropriate to resolve these sub-population dynamics.

3.1.2 Objectives of the Microfludic Device

The asynchronous nature of the exit of pluripotency renders population based assays, such as the use of flow cytometry, unsuitable to reveal the dynamics of the transition. Asynchronicity implies each cell develops on its own timescale, which is referred to as its developmental time. To gain new insight we aim to normalise this developmental time between individual cells so as to take into account the co-existence of cell stages at all time points during the exit, which conventional population based assays are unable to do.

Achieving the resolution required for this approach, necessitated the development of new technology to address the limitations of the traditional approaches. Traditionally we are able to observe single cells within a population using time-lapse microscopy. This could be used, for example, with the Rex1:GFPd2 cells to observe the downregulation of Rex1 in a number of individual cells within a population. This technique is however unsuitable for our aim to characterise the release from the ground state given that the observed cells cannot be linked to functional or molecular data [81].

As an alternative to single cell observation combined with population based functional or molecular data, we can perform single cell transcriptomics to analyse expression levels in single cells, however we rely on pseudotime ordering in the traditional approach. The process of pseudotime ordering is used for retrospective inference of cell state without functional validation[82]. This technique plots a pseudo-temporal path from single cell RNA-seq data to order cells of a heterogeneous population as the transcriptional network of the cells within progress. With traditional methods we are thus left with a choice: a known cell history through continuous imaging with non-specific functional or molecular analysis; or single cell analysis with imperfect knowledge of the history of the analysed cell.

Circumventing these issues is the first objective in developing our microfluidic device, facilitating the acquisition of single cell history combined with single cell transcriptional or functional analysis. In doing so, we primarily aim to profile the transition from naive pluripotency to lineage commitment. We plan to establish normalised developmental time to assess the transcriptional landscape at points at well-defined intervals around the loss of self-renewal. Such resolution requires single cell history with single cell molecular data.

We will achieve this by establishing a developmental time from the expression of Rex1 using Rex1:GFPd2 cells. Downregulation of Rex1 expression occurs within cells at a range of times following the removal of 2i, given the asynchronous nature of the stem

cell transition. We aim to observe individual cells as they downregulate Rex1 within our microfluidic platform, independently of other cells in the population. This is the basis of our developmental time normalisation: comparing cells based on their Rex1 expression, rather than time after 2i removal. This will enable us to build a full transcriptional profile of cells at a range of Rex1 expression levels, which can include time points beyond Rex1 extinction.

3.1.3 Technical Requirement for Microfluidics

The development of the protocol for single cell observation and analysis has been divided into two parts; the development of the microfluidic culture platform and the development of the ESC encapsulation process. Timo Kohler and Dr Carla Mulas have been responsible for developing the encapsulation of ESCs into 80μm beads, capable of sustaining ESCs with and without 2i conditions. Using a microfluidic platform developed by the Hollfelder group (Department of Biochemistry, Cambridge), the beads produced have been used in all of the following designs presented which aim to manipulate the flow and position of beads.

This project has centred on the development of a microfluidic platform which will form the basis of our investigations into the transition between naive and primed ESCs. The overall goals of the project translate into specific design requirements for the device: First, we require precise control over individual beads to allow for single cell/colony observations with the ability to then analyse the observed cells at a functional or molecular level. The beads must be held stationary for imaging purposes and the removal of a bead for analysis must not impact on the culture or imaging of the remaining cells.

Beyond the technical requirements of bead manipulation, the culture environment of ESCs must be carefully controlled on-chip while the imaging is performed. This may require cells to be cultured on-chip while the chip is positioned on a microscope stage for up to 72 hours.

Second, for the microfluidic platform to be of use to a stem cell researcher, we must be able to observe multiple beads, and therefore cells, within a single experiment. Given the imaging time could exceed 72 hours, it would not be practical to observe only one cell in this time.

Finally, the design of the device should take into account the technical challenges of setting up a microfluidic experiment while simultaneously preparing cells. Timing is often difficult when working with live cells, thus a device which requires minimal attention and set-up will be of benefit to the researcher.

3.2 Developing the Chip

This section presents a selection of the considerations and achievements along the design process of developing the device and its application for live cell imaging in Section 3.2.4. Each round of development included the drafting of new ideas to both overcome technical issues in the previous version and to anticipate potential problems in the following version. Each round, the designs deemed most promising were selected to fill the available space on an emulsion film photomask, with a total of 37 designs printed onto masks. Not all of these designs will be presented here, as many were not used to produce moulds; some designs were rendered obsolete from lessons learned during testing and sometimes unforeseen issues would arise requiring a new set of designs on a new mask.

3.2.1 Generation One: Trapping Cells Without Beads

The first stage in the development process consisted of a characterisation of the ESCs' compatibility with a microfluidic environment. Cells were maintained within a repurposed construction channel device, as presented in Chapter 2. This device, as shown in Fig 2.5, contained the largest internal volume of the readily available chips and we anticipated that with a low initial flow, cells would rest against the inlet of the constriction regions.

We performed a simple trial in which we injected a suspension of Rex1-GFP ESCs into the device and incubating for 24 hours. We found that cells could not survive in the untreated internal environment of the microfluidic device and hypothesised that a coating layer within the chip may be required, similar to the gelatin coating used on tissue culture plastic when culturing ESCs. The chip was thus bonded to either a superfrost^{+} or a poly-d-lysine coated slide, in an effort to ascertain the superior slide coating method, and filled with laminin immediately after bonding and left overnight. The chip was filled with 10^5 cells/ml in 2i media to inhibit differentiation, and cultured at 37^{o}C with 7% CO_2. From this round of investigation, we observed a large amount of cell death in both environments, although some cells survived and formed colonies within the superfrost^{+} variation, shown in Figure 3.1. Interestingly, we visually identified a gradient of cell death leading to the centre of the chip indicating a higher chance of survival at the inlets. We believed this to be due to a greater volume of media being held at the inlets which was better able to sustain the cells than the small volume of media at the chips centre. In an attempt to remove the surviving cells, we used a Fluigent pressure pump connected to the chip inlets by FEP tubing to flow the cells into the outlet. We found, however, that the cells were too strongly adhered to the chips such that they could not be removed without applying enough pressure to physically damage the cells due to a high shear stress. We learnt from these initial experiments that cells were unable

to survive in suspension within the chip, but also could not be removed if they survived by adhering to a coating. Furthermore, the pattern of cell death indicated a requirement for a constant supply of fresh media. This provided the initial design parameters for the first specifically designed device for the task: we required a constant supply of media combined with a surface for the cells to adhere to which can be easily removed from the chip with low pressure.

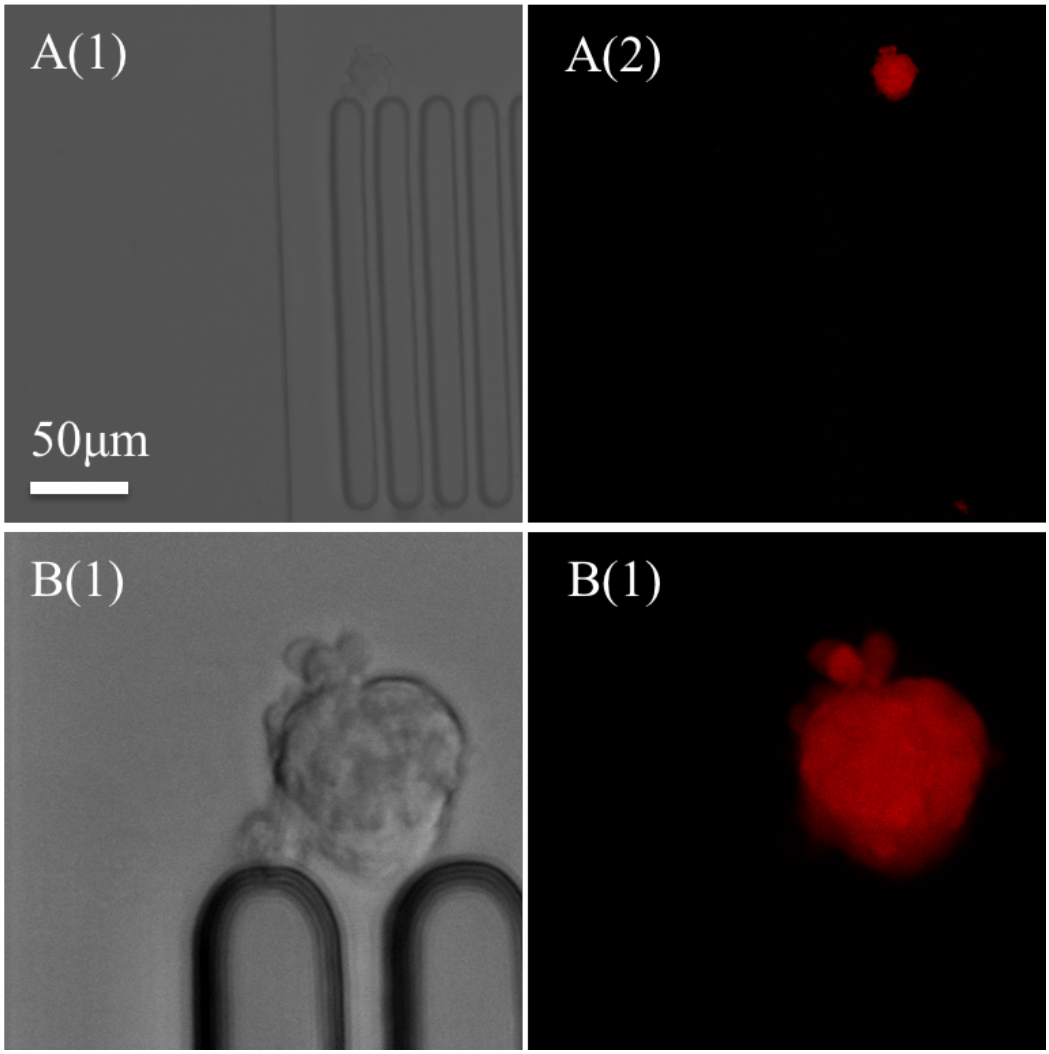

Figure 3.1: **Small Colonies after 24 hours in 2i**
A(1) and A(2): 20x objective image of ESCs cultured for 24 hours in a constriction channel microfluidic chip (chip as detailed in Chapter 2). (2) is the flourescence image of Rex1:GFPd2 cell colony. (B): images of the same colony taken with a 50x objective. The cells in this figure adhered to the chip interior and could not be removed without damage.

3.2.2 Generation Two: Trapping Beads Without Valves

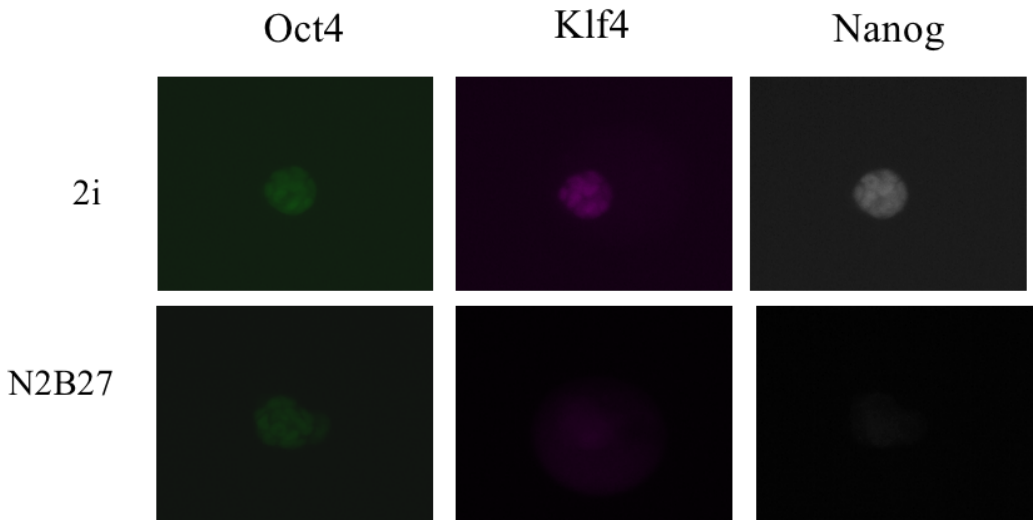

Figure 3.2: **ESC Downregulation of Pluripotency Markers Within Beads Over 24 hours** This figure shows a comparison between expression levels of certain transcription factors between cells with and without 2i. Klf4 and Nanog are naive transcription factors which will not be expressed in cells 24 hours after the removal of 2i. Oct4 is a marker for undifferentiated cells which will continue to be expressed into the primed phase of pluripotency.

To overcome the issue of ESCs adhering to the microfluidic chip, we encapsulated cells within agarose-fibrin droplets with finely tuned dimensions. Cells can be suspended in the liquid agarose-fibrin, such that beads are produced by the device shown in Figure 1.4 encapsulating single or multiple cells. The beads provide a matrix for ESCs to interact with whilst not themselves adhering to the chip. As shown in Figure 3.2, the beads are able to maintain pluripotency using 2i conditions over at least 24 hours and also to support the downregulation of pluripotency in the absence of 2i. It was at this stage that the project to produce a lab-on-a-chip culture platform for investigating the exit from pluripotency in ESCs split into two components. One one hand, I was responsible for the development of technology to manipulate the cells, encapsulated in beads, satisfying the requirements detailed in Section 3.1.3. On the other hand, Timo Kohler and Dr Carla Mulas were tasked with developing an agarose and fibrin based compound capable of supporting ESC differentiation along all lineages.

All of the following devices are designed to control the position and facilitate imaging of the ESCs encapsulated within 80μm beads. The first of such is depicted in Figure 3.3 in which beads are injected into Inlet 1 and flowed across the chip to Outlet 1. The user applies a cross flow from Inlet 4 when an isolated bead containing a single cell crosses the

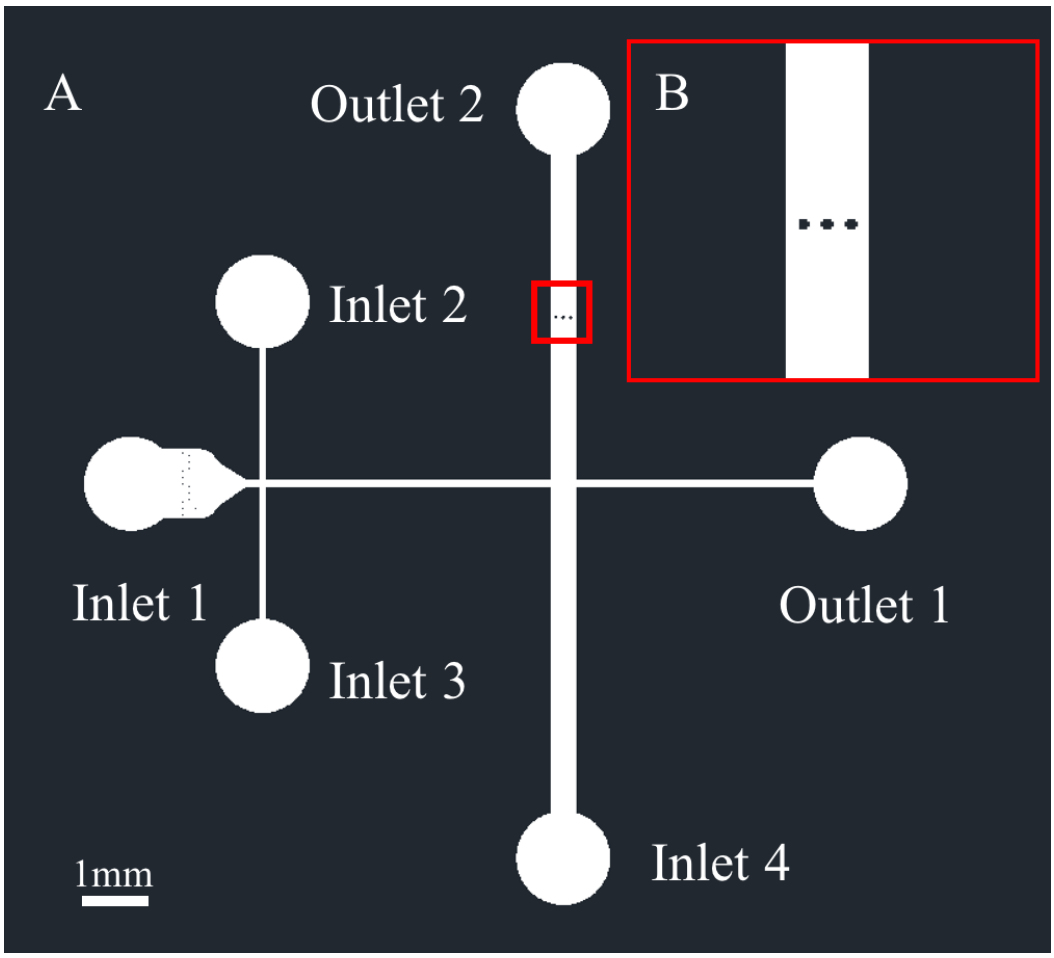

Figure 3.3: **Culture Chip to Direct the Flow of Beads**
This early version of the culture chip is designed to store a bead under constant media perfusion against the columns displayed in inset B. Using syringe pumps connected to each inlet, beads enter the chip from inlet 1. The design intended to direct a single bead into the traps using a carefully timed cross flow from inlet 4. Inlet 2 and 3 were to provide various media conditions. This design highlighted the necessity for valves to direct the flow.

intersection. This moves the bead in the direction of Outlet 2 where it becomes trapped on the columns (Figure 3.3 B). The aim was for media to continually flow around the bead from Inlet 4 whilst imaging until a reverse flow from Outlet 2 could move the bead from the chip.

Applying this device uncovered the difficulties of controlling fluid flow within the chip when using a combination of multiple inlet flows. With flow from a single layer alone, it was extremely challenging to direct a single bead in a new direction without the interference of other beads. This was a particular concern as more than one bead must be controlled and maintained on the device for it to be useful in biological applications (so as to achieve the required statistical power); such difficulty in coordinating flows to trap a single bead made up-scaling unrealistic.

From experiments with this design, we learned that controlling flow directions by simply combining flows from multiple inputs was very inefficient. Furthermore, consideration was required into how the device could be up-scaled to trap more beads whilst maintaining ease of use.

3.2.3 Generation Three: Quake Valves

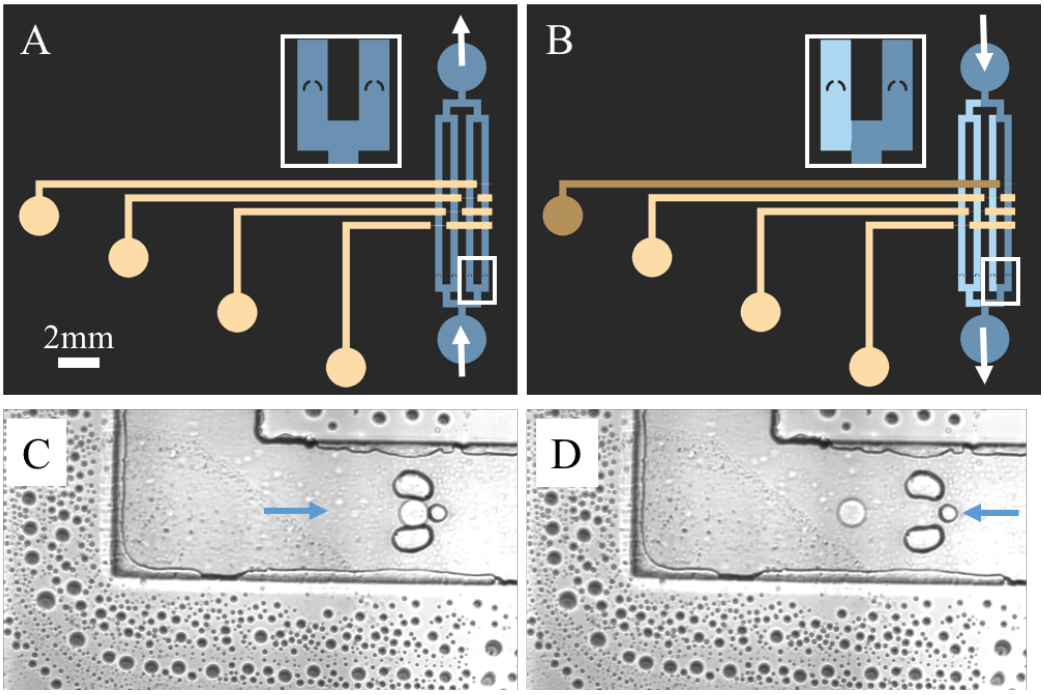

Figure 3.4: **First Generation of Quake Valve Chips**
Blue tones represent flow layer, yellow tones represent valve layer. (A): No valves actuated with beads in media flowing from the inlet across the traps (see inset) to the outlet. (B): Actuation of a single valve, represented by the darker tone, and reversing the media flow causes a single bead to be ejected from the chip. (C): Image of a bead caught in trap with media flow in the direction of the arrow. (D): Actuating a valve and reversing the flow (blue arrow) releases the corresponding bead from the chip.

To better direct the flow of beads, we next designed chips with microfluidic valves. The theory of these 'Quake valves' is described in Section 1.2. The principle relies on two layers of channels separated by a thin PDMS membrane. The valve layer is aligned over the top of the membrane on the flow layer. Pressure applied to the valve layer causes the membrane to expand into the flow channels below, closing them. In using this method, we were able to alter the flow path using a single input, removing some of the difficulties caused by the multiple flow inlets of the previous generation of chip. In addition to this, a particularly powerful feature of the Quake valve is the potential for multiplexing. An example of Quake valves is shown in Figure 3.4 which depicts an early version of a 4-trap chip with single inlet and outlet. This design possesses numerous advantages over the previous generation. Primarily, there is no complicated manipulation of flows required to direct the beads into the traps and secondly, this design incorporates multiple traps. The symmetric design means

each bead has approximately a 50% chance of travelling left or right as it leaves the inlet (shown as the white arrow going into the chip on Figure 3.4 A). This splitting occurs again for each of the channels therefore close to one quarter of the beads will travel down each of the four bead trap channels. The inset of Figure 3.4 A displays the cup shaped traps in two of the four channels. This offers a second advantage over the previous version; excess beads flow around the trapped beads. Once all beads have entered and all but four have exited, a constant flow of media continues to be delivered to the trapped cells. To remove a bead, the corresponding valve is actuated by applying pressure to the valve channel. This is shown as a dark yellow valve in Figure 3.4 B, whilst the unactuated valves remain light yellow. For the valve to impact on the flow channel below, the width of the valve channel must be similar to the width of the flow channel [32] with an appropriate pressure. This means the valve channels may cross the flow channels without effect if the width of the valve channels in this area is sufficiently low. This bypassing technique allows a valve to leave certain flow channels open while closing others. In Figure 3.4, actuating a valve closes three of the 4 channels. Combined with a reverse of flow direction, this removes the bead in that channel whilst the others remain stationary in the traps. Panels C and D display images of the bead within the trap then again after the release valve is actuated and flow reversed.

Whilst this design is able to store and release individual beads, specific features of the chip required improvement. Primarily, in an attempt to keep media inlets and outlets to a minimum for simplicity, the outlet for the waste beads and media becomes the inlet for flow when removing a bead which leads to potential problems. Primarily, if the same tubing is used to provide the removal flow, beads may flow back into the chip. A possible solution consisted in removing the waste tubing and inserting clean tubing to provide the removal flow. A caveat remained, in that removing and reinserting tubing introduces a significant risk of air bubbles entering the chip. Furthermore, the physical disruption of the system could dislodge the trapped beads. It was concluded from using this device that the bead trapping system and Quake valves had potential to deliver the results we required. However, a clean source of media for the removal flow was required when ejecting the beads.

The following device expanded on the design of Figure 3.4 to include separate inlets for waste flow, reverse flow, bead input, media input and bead output. The aim was to correct issues with the previous design, while the addition of valves meant the flow difficulties of our very first chip were not repeated. As shown in Figure 3.5, beads are loaded into the chip at inlet 1 while a simultaneous cross-flow of media from inlet 2 directs the beads to the traps shown in inset A. Using the same principle as the previous chip, releasing a bead requires activation of the corresponding valve (shown in dark yellow of panel B) and flowing media from behind the bead, directing it towards the inlet/outlet. This generation, however, uses

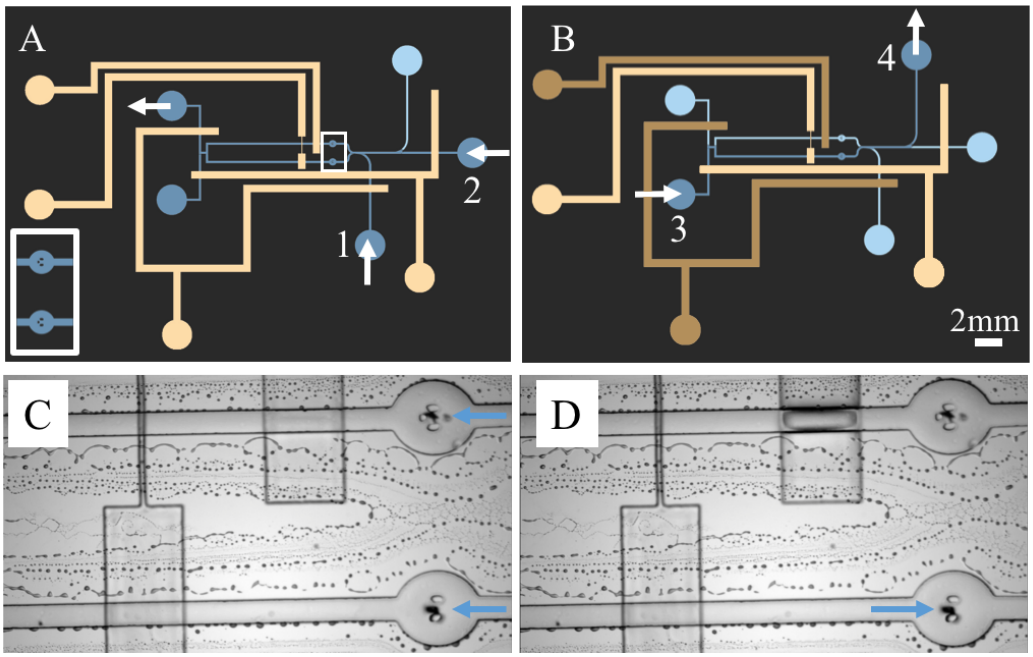

Figure 3.5: **Quake Valve Chip with Extra Inputs**
Blue tones represent flow layer, yellow tones represent valve layer. Access holes are punched in the large circular features. (A): No on-chip valves are actuated, beads are injected into input one with a media cross-flow from input 2. At this stage, an off chip valve in-line with input 3 is actuated so no beads may flow into the tubing. Beads become lodged in the bead trap (inset A) with excess exiting the chip further down the channel. (B): To remove a bead, the valves in dark yellow are activated and the flow is reversed through the inlet marked with a white arrow. The bead flows to an outlet to exit the chip. Stopping the flow at inlet 2 forces flow from inlet 3 to outlet 4. (C): Photograph of the traps depicted in (A). (D): Photograph of actuated valve and reversed fluid flow to remove bead from trap.

an inlet to provide the reverse flow which has not been contaminated by discarded beads. This is achieved by using an off chip valve in-line with the tubing entering inlet 3 shown in Figure 3.5 B. Opening this valve and applying pressure flows media into the chip to remove the bead, as shown in panel D, via outlet 4. Whilst this addition to the design succeeded in providing a clean source of media to remove the beads, the number of inlets and outlets led to an increase in problems with air bubbles entering the chip (each tube inserted comes with risk of including air, the fewer the tubes injected, the lower the risk) along with a flow dynamic which was difficult to control even with the addition of valves. To develop on this design required a simplified inlet/outlet system which maintained the improved delivery of the reverse flow.

A solution to difficulties of the reverse flow was developed as part of the ‘8’-shaped chips. Two versions of this are shown in Figure 3.6. In this design, the filling and removing flow

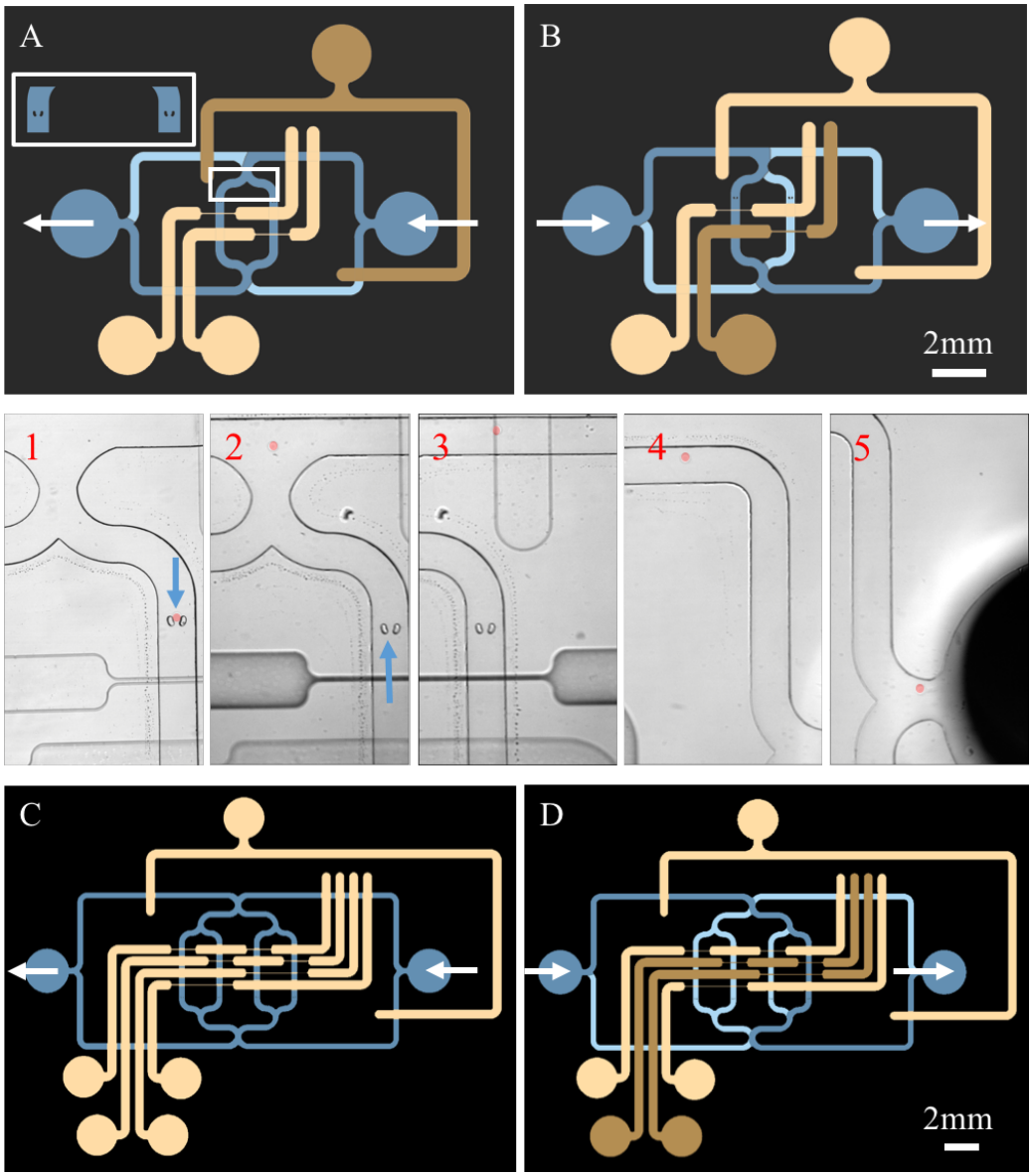

Figure 3.6: **Figure 8 Culture Chip: First and Second Versions**
Blue tones represent flow layer, yellow tones represent valve layer. Access holes are punched in the large circular features. (A): Actuation of dark yellow valve forces media and bead flow across the entrance to the bead traps (inset A), lodging two beads. Excess beads continue and exit the chip. Media is constantly perfused to sustain the cells within the bead. (B): To remove a bead, the appropriate valve (dark yellow) is actuated to reverse the flow of media as experienced by the trapped bead. (Panels 1-5): Sequence of photographs capturing a bead being removed from the chip. (1): Media flows across the bead, holding it in place. (2): The release valve is actuated (which is seen as being darker in the photo) to reverse the flow and eject the bead. (3-5): Photographs following the path of the bead (false coloured in red for clarity) as it exits the chip. (C and D): Schematic of a scaled-up version of (A) and (B) to capture four beads.

originates from the same input. The determining factor to the flow being filling or reversing in nature is the actuation of certain valves. In Figure 3.6 A, the actuated valve (dark yellow) directs the flow from the inlet across the bead traps (shown in inset A and panel 1) to fill them with beads. The discarded beads and waste media continue past trapped beads to the output. To remove the bead, as shown in panel B and the sequence of panels from 2-5 in Figure 3.6, the appropriate valve is actuated to redirect the flow to approach the bead from the back of the trap. Panel C and D depict how the device was scaled-up to capture 4 individual beads.

The operational stability of this design, both in terms of controllable fluid flow and far fewer instances of bubbles than previous generations, highlighted a new issue. The reverse flow would often disturb the beads in traps which should remain in the chip. This is due to an incomplete closure of the flow channel by the compressing valves. As introduced in Section 1.2, the efficacy of a Quake valve in its ability to close a channel has a strong dependence on the cross-sectional geometry of the channel being closed. In summary, a rectangular flow channel will remain open at the corners under valve compression whereas a rounded flow channel will close completely. The flow layer for all of the devices presented up to this point are fabricated with an SU8 photoresist mould and thus have rectangular cross-sections. To improve this design, therefore, the areas of the flow channels to be closed by valves must have a rounded cross-section.

3.2.4 Generation Four: AZ and SU8 Combination Chip

An important development following the implementation of the 'figure of 8' design was the combination of rectangular and semi-circular cross-sections for the flow channel. The rectangular sections are required for the bead traps to maintain their profile while the semi-circular regions are necessary to achieve complete channel closure upon valve actuation. To fabricate these contrasting profiles requires the use of two photoresists, in this instance and shown in Figure 3.7, AZ 40XT and SU8 2100. Upon heating of the AZ and SU8 resists up to 110°C, AZ 40XT re-flows into a rounded cross-section (see Figure 3.10 C). An 8 trap implementation of this technique is given in Figure 3.7 in which the rounded sections are represented by the rectangular areas in line with the narrower flow channels (both shown as blue tones). Photographic images of the rounded flow sections are shown in panel C and D. The rounding can be observed from the gradient of tone on the channels in these images, with the darkest regions representing the thinnest sections. In Figure 3.7 D, the membrane separating the flow channel and valve layer is in contact with the glass base of the chip. Improving on the previous designs, these valves block flow effectively, prohibiting trapped beads intended to remain within the chip from leaving when the reverse flow is applied. A visual guide to the effectiveness of the valve system is displayed in Figure 3.8, in which a purple dye has been used to show the path taken by incoming beads (A) and the media flow when a bead is being removed (B).

In addition to the improvements in valve closure stemming from flow layer refinements, the valve layer is also augmented in this generation by reducing the volume of the valve channels. In previous generations, the valve channels were broad enough to enable channel closure along their total length, except for the narrow areas for flow channel crossing. By making the length of the valves the width of the crossing sections, excluding the broad closing sections, the internal volume is reduced. As the valve channel is filled with water to prepare the chip for an experiment, the lower volume considerably reduces set-up time. It is necessary to fill with water as an empty valve channel will force air though the membrane into the flow channel upon actuation. The gas permeability of the PDMS which enables air to be forced into the flow channels, enables the closed volume of the valve channel to be filled with water, as the air escapes though the PDMS and is replaced by water. To further reduce filling times, the junctions between thin and wide valve sections are gradual as perpendicular angles could also trap pockets of air.

Having established a convenient method for separating, trapping and controlling single beads, the formation of air bubbles within the flow channel still prevented experiments to be completed successfully. We identified a number of potential causes for air to enter the

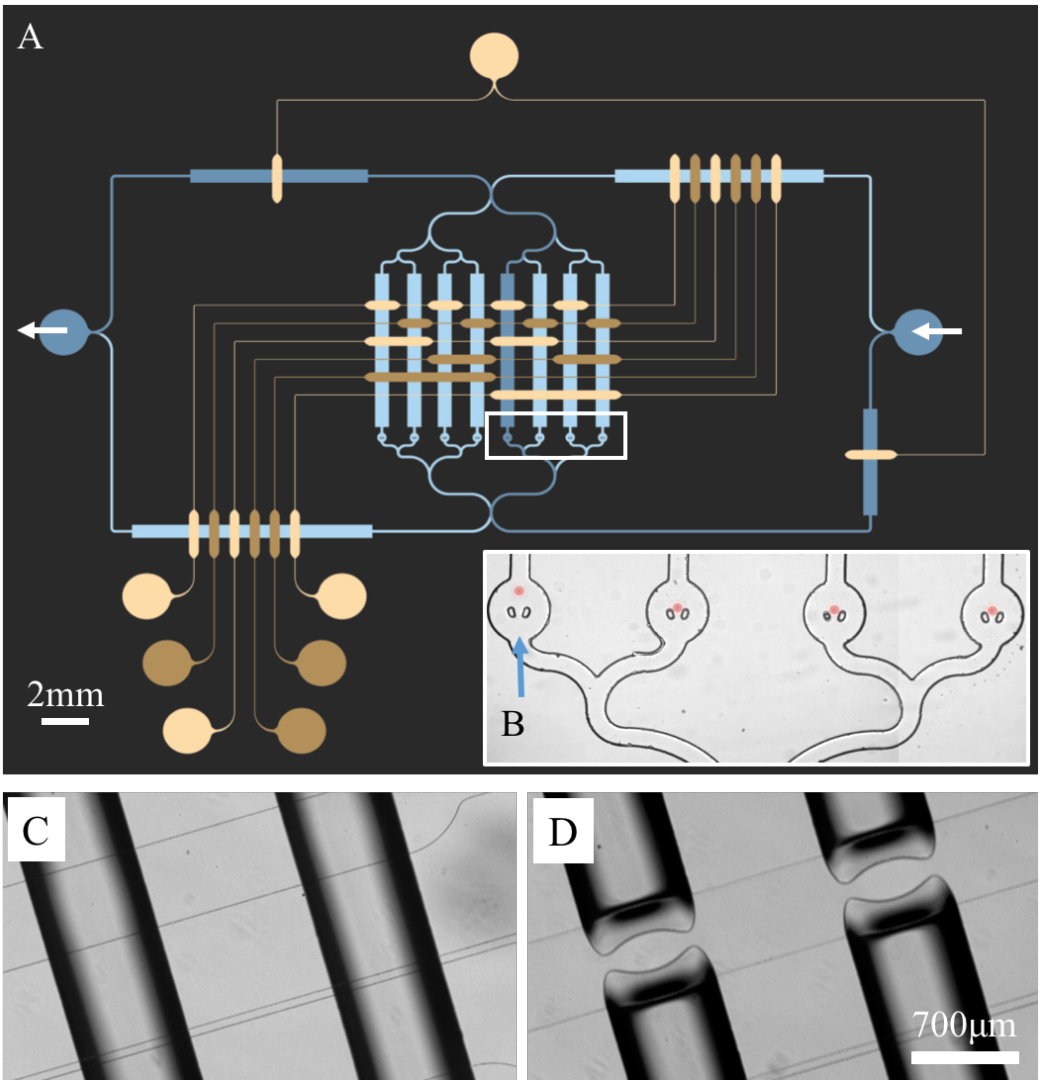

Figure 3.7: **AZ and SU8 Combination Chip**
Blue tones represent flow layer, yellow tones represent valve layer. Access holes are punched in the large circular features. (A): Schematic of an 8 trap chip fabricated from a combination AZ and SU8 mould. The broad rectangular sections of the flow layer (blue) are regions fabricated with AZ protoresist and can thus experience complete closure on valve actuation. The appropriate valves have been actuated (dark yellow) to release the bead shown leaving the trap in (B), where a false colour (red) has been added to the beads for clarity. (C): Unactuated valve (outlined from left to right) overlaying a rounded section of the flow channel (outlined from top to bottom). (D): Pressure applied to the valve layer forces the membrane separating valve layer from flow layer into the flow channel below.

system, discussed in the following section. In this generation of device, however, bubbles arose mainly from our method of filling the chip.

Before filling the devices, when bonding the PDMS to glass, the interior surface becomes hydrophilic making this the ideal moment to fill the device. Filling all channels however, requires the actuation of a valve to guide the flow. Valve actuation whilst the surface is hydrophilic causes the membrane to bond to the glass base, permanently closing the flow channel. Thus, we must wait for the interior to once more become hydrophobic before filling the valves.

The initial protocol to prepare this generation device for experiment was to initially fill the valve channels with water using a pressure source of approximately 0.5 bar more than 30 minutes after bonding. To then fill the flow channels below, a syringe pump was used to fill the bead trap channels one by one. We found using the valves to direct the flow to be very inefficient. Primarily, this 'flushing' approach required large volumes of fluid, generally PBS, to remove the air bubbles. If a small pocket of air remained in a channel after filling, increasing the flow rate could be used as a brute force method of removing it, but there were instances where the force required to remove the air in this fashion became more than the valve membrane could withstand.

As an alternative, we developed a method of filling the flow layer which followed the same principles as filling the valve layer. We mimicked the closed volume of the valves by blocking the flow layer outlet tubing with an off chip valve, then used a pressure source to fill the chip from the inlet with PBS. If the pressure in the valve layer is set to match the pressure filling the flow channels, the air from the channels will escape though the PDMS but not into the already filled valves. This method enabled the user to leave the system under pressure until either the air has left the chip or later without any further effort. Once filled and ready to be used, the next task was to inject the beads into the device.

Whist the concerns regarding air bubbles within the system from the initial filling were overcome with this generation of device, the propensity for air to enter the chip during bead injection remained unacceptably high. The root of the problem lay in having to remove the inlet tube between chip filling and bead injection. After filling the chip with media, the inlet tube was removed to be filled with bead suspension before being reinserted to inject the beads into the chip. During this process, maintaining a volume of media over the inlet hole and at the end of the tubing was effective at providing an air free interface. This method is successful when performed effectively, however the application of it is quite difficult for the user and a small mistake in moving the tubing into the chip can lead to bubbles. We found that when using a full experimental set-up, including heated environment chamber for cell culture with the microscope, set up became increasingly difficult. Experiments with this chip,

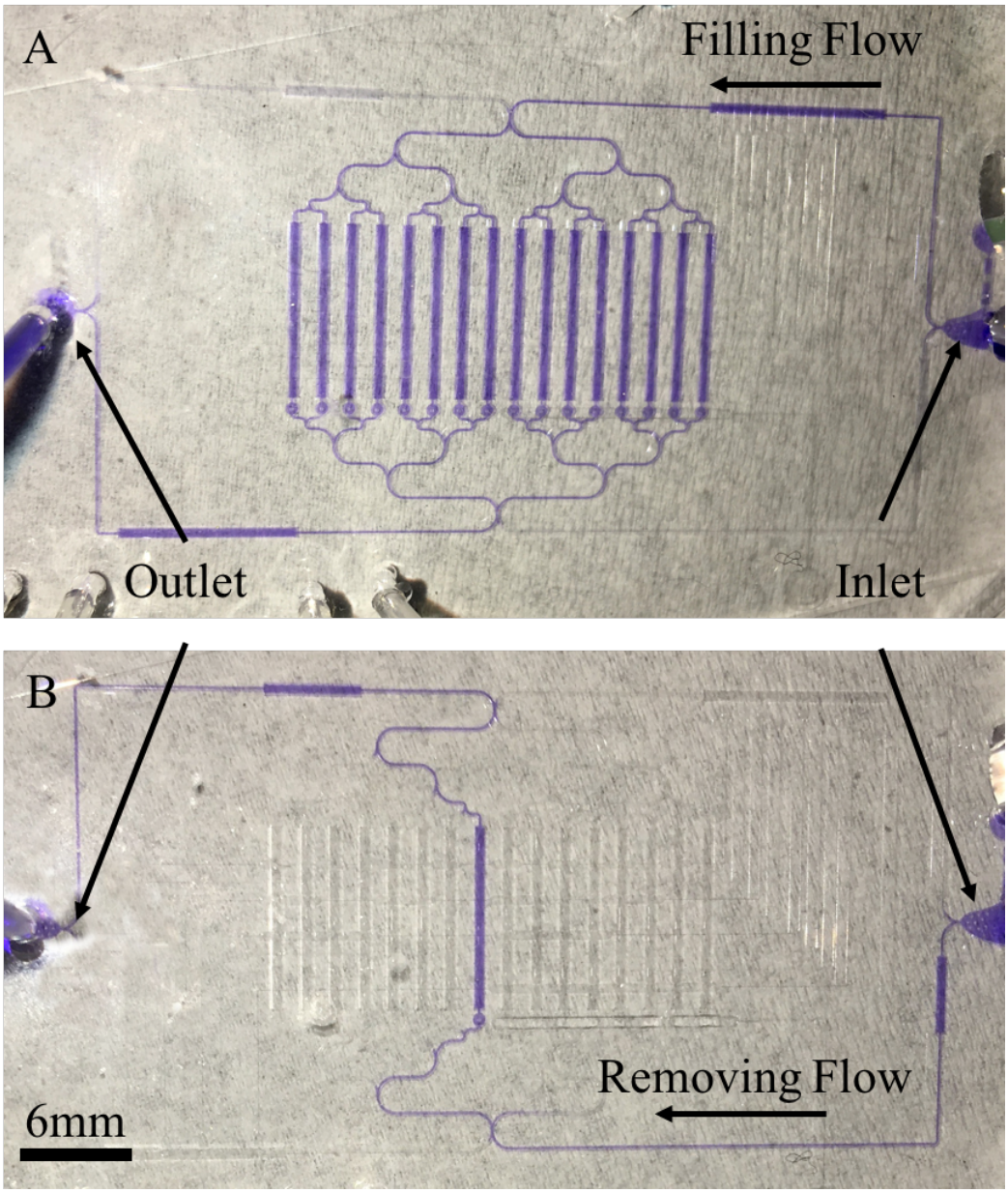

Figure 3.8: **Filling and Removing Flows with Dyes**
These photographs are of a 16 trap chip in which a purple dye has been used in (A) to identify the flow when the filling flow valves have been actuated. B: The valves have been actuate to flow the inlet media, here again dyed purple, across a single trap in its own channel.

particularly when using live cells, elucidated the need to have all tubing in place with the chip contained within the environmental chamber before the beads were injected. A redesign addressing this problem is presented in the following section.

3.3 16 Channel Bead Trapping Device with Secondary On-Chip Culture Section

The sections above describe the stages of development to produce the final device which is presented here, a schematic of which is displayed in Figure 3.9. I introduce the additional features and improvements of this generation, followed by the fabrication methods and the experimental procedure we formulated to observe ESCs exit from naive pluripotency within the device.

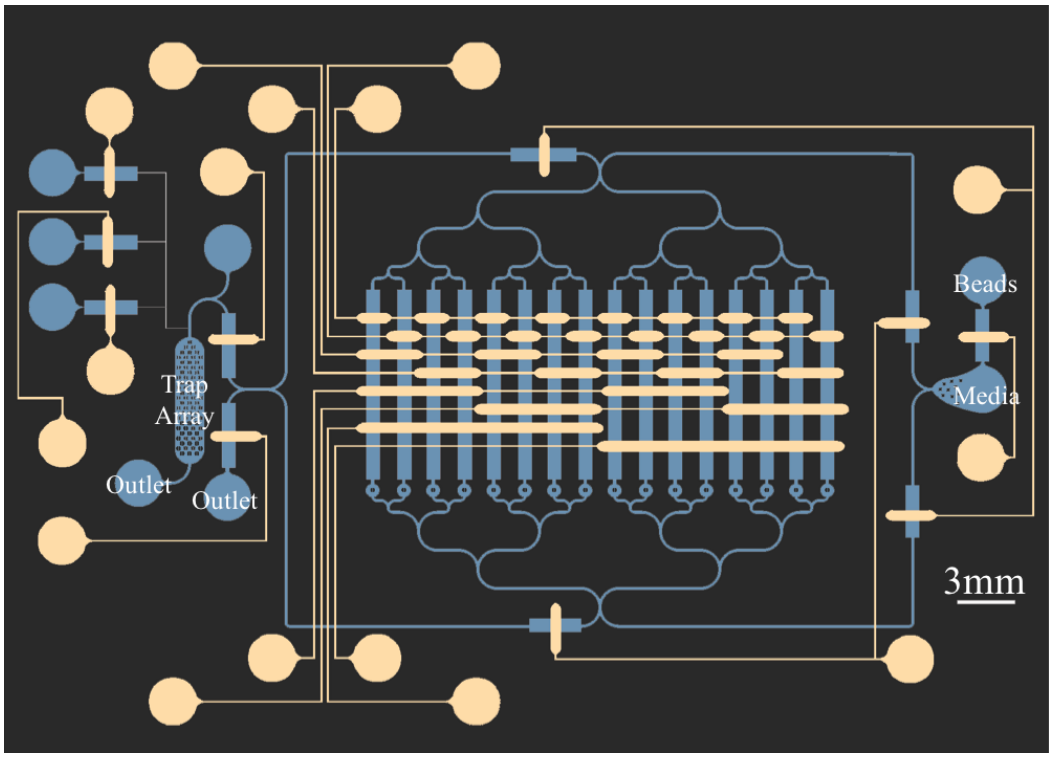

Figure 3.9: **Modular 16 Trap Chip Schematic**
Blue represents flow channels and yellow represents the valves. In this design, the filling and removing flow directing valves are uncoupled from the channel selection valves. There are separate inlets for beads and for media cross-flow. The module at the left of the figure contains an array of traps to which beads can be moved and cultured in different conditions. Further detail is given in Figure 3.11.

3.3.1 Improvements from Previous Designs

This iteration of the '8'-shaped design aims to address a number of issues which arose while using earlier versions. In the preceding design, the user removes and reinserts tubing to inject

beads into the chip. We found that this increases the risk of air bubbles being introduced or forming within the chip. An extra inlet was added in line with the main inlet and separated by a valve to address this. This provides a single inlet for media and a second inlet for beads. Additionally, this enables precise control over bead injection timing and volume due to the dedicated valve separating the inlets.

A further advancement from the previous generation device is the inclusion of the first modular element to be attached to the '8'-shaped structure. The module offers the user the choice between simply ejecting a bead off-chip as with previous designs, or to move the bead into a secondary culture array in which media conditions can be adjusted independently from the main chip. A single bead can be removed from its trap and moved to the culture array shown in Figure 3.10 D and E by actuating the appropriate valves. Using up to 4 dedicated media inlet and valve pairs, the bead stored in the culture array can be subjected to a range of culture protocols, including separate steps and washes while it continues to be imaged on-chip.

A major alteration in this round of design was a consequence of adding a secondary culture array module. This inclusion increases the total area of the device's operational components, thus introducing the need to save space elsewhere. This was achieved by uncoupling the valves which dictate filling or removing flow from the valves that determine which bead trap channel is open. This required two additional valve inlets, but in doing so we were able to double the number of traps whilst occupying slightly less area. This is an important consideration given the desire to upscale these devices to feature many more traps. Furthermore, the decoupling of flow direction and channel selection allows the traps to be selectively filled and ejected (previously a single bead trap channel could only be isolated when the removing flow was engaged.) This development better enables us to remove unwanted beads during the filling procedure and replace them with more desirable alternatives, all without disturbing beads trapped in the other channels.

The final adjustment to this iteration of the device was in the design of the traps. To promote flow through the centre of the trap, and thus have a high trapping efficiency, the original traps were designed to be as unobstructive to the laminar flow profile as possible. This required the traps to occupy as little space as practicably possible. Whilst the trapping efficiency of a well formed trap appeared high, the small size of the traps made them difficult to consistently reproduce from the mould; it was commonplace for at least one trap to be damaged during fabrication. To correct for this, the size of the traps was increased in an effort to improve rigidity and reduce the amount of spoiled devices.

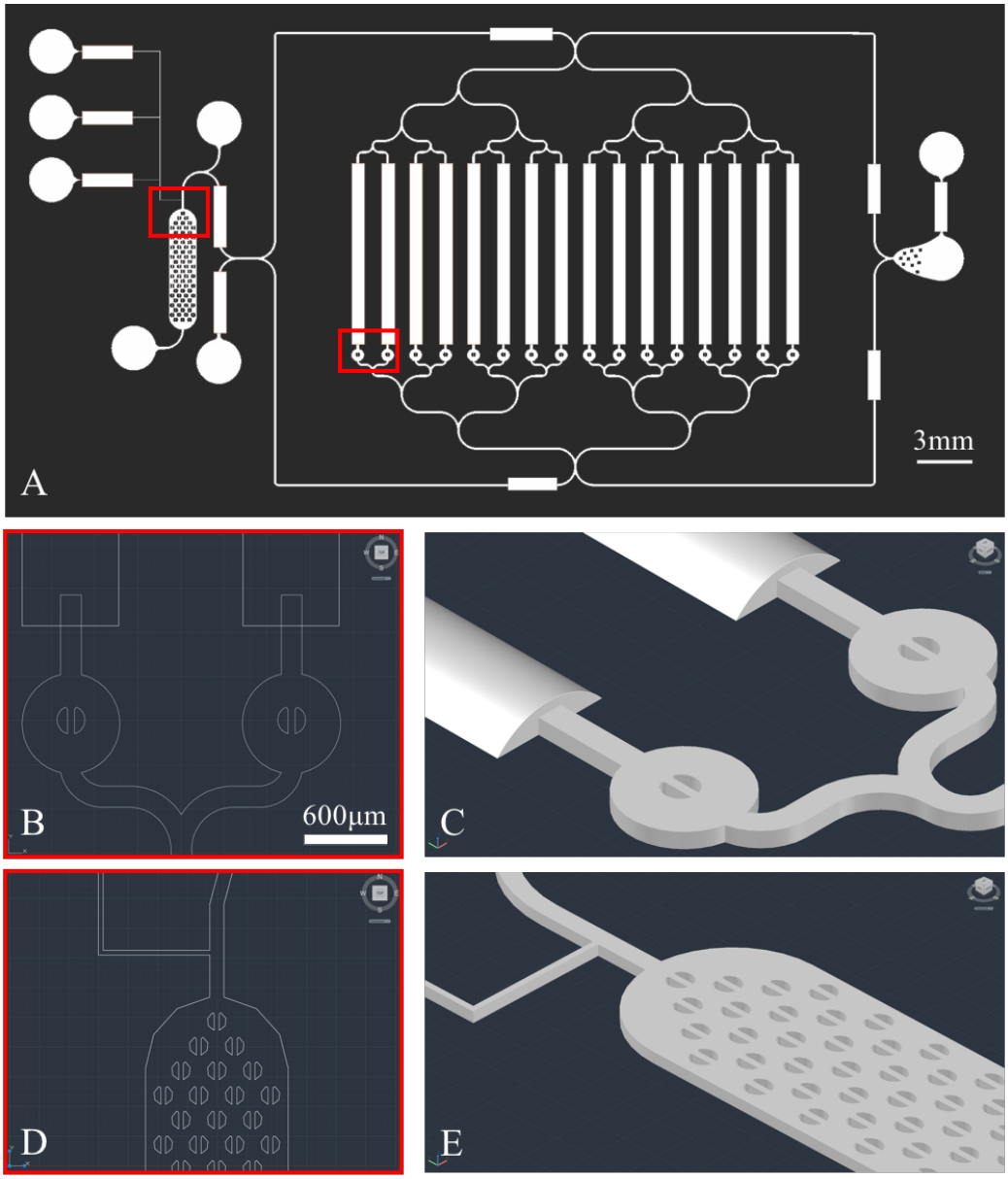

Figure 3.10: **Flow Layer Schematic**
A: CAD drawing of the combined AZ and SU8 sections of the flow layer, shown without the valve layer. The rectangular sections along the channels represent the AZ sections which re-flow to form curved profiles (see panel C). B: Expanded view of two traps taken from CAD drawings with AZ and SU8 masks overlaid. The rectangles are part of the AZ mask shown in Figure 3.11(B). C: To-scale 3D profile of the flow layer at the intersection between AZ and SU8 regions. Heating of the mould causes the re-flow of AZ to produce the rounded cross-section, leaving the SU8 channels and traps well defined and angular. D: CAD drawing of the array of traps for secondary culture conditions in which beads can be transferred from the primary traps shown in (A). E: 3D profile of panel D.

3.3.2 Fabrication Methods

Mould Fabrication

The underlying principles of the fabrication methods are detailed in Section 1.3.1. Additionally, Quake valves were employed in many of the devices presented in this chapter to control flows in 'flow channels' using 'valve channels'. A review of the principles of Quake valves is given in Section 1.2.1. In summary, they comprise of a thin PDMS membrane separating a flow channel from a valve channel. Pressure applied to the valve channel forces a reversible closure of the flow channel below by the membrane. This process complicates the protocol given in Section 1.3.1 as well-defined traps within the flow channels are required. The flow channels should also be able to close completely to ensure the beads do not escape. Complete closure of a channel requires a curved cross-section. So only the valve sections of the chip deform and round on heating whist the well-defined bead trap sections are unaffected, we used a different photoresist for each: AZ which rounds on heating for the valve sections and SU8 which remains rigid on heating for the trap sections.

Section 1.3.1 discussed both SU8 and AZ type photoresists, both of which have been used for the valve devices. Combining the two varieties on a single layer enables us to have sealable sections of the flow layer while maintaining well-defined features in others. At temperatures of 110°C and above, AZ 40XT melts and re-flows, rounding the corners of the features as shown in Figure 3.10 C. A temperature of 110°C is, however, not sufficiently high to have any deforming effect on the SU8 2100 used to form the bead traps, introducing selectivity in the rounding effect of the channels. The design, therefore, features distinct sections of the flow layer to be closed (AZ 40XT) and sections to trap the beads (SU8 2100).

Fabricating a master with a dual photoresist composition requires a two-step photolithography process, similar to that detailed in Section 2.2.2. Given the sensitivity of AZ 40XT to temperature, the first layer deposited on a silicon wafer is SU8 2100. Each layer has its own mask, as displayed in Figure 3.11

The beads used in our experiments are 80μm, so the early versions of the device aimed for a channel height as close to this as possible, given that low aspect ratios are generally easier to fabricate. We found, however, that drooping of the membrane separating valve and flow layers impedes the flow of beads. This was confirmed by imaging a Z-stack along the height of the flow channel section underneath valve. Figures 3.12 and 3.13 display the effect of a open and closed valve respectively. While we are able to achieve good valve closure, the membrane bows into the channel, thereby reducing the height when the valve is off. We found a higher channel resolves this problem, thus in later iterations the SU8 layer was fabricated at 110μm by spinning SU8 2100 at 2100 RPM followed baking for 5 minutes

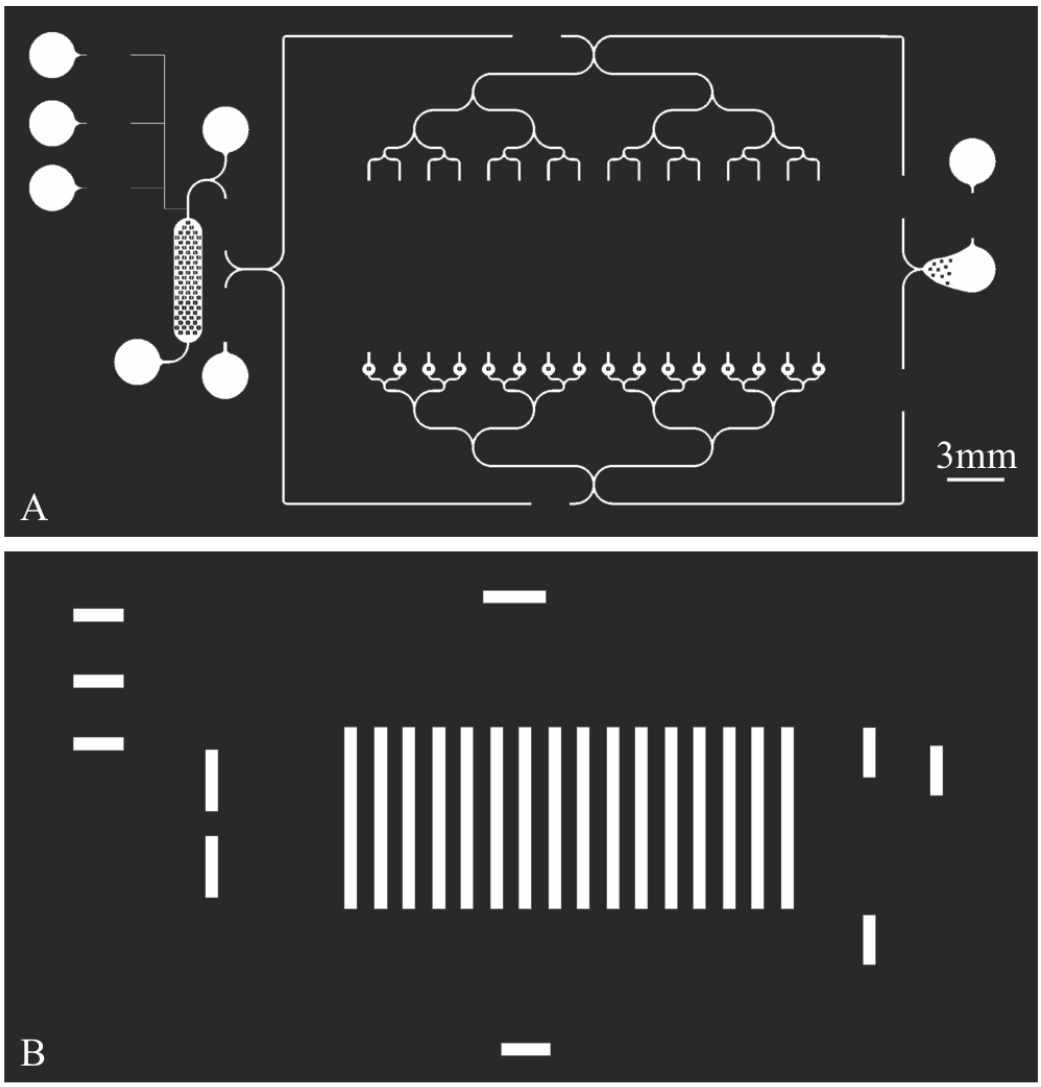

Figure 3.11: **AZ and SU8 Flow Channel Photomasks**
A: CAD drawing of the photomask used to produce the SU8 section of the flow channel. This layer is deposited onto the silicon wafer mould base first. B: A CAD drawing of the photomask used to produce the AZ section of the flow channel. This layer is deposited over the SU8 features produced previously.

at 65°C and 35 minutes at 95°C. For thick films such as the one fabricated here, the edge can bead into a thicker region around the perimeter of the wafer. As the thicker boundary around the wafer creates a gap between the mask and the centre of the wafer during exposure, it must be removed. Conventional approaches involve using developer to clean the edges away. However, we found that to simply scrape away the edge whilst the wafer is still hot, is more time-efficient without affecting the quality of the end product. Next, the wafer is exposed for 18s by a UV lamp (365-405nm, 20mW cm^{-2}) on an MJB-4 contact mask aligner (Karl Suss, Munich, Germany) using the mask shown in Figure 3.11 A. The wafer is then baked at 95°C for 15 minutes before developing in propylene-glycol-mono-methyl-ether-acetate (PGMEA) for 7 minutes. After baking, more PGMEA is poured over the wafer, immediately followed by an isopropanol wash. If at this stage the wafer is fully developed, a further acetone, isopropanol and water wash is performed, followed by a 10 minute bake at 200°C to clean the surface in preparation for the next layer.

The SU8 layer forms the mould for those flow channel areas which are not to be deformed by the valves above. In contrast, sections of the flow channel which should respond to valve pressure are left open as gaps in the SU8 layer. These gaps are subsequently filled with an AZ 40XT layer to form a continuous channel by spin-coating a AZ 40 XT at 900 RPM. As this resist is considerably more sensitive to temperature fluctuations than SU8, a slow-ramped bake from 65°C to 126°C over 20 minutes is performed. After the solvent is evaporated in the AZ resist, the process is repeated to produce a second layer, thus doubling the height of the features. The mask aligner is used to align the channels viable on the mask to the existing SU8 channels protruding through the AZ surface. Two 90s exposures in contact gap mode by a UV lamp (365-405nm, 20mW cm^{-2}) exposes regions to be removed using the mask shown in Figure 3.11 B. Following a post-exposure bake at 105°C, the wafer is immersed in AZ 726 developer until the surface appears clean. Finally, a further bake at 110°C for 5 minutes is sufficient to re-flow the AZ features, achieving the rounded cross-section necessary for full valve closure. Following this protocol, a stylus profilometer (Dektak, Bruker, Billerica MA, USA) was used to measure a height of 110μm for the SU8 features and 130μm at the highest point of the AZ features.

A second mould was produced for the valve layer to be placed over the flow layer. This was fabricated with SU8 2025 spun at 1700 RPM to achieve a feature height of 35μm.

Epoxy Replica Mould Fabrication

The first step in the protocol for production of the flow layer was to produce a replica mould of the silicon/photoresist mould described above. Given the difficult and time-consuming process in producing the silicon/photoresist mould, producing replicas enables a higher

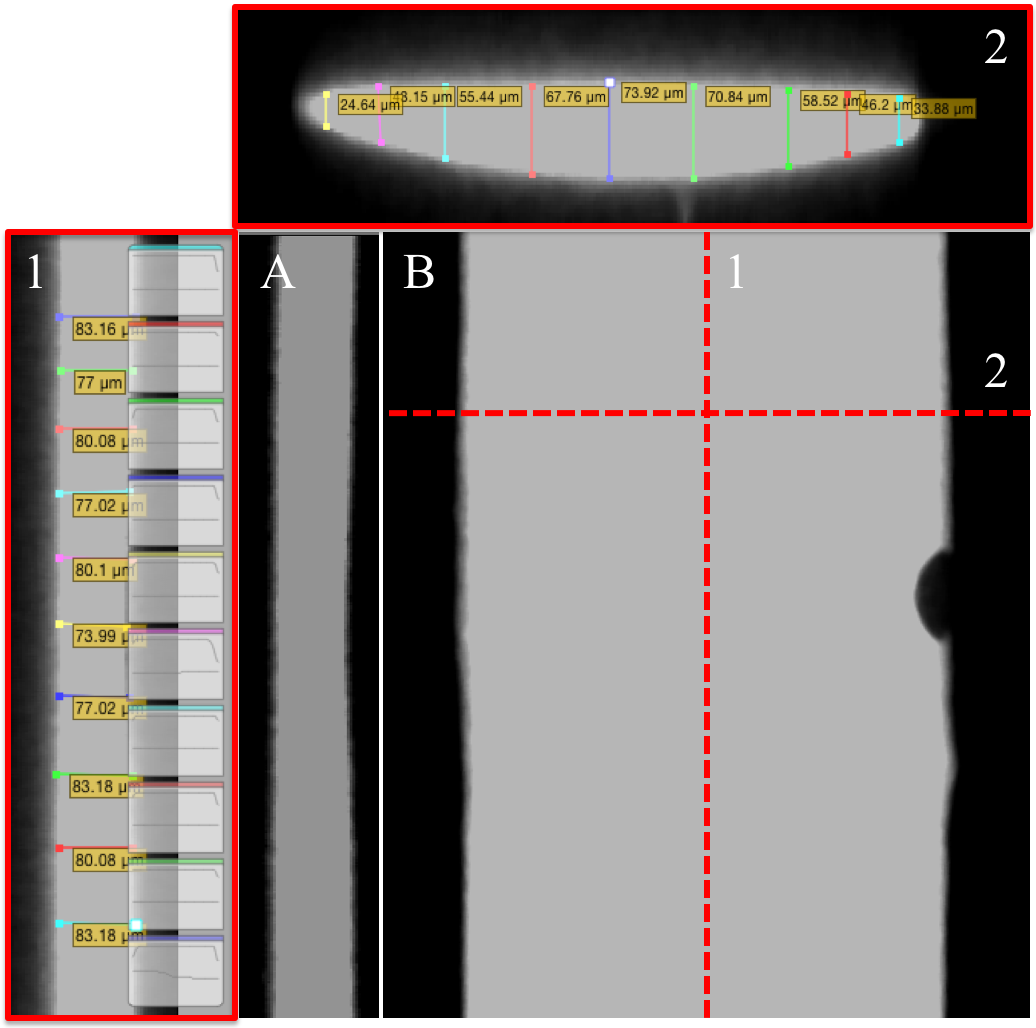

Figure 3.12: **Image Series for Open AZ Section of Flow Channel**
These images are of the rounded AZ section of the flow channel filled with a fluorescent dye. A: Side profile of the channel taken along line '1' shown in B. The lowest part of the channel occurs where a valve passes over the top. In these areas, the membrane can droop into the flow channel, as seen by the decrease in height in panel 1. B: Top-down view of flow channel. The line labelled 2 is the location of the cross-section displayed in panel 2.

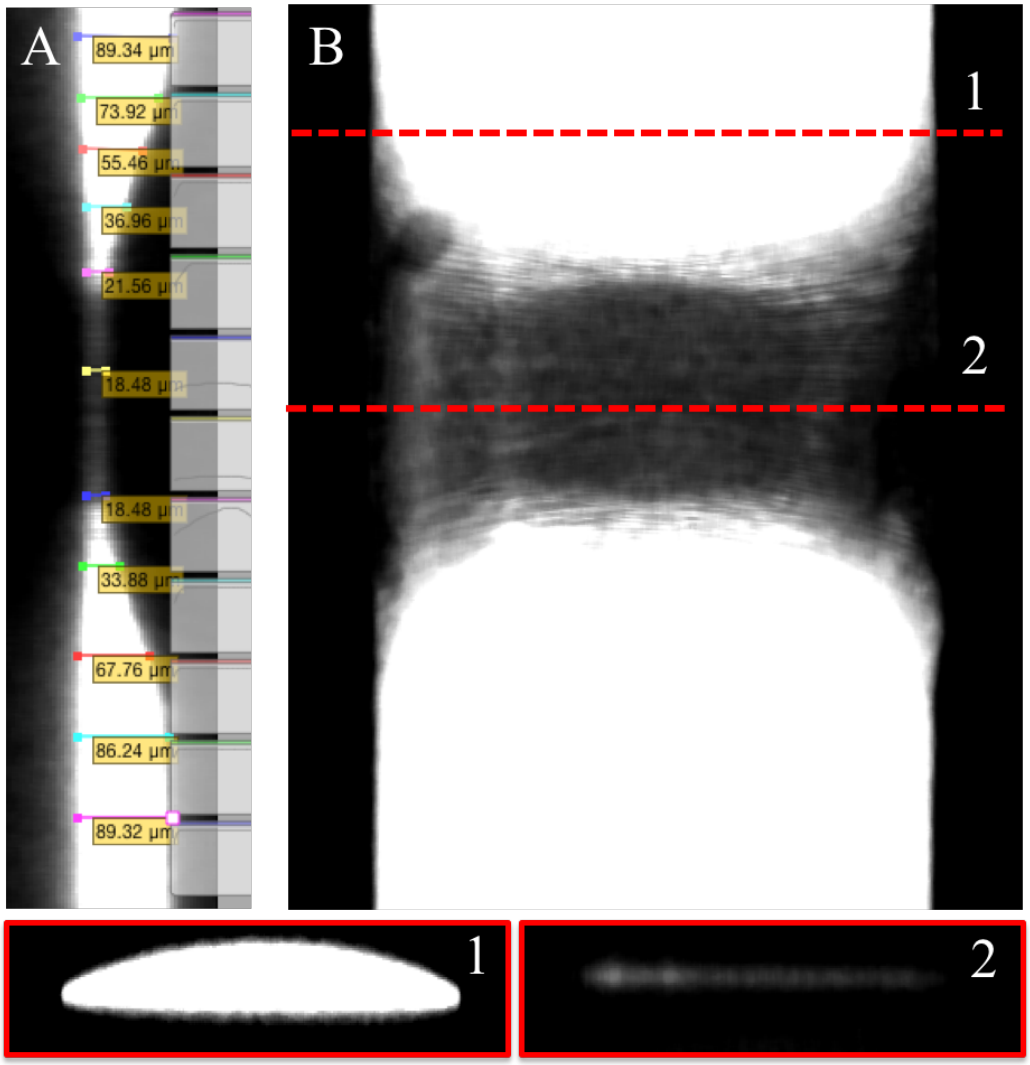

Figure 3.13: **Image Series for Closed AZ Section of Flow Channel**
These images are of the rounded AZ section of the flow channel filled with a fluorescent dye. A: Side profile of the channel taken along length of the channel. The actuation of a valve forces the membrane into the flow channel below. B: top down view of flow channel. The lines labelled 1 and 2 is the location of the cross-section displayed in panels 1 and 2 respectively.

output of chips and a back-up should the original become damaged. The silicon wafer in particular is brittle and prone to fractures, PDMS may become lodged in the small features, or the AZ section of the chip can deform over time following the repeated bakes during chip production. To produce a replica, a 1 cm block of 15:1 (base:curing agent) PDMS is cured on the flow layer mould, this ratio is required to maintain softness and ensure that the PDMS does not tear in subsequent steps. Following curing, the PDMS is removed from the silicon and an epoxy adhesive (Loctite EA 9483) is poured over the featured surface to a thickness of 0.5 cm and then degassed. The epoxy-coated PDMS is left overnight to set, following which the PDMS is removed from the surface. The epoxy-layer is then baked at 60° for 24 hours, allowing the epoxy mould to be used in the same way as the silicon/photoresist version. Post-bake characterisation of the epoxy replica with a stylus profiler (Dektak, Bruker) confirmed that the dimensions of the features remained unaltered from the original.

PDMS Chip Fabrication

The PDMS chip for experiments is fabricated in two parts. First, the valve layer is produced by making a 1-1.5cm PDMS impression of the valve layer mould using a ratio of 5:1 (base:curing agent). Second, the flow layer is fabricated by spin-coating 20:1 ratio PDMS over the flow layer mould. The raised features of the mould will leave channels in the PDMS coating once it is pealed away after curing. The spin coating is performed to only marginally cover the tops of the features. This thin covering over the channels acts like a membrane between the flow channels and the valve channels which will be bonded over the top. A trade-off exists between greater resilience and resistance to tears of the thicker membranes and the easier deformity of the thinner membranes for a given pressure. We found that a spin rate of 450rpm produced a membrane which both rarely tears and facilitates complete channel closure on valve actuation. The 20:1 layer is cured for 6 hours at 60°C while the 5:1 valve layer is cured for 1 hour.

A 1.5mm biopsy punch is used to punch holes in the valve layer to allow access to the valve channels. The feature side of both the valve layer and spin-coated mould are exposed to oxygen plasma for 20s at 100W. The two layers are then aligned by hand under a microscope and placed in contact to bond. The differing levels of curing agent in the two layers, plus the soft, partially-cured valve layer, improves the contact and bonding. The mould is returned to 60°C to further improve the bonding and completely cure the 5:1 section. A scalpel is used to free the chip from the mould. Holes are once more punched for fluidic access to the chip before plasma bonding (20s at 100W) of the feature side to a glass slide (76x52x1.2mm,

Fisher Scientific). The bonded chip is returned to the oven for 15 minutes to complete the bonding.

3.3.3 Experimental Methods

To prepare the device for our experiments, we used a similar filling protocol to that used previously. Water was initially injected into the valve inlet using a syringe and needle before tubing was added. Each of the valve tubes were connected to a specific outlet of a MUX microfluidic flow switch matrices (Elveflow, Paris, France). The MUX unit connects to a Fluigent MFCS-EZ microfluidic flow control system which can deliver a pressure of up to 1.3bar to the MUX. The MUX has 16 outlets to which FEP tubing can be inserted, connecting the unit to valve inlets of the microfluidic chip. As the valves are closed volumes, each of these outlets can simultaneously deliver the pressure specified by the Fluigent pump to the valves. Computer software can open and close any of the 16 MUX valves with any combination thus delivering full control of the valves on chip with a pressure specified by the Fluigent pump. To fill the valves, a pressure of 0.5bar is requested from the Fluigent unit and all of the valves are opened on the MUX unit. This therefore applies 0.5bar of pressure to each of the valves on the chip, which is sufficient to force air out of the valve channels, replacing it with water. This process takes approximately 30 minutes, following which the flow layer can be filled.

As before, to account for the hydrophobicity within the flow channels, an off-chip valve is used to create the closed volume required to fill the flow layer. For this design, an off chip valve is required for all inlets and outlets apart from one which is connected to both a reservoir of PBS and the Fluigent pressure unit via FEP tubing. A pressure of 0.5bar is used to force PBS from the reservoir into the flow channels, replacing the air within. This process is much more time consuming than the filling of the valves and can take up to a number of hours to fully remove all of the air within. The other drawback is that only a single chip can be prepared using this method, which can potentially derail an experiment if a fault is found in the chip after the filling procedure. As an alternative, we thus adjusted the protocol to enable us to prepare multiple chips simultaneously to be used should a chip fail. The updated protocol requires that the chips be submerged in sterilised PBS following a 10 minute bake at 60°C post plasma bonding. The container of PBS and microfluidic chips is placed in a vacuum desiccator and held under vacuum overnight. This simultaneously fills the flow and valve layers in as many chips that are held in the container.

Having filled, a chip is then placed in a stage mount and the valve tubing is attached. The valves are actuated by the opening and closing of valves on the MUX unit. To make use of the multiplexing element of the design, specific combinations of valves must be open simultaneously to access a specific bead. In order to control this, a custom MATLAB GUI was developed with which the user can conveniently control the flow directions and thus bead positions. This is enabled by consistently matching up a specific MUX outlet to a specific

valve inlet. The MUX unit has 16 outlets, each with their own co-ordinate between A-D and 1-4 and each of which have assigned their own on-chip valve. The co-ordinates are written into MATLAB using a 16-digit array in which a '1' opens an outlet and '0' closes it. For example, to open MUX outlet A1 and thus actuate the corresponding on-chip valve, MATLAB feeds $A1 = [1\ 0\ 0\ 0\ 0\ 0\ 0\ 0\ 0\ 0\ 0\ 0\ 0\ 0\ 0\ 0]$ to the MUX unit. Similarly $B1 = [0\ 1\ 0\ 0\ 0\ 0\ 0\ 0\ 0\ 0\ 0\ 0\ 0\ 0\ 0\ 0]$ This provides a convenient method of multiplexing if the arrays for various outlets are summed to actuate a combination of valves, which in this example would be $A1 + B1 = [\ 1\ 1\ 0\ 0\ 0\ 0\ 0\ 0\ 0\ 0\ 0\ 0\ 0\ 0\ 0\ 0]$. Incorporating this approach in a graphical user interface (GUI), enables powerful control over the device. Indeed, selecting a command to release a certain bead automatically releases the bead and actuates all required valves instantly and simultaneously. Deselecting the command then resets the valves to as they were previously. This process is demonstrated in Figure 3.14 showing the GUI, the MUX outlet array and the corresponding locations of the valves on the chip schematic.

The connected valves are shown in the photograph in Figure 3.15. Also displayed are three clamped sections of tubing used to block three of the four outlets punched. For the initial rounds of testing, the media inlets of the modular section were left unpunched for simplicity.

The experiment involves the use of both a pressure pump and a syringe pump. The pressure pump is used only at the preparation phase for removing any remaining air within the device. The pressure source is connected to the chip via a PBS filled tube and set to 400mbar. The other inlets and outlets are blocked off using clamps on the tubing, thus the applied pressure works to dive air from the channels and out of the chip though the PDMS. During this process, the syringe pump (at this stage not connected to the chip) is prepared to deliver media and beads to the chip. This is done by thoroughly cleaning the syringe with multiple ethanol washes followed by multiple PBS rinses. Finally, the syringe pump is filled with the media which is to be used to maintain the cells through the experiment. Once this is completed, if no bubbles are present within the chip following the use of the pressure pump, the main media inlet can be opened. Using the pressure source, a small amount of PBS is made to form a bubble over the inlet. The syringe pump is activated to form a bubble of media at the end of the tubing which is brought into contact with the PBS bubble covering the inlet and then inserted into the device. This creates an air-free interface between the tubing and the chip.

At this stage the tube which is connected to the pressure source in order to fill the flow layer can be re-purposed as the waste outlet while the syringe pump flows media though the chip. The syringe pump is made to flow 1ml of media to replace the PBS at a flow rate of 5ml/hour to prepare the chip for the encapsulated cells. To inject the beads, a suspension of

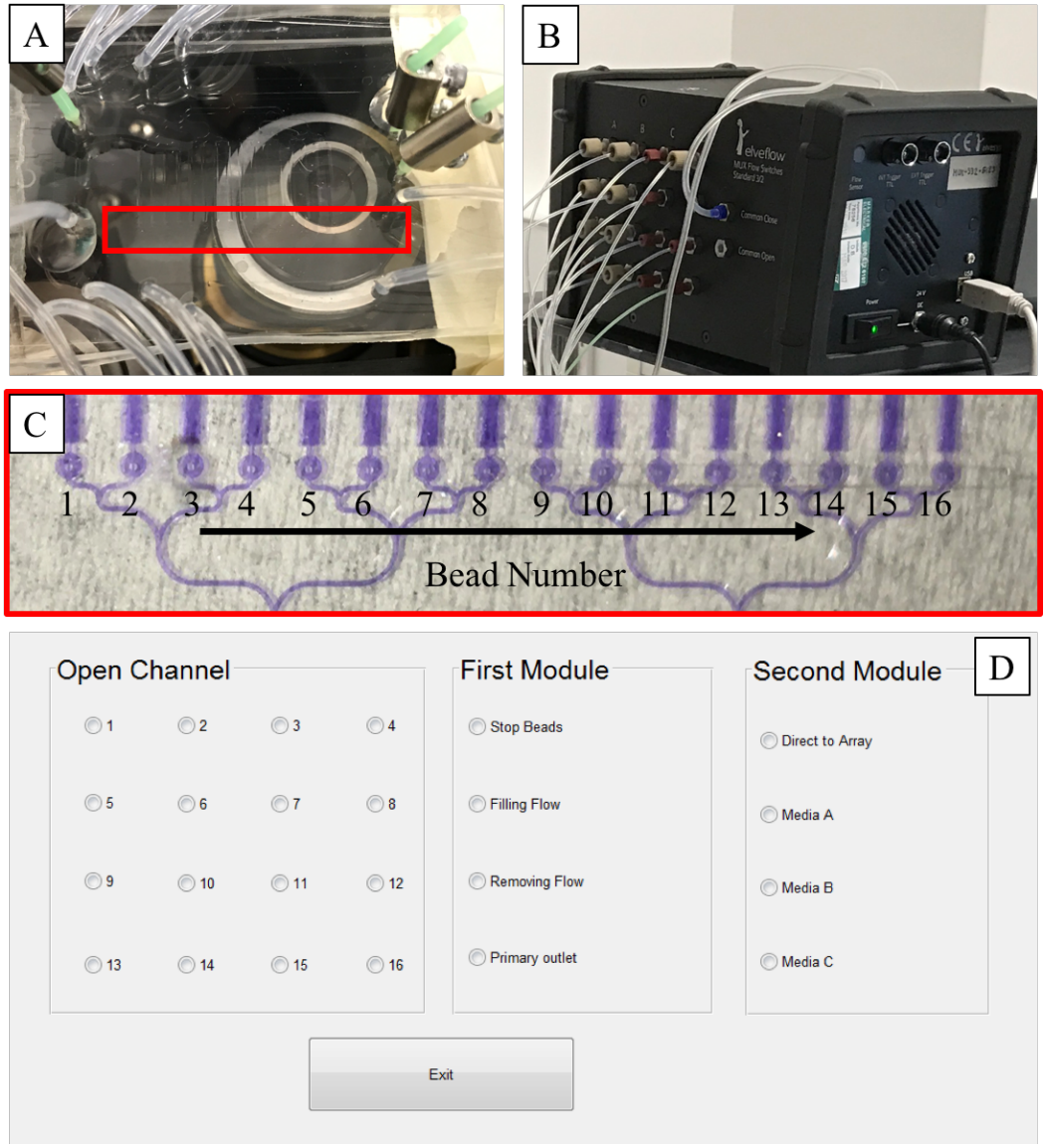

Figure 3.14: **Experimental Set-up with MATLAB GUI**
A: Clear FEP tubing connects the valve inlets to the MUX flow controller unit shown in B. The green tubing shown in A is mechanically clamped to block three of the four punched inlets to the flow channels. C: A purple dye is used to highlight the traps as part of the flow layer. The traps are numbered from 1 to 16, which corresponds to the 'Open Channel' section of the GUI displayed in D. D: The MATLAB GUI for controlling the MUX unit, which in turn controls the on-chip fluid flow. The 'Open Channel' section allows the user to direct the flow to a specific channel. The 'First Module' sections stores options to make the beads enter or exit the traps. The 'Stop Beads' button actuates the valve separating the bead inlet from the rest of the chip. The 'Primary Outlet' button directs the flow out of the chip without encountering the trap array section. The 'Second Module' includes buttons to send ejected beads to the trap array and to add from from 3 additional inlets.

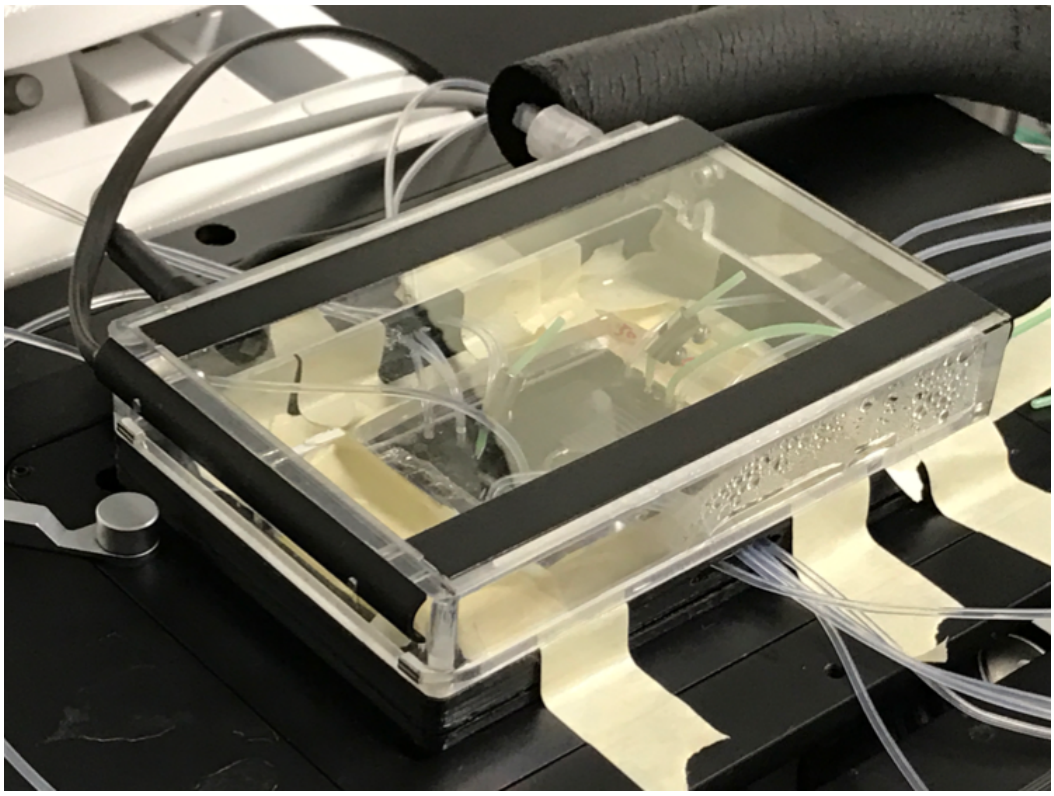

Figure 3.15: **Atmospheric Chamber for the Microfluidic Chip**
Photograph of the microfluidic chip connected to the syringe pump and MUX unit. The device is enclosed within an atmospherically controlled chamber which fits into the microscope stage mount. This keeps the chip at 37°C and in 7% CO_2 throughout the experiment.

beads and media is drawn into an FRP tube by a second syringe pump. The tube closing the bead inlet is then removed and 'filling flow' valve and 'removing flow' valves are actuated. This effectively closes off the main body of the device, diverting the flow from the media inlet syringe out of the bead inlet, removing any air and forming a media bubble over the hole. Both syringes are set to flow at 100μl/hr as a droplet of bead/media suspension forms on the end of the bead inlet tube. The bead inlet tube is then inserted as the 'removing flow' is turned off thus causing the beads to flow over the traps.

As the beads become lodged in the bead traps and the excess flows round them and out of the chip, the environment chamber is secured over the device as shown in Figure 3.15. This aims to recreate the conditions of the incubators normally used to culture these cells by setting CO_2 to 7% and humidity to 100%.

Once the atmospheric conditions have been established, the user can then use the microscope to inspect the trapped beads. There are occasions when an empty bead becomes trapped and we require its removal. To do this, the control GUI is used to isolate the flow to

the channel where the bead is to be replaced. The flow can then be reversed by un-clicking 'filling flow' and selecting 'removing flow'. This will remove the unwanted bead from the chip, leaving a free trap to be refilled when the filling flow is selected again. This process can be repeated as many times as is necessary to fill the traps with beads containing cells. When this is achieved, the syringe pump injecting the beads can be stopped and the bead stopping valve separating the bead inlet from the media inlet can be activated to ensure no unwanted beads enter the chip after this point.

When the traps have been filled with beads containing cells, the flow rate on the syringe pump is increased to 800μl/hour, ensuring a continuous flow of fresh media to the cells. With a 10ml syringe this means the chip can run continuously for 12.5 hours before it must be refilled which can be achieved without disturbing the chip. As the experiment is running, the computer controlled microscope can be programmed to take images of the cells within the beads at various time points. At the end of the experiment, the GUI enables the user to either send the beads one at a time to the culture array module or out of the chip to be collected.

3.3.4 Troubleshooting

The protocol described above is the result of numerous rounds of testing. This section lists current issues uncovered while culturing ESCs on chip over a 24-hour period. Currently, the greatest problem faced is the presence of air bubbles within the flow channels. At the time of writing, we have made refinements to the experimental set-up which reduces the likelihood of air, although have not completely eliminated the chance of air bubble forming in the chip and thereby influencing the experiment. We regularly found that at some stage during the imaging process, air bubbles arrive at the traps, arresting the delivery of media to cells or dislodging the beads.

One of the initial attempts to overcome the formation of bubbles consisted of filling the chips using the vacuum desiccator, which had the additional benefit of reducing experimental preparation time. We hypothesised that air within the PDMS may lead to the formation of bubbles within the channels, or potentially the media within the flow channels was absorbed into the PDMS. This idea was reinforced as we observed a discolouring of the PDMS following prolonged contact with our culture media. We found, however, that the chips filled in this way were still susceptible to air bubbles appearing during our experiments.

Whilst we witnessed air bubbles with the new filling method, we were able to observe the cells in culture on the chip long enough to identify another issue. At approximately 5 hours into imaging, the presence of bacteria became visible within the imaging window for the beads. This highlighted two new concerns: the environment within the chip, even with the inclusion of Penicillin-Streptomycin (1:100 dilution) in the media, was not sterile and

that our flow rate was very low given there was no apparent disruption to the bacteria. We hypothesised that the flow rate in particular may be having an effect on the formation of bubbles as very small bubbles may have more time to increase in size and become a problem with a low flow. For the next attempts, we thus increased the flow from the initial speed of 300μl/hr to 800μl/hr and added the ethanol wash to the chip preparation protocol.

By temporarily replacing the atmospheric chamber with a simple 37°C hot plate, we found that the chamber forces a sharp change in direction to the inlet tubes. This has two effects: the first is a laxity in contact between the chip and the tubing. The second is the creation of tight curvature radii in the tubing may cause, a flow profile which enables bubbles to form. A further potential problem with the atmospheric chamber is the steep temperature gradient between the 37°C environment within and the room temperature environment leading to the formation of bubbles at the interface. Finally, we hypothesised that a potential cause for the air bubbles in some chips may be due to the presence of small tears in the membrane between the flow channels and the valves. After numerous rounds of testing, we found we could achieve consistent air-free delivery of media though the chip by using a chip with a thicker membrane, having a secure connection between the chip and tubing, by ensuring no bends in the tubing between the syringe pump and the chip and finally by using the increased flow rate of 800μl/hr.

When using this protocol with live cells, however, with the inclusion of the atmospheric chamber with an interface between the chip and the syringe pump, we observed the arrival of bubbles to the chip during imaging. As an attempt to reduce the temperature differential at the entrance of chamber, we wrapped thin heating elements around the syringe and inlet tubing. This, however, led to the formation of bubbles at the points where the heating wire was closest to the inlet tubing, supporting our hypothesis that a sharp temperature gradient in the system produces bubbles. We aim to address the remaining problem by constructing an environment chamber to enclose the syringe pump and tubing, this work is currently ongoing.

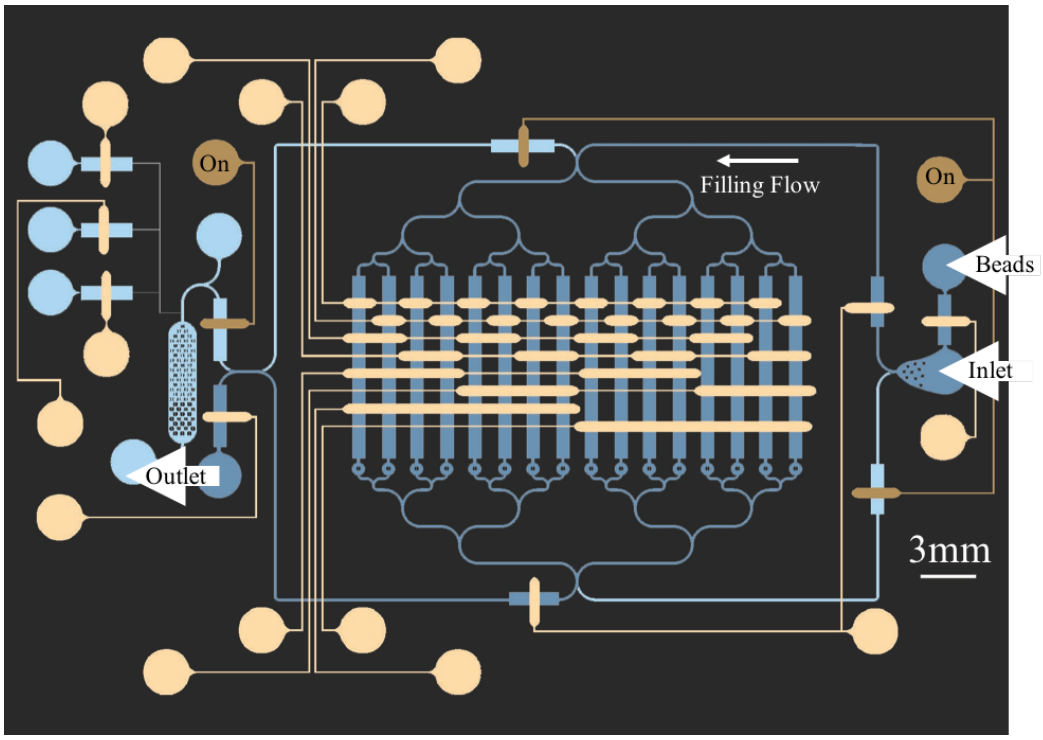

Figure 3.16: **Filling the 16 Trap Chip**
Flow layer is coloured with blue tones and valve layer is coloured with yellow tones. To capture beads in the traps, beads are injected in the 'Beads' inlet using a syringe pump. Media is simultaneously flowed into the second inlet whilst the valve to direct the flow to the traps is actuated. The actuated valves in the figure are labelled 'On' and are a darker tone than the unactuated valves. The beads not trapped move to the outlet and into a waste tube off-chip.

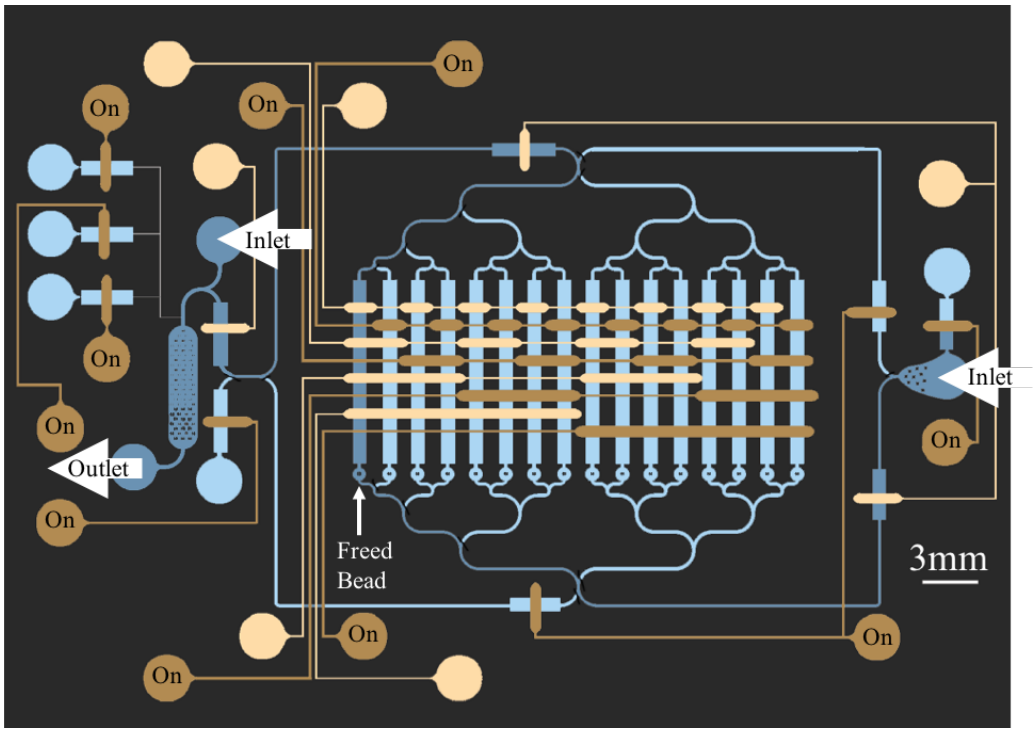

Figure 3.17: **Ejecting a Bead From a Trap**
Flow layer is coloured with blue tones and valve layer is coloured with yellow tones. To release a bead from a trap, a valve is actuated to flow media along the channel the bead occupies. Flowing from behind the trap removes the bead and moves it towards the trap array where the second media inlet can continue to supply fresh media without effecting the rest of the chip.

3.4 Results and Conclusions

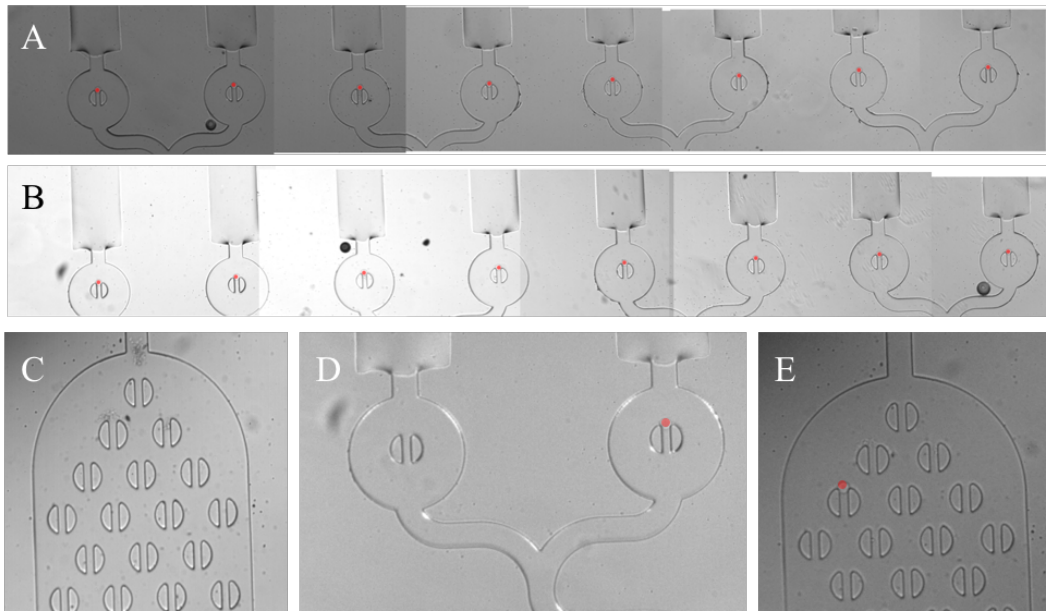

Figure 3.18: **Moving a Single Bead to the Secondary Culture Array**
A and B: 16 beads (false coloured red for clarity) occupy the 16 traps of the chip. C: The trap array is empty while all of the beads are in the primary traps. D: On actuation of the removing flow valve and the specific valves to remove a certain bead, that bead alone leaves its trap while all others remain stationary. E: The ejected bead arrives in the trap array to be cultured separately from the remaining beads.

The aim of the device presented in this chapter is to facilitate the continuous imaging of individual beads containing individual ESCs over a period sufficient for the down-regulation of naive markers following the removal of inhibitors. We aimed to possess the ability to manoeuvre individual beads either outside of the chip or to a secondary culture section in which conditions could be altered from the main chip. This section will review the success of these aims.

The ability to direct beads around the flow channels of our devices using Quake valves is well demonstrated in Figure 3.18. Using valves, we are able to direct a flow of media and beads towards the entrance of individual traps shown in Figure 3.18 A. Using a bespoke MATLAB GUI, the user can then guide a singe bead away from the trap towards an outlet or a secondary array of traps with the press of a button. We have thus achieved an excellent level of control over the directionality of the beads containing cells on-chip and may do so with minimal user input.

The device is able to function in this way due to the combination of photoresists used in the fabrication process, producing rounded regions to be closed by valves and angular regions to trap the beads. This, however, is a difficult and time consuming process. The development of the epoxy replica mould enabled us to reproduce many moulds, relaxing the fear that the delicate silicon/photoresist original would become somehow damaged. In addition, it enables us to produce multiple identical chips by producing multiple moulds.

The up-scaling of chip production enabled experiments with encapsulated cells to be performed more frequently. We could efficiently move single beads into the traps and due to the uncoupled valves, were able to remove unwanted beads from traps to be replaced by suitable alternatives. More difficult, however, was the prolonged duration of the experiment due to the formation of air bubbles.

Air bubbles have numerous causes and sources, not all of which we were able to overcome with the equipment available to us at time of writing. However, through the development process preceding the final device presented here, both design features and experimental protocols have been refined:

- Whilst there is a need for multiple inlets to avoid removing and reinserting tubing to the chips, this number should be kept to a minimum for simplicity. The flow direction is best controlled by on-chip valves as opposed to a combination of inlet flows.

- A low valve channel volume combined with gradual changes in width can reduce set-up times considerably. Set-up times can be reduced further by filling the chip using a vacuum desiccator while the chip is submerged in PBS.

- A thin membrane between the flow and valve channels is more easily deformable for a given pressure than a thick one. Thin membranes, however could regularly tear during fabrication. A trade-off between ease of closure and thickness is found by setting the membrane to be fully closable using no more than 90% of the available pressure. This was tested with a maximum pressure source of 1.3bar.

- To sustain cells within chips, there must be a constant supply of media flowed and appropriate atmospheric conditions.

- A thorough cleaning process is required before bonding the chip and then maintained within a sterile environment to prevent bacterial growth within the chip.

- We found that sharp temperature gradients could cause the formation of air bubbles within the delivery tubing connecting the syringe pump and chip.

- We were able to run the device without air bubbles for longer by increasing the tightness of the seal between the tubing and chip, minimising bending of the tubing as far as practically possible and ensuring the tubing does not pull against the inlets increased the time we were able to run the device without air bubbles.

Despite the partially unresolved problem of air bubbles, we were able to sustain those cells not dislodged or obstructed for 13 hours. This is shown in Figure 3.19 with images taken in both brightfield and florescence. In total, 26 images were taken of the trapped beads at 30 minute intervals. The first and last set for a specific bead are given in Figure 3.19. The culture in this instance included 2i thus we would not expect to see any decrease in the GFP signal as naive pluripotency is maintained.

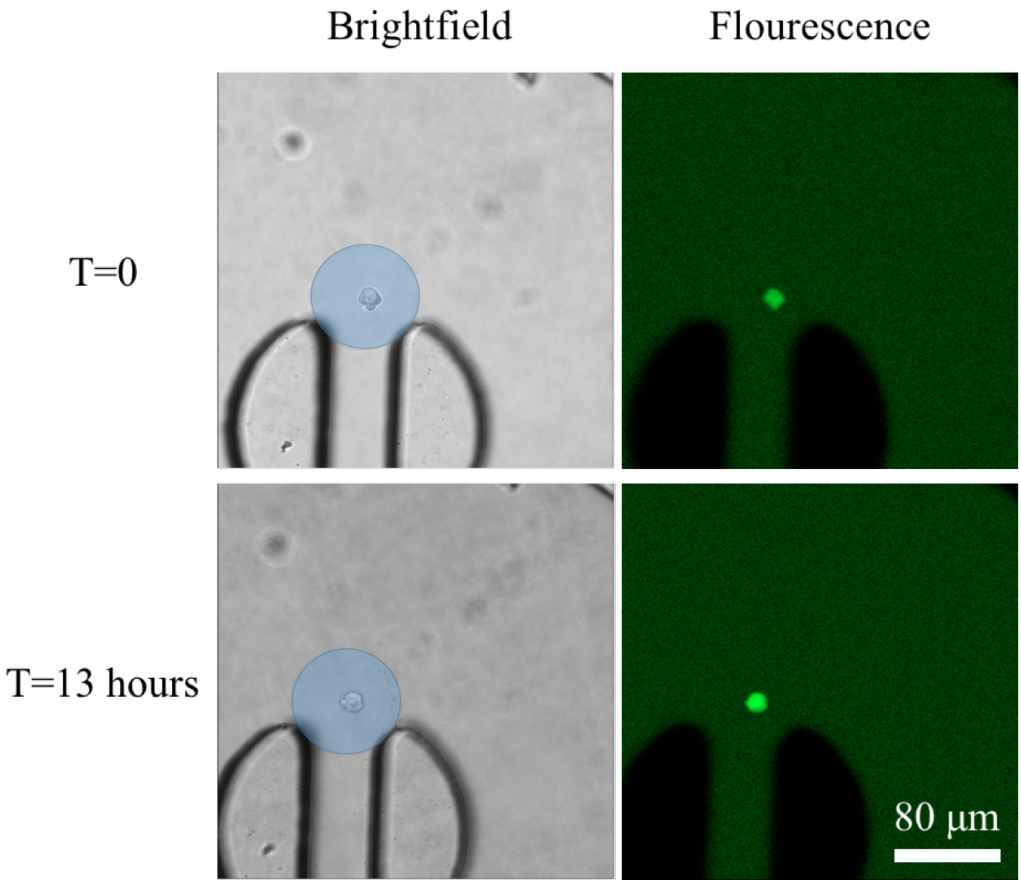

Figure 3.19: **13 hours in 2i Media On-Chip**
Images taken of encapsulated ESCs at 0 and 13 hours on-chip using 2i conditions. The florescence signal from the GFP indicates the continued expression of Rex1 and thus maintained naive pluripotency. The beads in the brightfield images have been false coloured blue to identify their position.

The ability to remove cells from the chip following culturing is shown in Figure 3.20, in which a 2i cultured cell is ejected from the trap with a removal flow (depicted by the white arrow of panel B). This was controlled using the MATLAB GUI control software with no further alterations to the system.

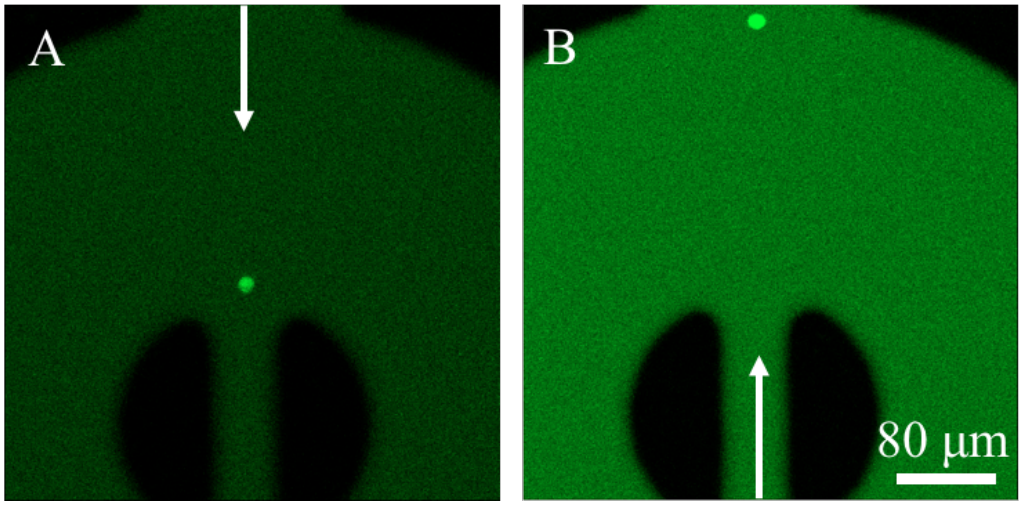

Figure 3.20: **Encapsulated ESC Before and After Removing Flow**
A: Encapsulated cell maintained in 2i conditions on-chip using a continual flow in the direction of the trap, indicated by the white arrow. B: Reversing the flow (indicated by the white arrow), the encapsulated cell can be removed from the chip or to a secondary location.

Presented in this chapter is a device capable of maintaining isolated cells in conditions suitable for both continued imaging and culture. The device enables the researcher to alter media conditions at will, with the option to have two separate conditions on-chip simultaneously. As proposed in our initial aims, we are able to remove single cells, or colonies, from their traps, without disruption to other cells. With adequate control of air bubble formation, we believe this will become a valuable and unique tool in the study of pluripotency.

3.5 Ongoing Work

Whilst I believe we were successful in accomplishing many of our goals, the final obstacle in the long term (72 hours and beyond) culture of ESCs on-chip, is in controlling the formation of air bubbles within the delivery tubes. We anticipate the construction of a culture box around the microscope which can house the syringe pump and tubing will address this issue by removing temperature gradients from the system.

In our experiments using the current generation, we noticed that many of the beads flowing in the direction of the traps would deviate around it; relying on a high volume of beads to catch one in the traps. Using finite element modelling (COMSOL Multiphysics 4.4), we assessed the flow pattern through this design (Figure 3.21) and used this data to redesign the traps so as to be consistently reproducible whilst capturing beads effectively. It is clear from the figure that there is almost no flow passing through the centre of the trap as the fluid is directed around the outside. This matches up well with what we observed in our experiments.

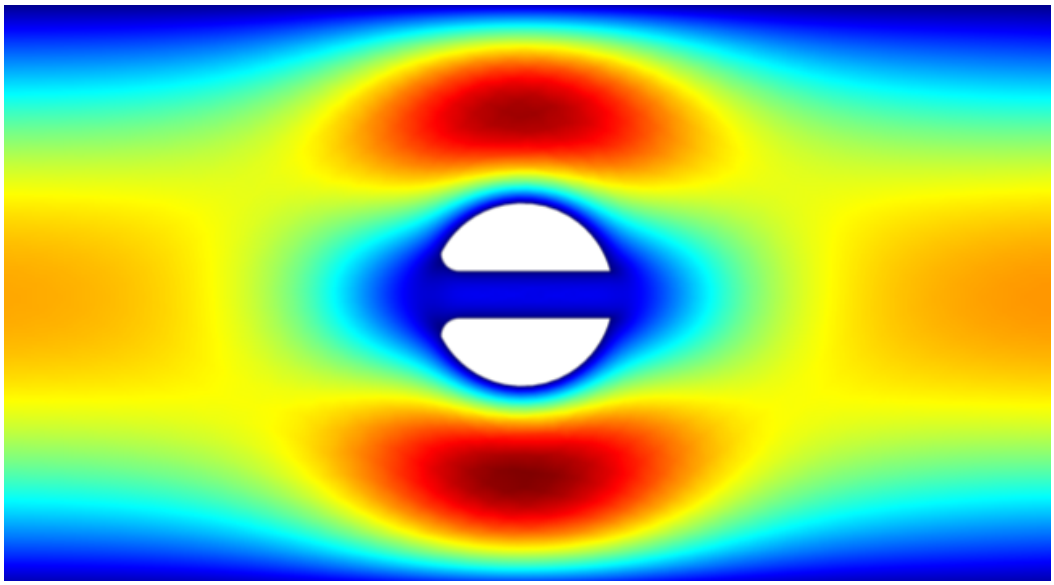

Figure 3.21: **Fluid Dynamics Around Bead Trap**
This figure was produced by importing CAD designs into COMSOL Multiphysics 4.4 for computational fluid dynamics. The red end of the spectrum represents areas of higher velocity profile, showing that the beads in this design will be directed around the side of the trap, not into it.

Having uncovered this, many new traps designed were drafted using AutoCAD and analysed. The design which will theoretically provide the greatest flow though the centre of the traps whilst having large enough features to produce consistent PDMS replicas is

shown in Figure 3.22. This version shows more flow passing though the centre of the trap than Figure 3.21, which will lead to a higher likelihood of a bead becoming trapped and not passing round the side of the trap.

The new trap design will also be used in the modular trap array section for secondary culture conditions. In this area of the chip, it is particularly important that every bead becomes lodged in a trap hence there are many more traps than potential beads. The arrangement of the traps is shown in Figure 3.23 A in which beads will arrive in the direction of the arrow. Panel B shows the fluid dynamics within this section in which all of the traps apart from the last one has a bead (depicted as a white circle) within it.

Beyond small alterations to the existing design, the next round of development will be to produce a chip capable of transferring a bead from the primary trap to a secondary culture array without losing individual control. Currently, we are able to move beads to the secondary array although we lose single bead control with the arrival of two or more beads to the module. The ability to change culture conditions for individual beads before being removed from chip independently of other beads would further improve our investigative powers in the study of pluripotency.

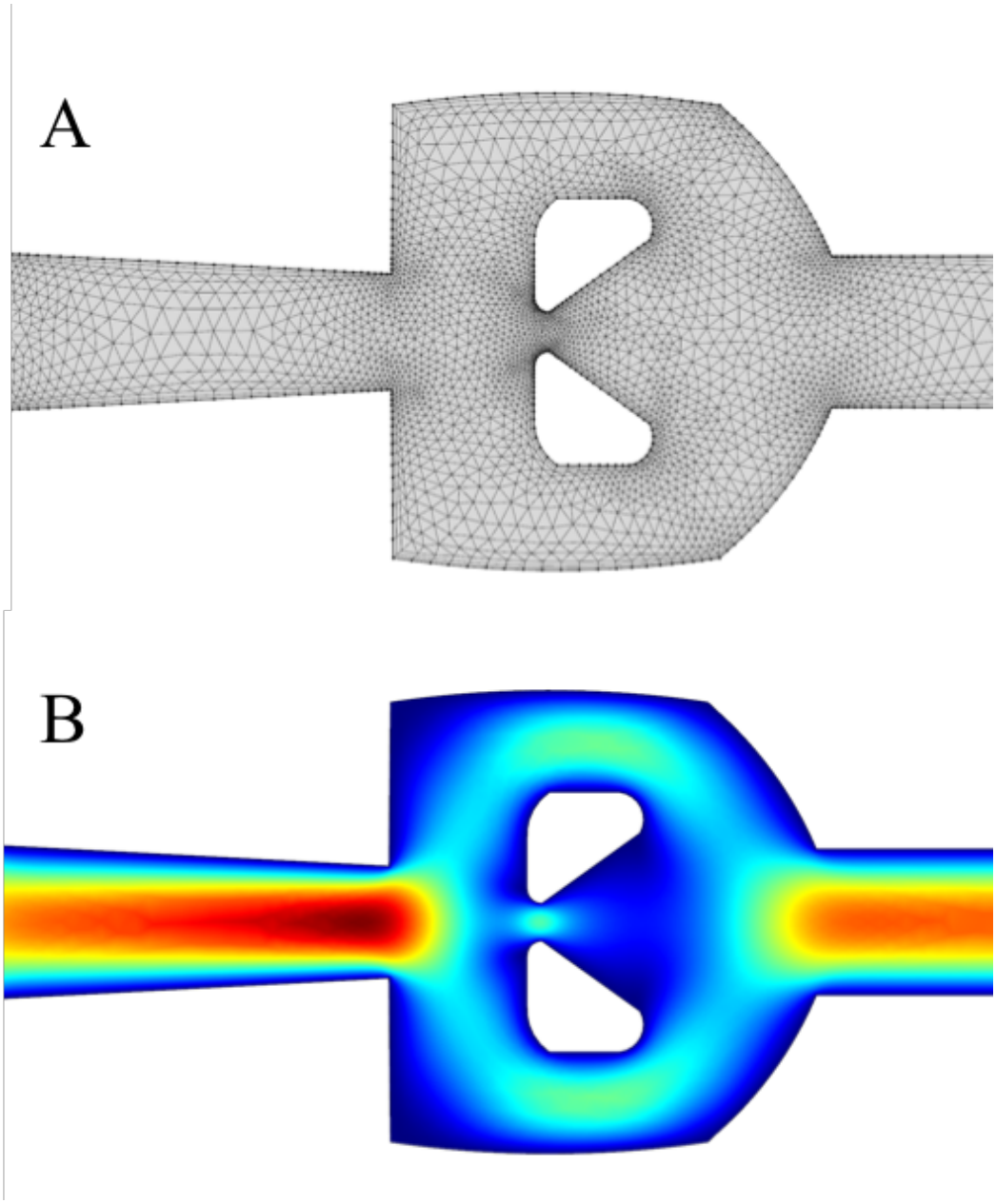

Figure 3.22: **Computational Fluid Dynamics Analysis of Proposed New Traps**
This figure was produced by importing CAD designs into COMSOL Multiphysics 4.4 for computational fluid dynamics. A: Finite element model used in the fluid dynamics analysis. B: The red end of the spectrum represents areas of higher velocity profile, showing that the beads in this design will be more likely that the previous designs to pass into the trap.

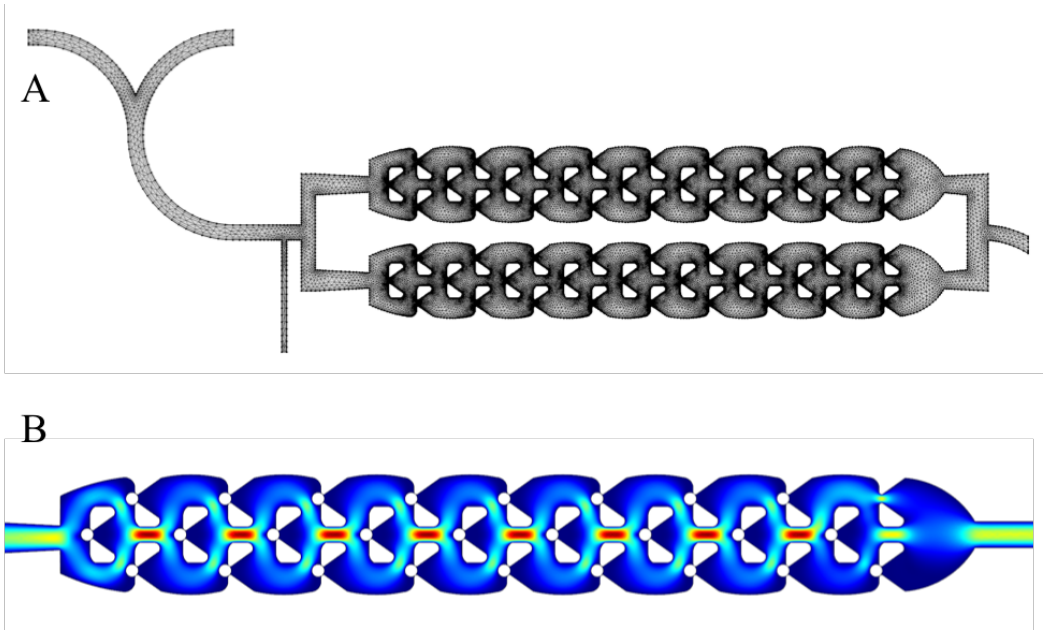

Figure 3.23: **Computational Fluid Dynamics for Secondary Culture Array**
This figure was produced by importing CAD designs into COMSOL Multiphysics 4.4 for computational fluid dynamics. A: Finite element model used in the fluid dynamics analysis, showing the entire secondary culture array for beads to be moved to. B: Expanded view of part of the secondary culture array. Beads are present in all but one of the traps (shown as white circles). The red end of the spectrum represents areas of higher velocity profile, showing that the beads in this design will be more likely that the previous designs to pass into the trap.

Chapter 4

Summary and Outlook

The work presented in this thesis forms two separate sections, utilising different forms of microfluidic technologies, each aiming to facilitate new means of investigating ESCs and pluripotency.

Chapter 2 developed upon the microfluidic device of Pagliara *et al.* (2014), which was used to identify the auxetic phenotype of transition ESC nuclei; cells which have down-regulated their naive pluripotency markers but have not yet gained competence for lineage commitment. We aimed to improve this device in a number of ways: its fabrication, throughput and image analysis being the primary motivators.

We identified that the number of cells per second across the chip increases linearly with flow rate only to a rate of 40μl/hr, at which point there is no observed increase in throughput with increased flow. We hypothesise that this may be due to a combination of factors including camera frame-rate of 110 fps not being sufficient to capture all translocating cells, and increased cell damage causing blockages at the inlet. As expected, we found that increasing the cell concentration has a linear relationship with increasing throughput.

The device presented in Chapter 2 is designed to apply a one dimensional compression to cells, opposed to the two dimensional compression of the device used in Pagliara *et al.*. We hypothesised that this would both remove any focal shift as cells transition from reservoir to constriction channel whilst being easier to fabricate and less likely to clog. We confirmed the constant focal plane between the two regions by imaging 10μm fluorescent beads in each, with measured diameters of 9.98$\pm$0.16μm within the reservoir and 10.07$\pm$0.16μm within the constriction channel (n=19, Figure 2.10). Finally, a bespoke MATLAB GUI was developed to streamline image analysis. Using the software, multiple images of the same cell travelling across the device can be conveniently used to produce mean values for axial dimensions. This function was adapted to assess the dependence of time under constriction

on cell shape. We found that there was no significant difference in cell dimension between the first, second and final thirds of the constriction channel (Figure 2.11 (C)).

We used our device to assess the cellular and nuclear reaction to compression for ESCs with and without treatment of the chromatin decondensing agent TSA. In comparing the two samples of the strain response to compression, we showed that the device and technique is capable of physically phenotyping cells in high throughput and resolution. Furthermore, we identified that ESCs cultured in the Serum/LIF, particularly for small nuclei, exhibit the auxetic phenotype of transition ESCs cultured in 2i medium (Figure 2.12).

Further demonstration of the devices phenotyping ability was given through assessing the translocation times of ESCs through the channels with and without the actin depolymerising agent Cytochalasin D. We showed that treatment with Cytochalasin D significantly reduces translocation time ($P << 10^{-4}$, $n>200$, Figure 2.11 (D)). This result supports our hypothesis that depolymerisation of the actin cytoskeleton eases the passage of cells though the constriction channels.

Chapter 3 presents a novel microfluidic platform capable of culturing ESCs on-chip. Single cells are encapsulated in agarose and fibrin beads which can be stored on-chip to be cultured and continuously observed. The device utilises microfluidic valves to enable parallel culture of up to 16 beads, thus 16 individual cells capable of forming colonies on-chip whilst under observation. Rex1:GFPd2 ESCs, enable observation of the expression level of the naive pluripotency marker Rex1, providing visual feedback to the differentiation state of the stem cell. At any moment during an experiment, the user can use a custom MATLAB GUI to remove a single bead from the device, or to move a bead to a secondary on-chip culture array. Computerised control of the bead position provides the potential for automated removal and manipulation of beads based on observed fluorescence signal or time.

Over the following two years, we aim to utilise this device to perform a number of experiments to test our hypothesis of ESC exit from pluripotency. Population data suggests that the loss of self-renewal in ESCs may be a cumulative process reflected in a gradual downregulation of Rex1 over approximately 40 hours [80]. However, the loss of self-renewal is effected in individual cells, which occurs with varying latency across the population [79]. Due to this, bulk population data for the time between removal of 2i and loss of self-renewal masks the profile of the transition occurring in individual cells. We initially aim to delimit the transition temporally though continued observation of individual cells and colonies on-chip following the removal of 2i. To initially assess the loss of self-renewal, cells will be returned to 2i/LIF conditions; inability to form colonies in this condition indicates loss of self-renewal. This will be performed on chip with use of automated thresholding of GFP

signal and the secondary culture array. Defining a time window for the extinguishing of self-renewal capacity will provide a profile for the decay.

Having defined the transition time window, we will use the device to retrieve cells specific times across this interval before applying single cell RNA-Seq to obtain transcriptome data. This will be performed using custom written automated thresholding software to be incorporated with the bead control software already written. The synchronised staging of cells will reduce variability compared with bulk population RNA-seq, providing a highly resolved transcriptional profile at developmentally important times. We will furthermore make use of the high resolution transcriptional profiling to construct new reporters for various stages of development.

This discussion within this thesis aims to provide a case for the importance of understanding the mechanisms of pluripotency; how the physical nature of cells correlates with both development and the impact of external factors; how the physical nature of a cells micro-environment can direct its developmental path and finally; how the various microfluidic technologies are ideally suited to probing all of the above. The devices developed as part of this PhD project approach the investigation into ESC pluripotency in contrasting yet complimentary ways. In doing so, we have produced two unique investigative tools with corresponding protocols and software plus a range of design parameters to be considered for following generations.

Bibliography

[1] Andrew C. Hodgson, Christophe M. Verstreken, Cynthia L. Fisher, Ulrich F. Keyser, Stefano Pagliara, and Kevin J. Chalut. A microfluidic device for characterizing nuclear deformations. *Lab Chip*, 17(5):805–813, 2017.

[2] Eric K Sackmann, Anna L Fulton, and David J Beebe. The present and future role of microfluidics in biomedical research. *Nature*, 507(7491):181–9, 2014.

[3] Eric M. Darling and Dino Di Carlo. High-Throughput Assessment of Cellular Mechanical Properties. *Annual Review of Biomedical Engineering*, 17(1):35–62, 2015.

[4] Paul J. Hung, Philip J. Lee, Poorya Sabounchi, Robert Lin, and Luke P. Lee. Continuous perfusion microfluidic cell culture array for high-throughput cell-based assays. *Biotechnology and Bioengineering*, 89(1):1–8, 2005.

[5] Adam J. Engler, Shamik Sen, H. Lee Sweeney, and Dennis E. Discher. Matrix Elasticity Directs Stem Cell Lineage Specification. *Cell*, 126(4):677–689, 2006.

[6] S Pagliara, K Franze, C R McClain, G W Wylde, C L Fisher, R J Franklin, A J Kabla, U F Keyser, and K J Chalut. Auxetic nuclei in embryonic stem cells exiting pluripotency. *Nat Mater*, 13(6):638–644, 2014.

[7] M J Evans and M H Kaufman. Establishment in culture of pluripotential cells from mouse embryos. *Nature*, 292:154–156, 1981.

[8] Eran Meshorer and Tom Misteli. Chromatin in pluripotent embryonic stem cells and differentiation. *Nature reviews. Molecular cell biology*, 7(7):540–546, 2006.

[9] Joe Swift, Dennis E Discher, J. K. Pritchard, and K. L. Reddy. The nuclear lamina is mechano-responsive to ECM elasticity in mature tissue. *Journal of cell science*, 127(Pt 14):3005–15, 2014.

[10] Philipp Isermann and Jan Lammerding. Nuclear mechanics and mechanotransduction in health and disease. *Current Biology*, 23(24):R1113–R1121, 2013.

[11] Nikhil Jain, K Venkatesan Iyer, Abhishek Kumar, and G V Shivashankar. Cell geometric constraints induce modular gene-expression patterns via redistribution of {HDAC}3 regulated by actomyosin contractility. *Proceedings of the National Academy of Sciences*, 110(28):11349–11354, 2013.

[12] Yeh-Chuin Poh, Sergey P Shevtsov, Farhan Chowdhury, Douglas C Wu, Sungsoo Na, Miroslav Dundr, and Ning Wang. Dynamic force-induced direct dissociation of protein complexes in a nuclear body in living cells. *Nature communications*, 3(May):866, 2012.

[13] Arash Tajik, Yuejin Zhang, Fuxiang Wei, Jian Sun, Qiong Jia, Wenwen Zhou, Rishi Singh, Nimish Khanna, Andrew S. Belmont, and Ning Wang. Transcription upregulation via force-induced direct stretching of chromatin. *Nature Materials*, 15(December):1–20, 2016.

[14] Alejandro De Los Angeles, Francesco Ferrari, Ruibin Xi, Yuko Fujiwara, Nissim Benvenisty, Hongkui Deng, Konrad Hochedlinger, Rudolf Jaenisch, Soohyun Lee, Harry G Leitch, M William Lensch, Ernesto Lujan, Duanqing Pei, Janet Rossant, Marius Wernig, Peter J Park, and George Q Daley. Hallmarks of pluripotency. *Nature*, 525(7570):469–78, 2015.

[15] Mika Tanaka, Anna-Katerina Hadjantonakis, Kristina Vintersten, and Andras Nagy. Aggregation Chimeras: Combining ES Cells, Diploid and Tetraploid Embryos. *Gene*, 530(FEBRUARY):15–27, 2009.

[16] Guoji Guo, Luca Pinello, Xiaoping Han, Shujing Lai, Li Shen, Ta-wei Lin, Keyong Zou, Guo-cheng Yuan, Stuart H Orkin, Boston Children, Computational Biology, Genetics Core Facility, Boston Children, and Open Labs. HHS Public Access. *Cell Rep*, 14(4):956–965, 2016.

[17] Hendrik Marks, Tüzer Kalkan, Roberta Menafra, Sergey Denissov, Kenneth Jones, Helmut Hofemeister, Jennifer Nichols, Andrea Kranz, A. Francis Stewart, Austin Smith, and Hendrik G. Stunnenberg. The transcriptional and epigenomic foundations of ground state pluripotency. *Cell*, 149(3):590–604, 2012.

[18] Qi Long Ying, Jason Wray, Jennifer Nichols, Laura Batlle-Morera, Bradley Doble, James Woodgett, Philip Cohen, and Austin Smith. The ground state of embryonic stem cell self-renewal. *Nature*, 453(7194):519–523, 2008.

[19] Kevin J. Chalut, Markus Höpfler, Franziska Lautenschläger, Lars Boyde, Chii Jou Chan, Andrew Ekpenyong, Alfonso Martinez-Arias, and Jochen Guck. Chromatin

decondensation and nuclear softening accompany Nanog downregulation in embryonic stem cells. *Biophysical Journal*, 103(10):2060–2070, 2012.

[20] Tüzer Kalkan and Austin Smith. Mapping the route from naive pluripotency to lineage specification. *Philosophical transactions of the Royal Society of London. Series B, Biological sciences*, 369(1657):20130540–, 2014.

[21] Jennifer Nichols and Austin Smith. Naive and Primed Pluripotent States. *Cell Stem Cell*, 4(6):487–492, 2009.

[22] Yi Liu and Hang Lu. Microfluidics in systems biology - hype or truly useful? *Current Opinion in Biotechnology*, 39:215–220, 2016.

[23] Delai L. Chen and Rustem F. Ismagilov. Microfluidic cartridges preloaded with nanoliter plugs of reagents: an alternative to 96-well plates for screening. *Current Opinion in Chemical Biology*, 10(3):226–231, 2006.

[24] David C Duffy, J Cooper Mcdonald, Olivier J A Schueller, and George M Whitesides. Rapid Prototyping of Microfluidic Systems in Poly (dimethylsiloxane). *Anal. Chem.*, 70(23):4974–4984, 1998.

[25] Janelle R. Anderson, Daniel T. Chiu, Rebecca J. Jackman, Oksana Chemiavskaya, J. Cooper McDonald, Hongkai Wu, Sue H. Whitesides, and George M. Whitesides. Fabrication of topologically complex three-dimensional microfluidic systems in PDMS by rapid prototyping. *Analytical Chemistry*, 72(14):3158–3164, 2000.

[26] Todd A Duncombe, Augusto M Tentori, and Amy E Herr. Microfluidics: reframing biological enquiry. *Nature reviews. Molecular cell biology*, 16(9):554–567, 2015.

[27] Guansheng Du, Qun Fang, and Jaap M J den Toonder. Microfluidics for cell-based high throughput screening platforms-A review. *Analytica Chimica Acta*, 903:36–50, 2016.

[28] Todd M. Squires and Stephen R. Quake. Microfluidics: Fluid physics at the nanoliter scale. *Reviews of Modern Physics*, 77(3):977–1026, 2005.

[29] Oliver Otto, Philipp Rosendahl, Alexander Mietke, Stefan Golfier, Christoph Herold, Daniel Klaue, Salvatore Girardo, Stefano Pagliara, Andrew Ekpenyong, Angela Jacobi, Manja Wobus, Nicole Töpfner, Ulrich F Keyser, Jörg Mansfeld, Elisabeth Fischer-Friedrich, and Jochen Guck. Real-time deformability cytometry: on-the-fly cell mechanical phenotyping. *Nature Methods*, 12(3):199–202, 4 p following 202, 2015.

[30] Marc A Unger, Hou-pu Chou, Todd Thorsen, Axel Scherer, and Stephen R Quake. Monolithic Microfabricated Valves and Pumps by Multilayer Soft Lithography. *Science*, 288(April), 2000.

[31] T Thorsen, SJ Maerkl, and SR Quake. Microfluidic Large-Scale Integration. *Science*, 4437(2000), 2002.

[32] Vincent Studer, Giao Hang, Anna Pandolfi, Michael Ortiz, W. French Anderson, and Stephen R. Quake. Scaling properties of a low-actuation pressure microfluidic valve. *Journal of Applied Physics*, 95(1):393–398, 2004.

[33] Jaemin Shin, Hobin Park, Van Bac Dang, Chang-Wan Kim, and Sung-Jin Kim. Elastomeric microfluidic valve with low, constant opening threshold pressure. *RSC Adv.*, 5(30):23239–23245, 2015.

[34] Chad I. Rogers, Kamran Qaderi, Adam T. Woolley, and Gregory P. Nordin. 3D printed microfluidic devices with integrated valves. *Biomicrofluidics*, 9(1), 2015.

[35] Yusuke Sugiura, Hirotada Hirama, and Toru Torii. Fabrication of Microfluidic Valves Using a Hydrogel Molding Method. *Nature Publishing Group*, pages 1–2, 2015.

[36] Aaron J Dy, Alin Cosmanescu, James Sluka, James a Glazier, Dwayne Stupack, and Dragos Amarie. Fabricating microfluidic valve master molds in SU-8 photoresist. *Journal of Micromechanics and Microengineering*, 24(5):057001, 2014.

[37] Nobuyuki Futai, Wei Gu, and Shuichi Takayama. Rapid prototyping of microstructures with bell-shaped cross-sections and its application to deformation-based microfluidic valves. *Advanced Materials*, 16(15 SPEC. ISS.):1320–1323, 2004.

[38] P. M. Fordyce, C. a. Diaz-Botia, J. L. DeRisi, and R. Gomez-Sjoberg. Systematic characterization of feature dimensions and closing pressures for microfluidic valves produced via photoresist reflow. *Lab on a Chip*, 12(21):4287, 2012.

[39] Axel Scherer, Clive R Taylor, and W French Anderson. NIH Public Access. *Electrical Engineering*, 101(6):1–9, 2009.

[40] Joshua S. Marcus, W. French Anderson, and Stephen R. Quake. Microfluidic single-cell mRNA isolation and analysis. *Analytical Chemistry*, 78(9):3084–3089, 2006.

[41] Jessica Melin and Stephen R. Quake. Microfluidic large-scale integration: the evolution of design rules for biological automation. *Annual review of biophysics and biomolecular structure*, 36:213–231, 2007.

[42] D. R. Gossett, H. T. K. Tse, S. a. Lee, Y. Ying, a. G. Lindgren, O. O. Yang, J. Rao, a. T. Clark, and D. Di Carlo. Hydrodynamic stretching of single cells for large population mechanical phenotyping. *Proceedings of the National Academy of Sciences*, 109(20):7630–7635, 2012.

[43] Henry T K Tse, Daniel R Gossett, Yo Sup Moon, Mahdokht Masaeli, Marie Sohsman, Yong Ying, Kimberly Mislick, Ryan P Adams, Jianyu Rao, and Dino Di Carlo. Quantitative diagnosis of malignant pleural effusions by single-cell mechanophenotyping. *Science translational medicine*, 5(212):212ra163, 2013.

[44] Amy C Rowat, Diana E Jaalouk, Monika Zwerger, W Lloyd Ung, Irwin A Eydelnant, Don E Olins, Ada L Olins, Harald Herrmann, David A Weitz, and Jan Lammerding. Nuclear Envelope Composition Determines the Ability of Neutrophil-type Cells to Passage through Micron-scale. *J. Biol. Chem*, 288(12):8610–8618, 2013.

[45] Hawa-Racine Thiam, Pablo Vargas, Nicolas Carpi, Carolina Lage Crespo, Matthew Raab, Emmanuel Terriac, Megan C King, Jordan Jacobelli, Arthur S Alberts, Theresia Stradal, Ana-Maria Lennon-Dumenil, and Matthieu Piel. Perinuclear Arp2/3-driven actin polymerization enables nuclear deformation to facilitate cell migration through complex environments. *Nature communications*, 7:10997, 2016.

[46] Takamasa Harada, Joe Swift, Jerome Irianto, Jae-won Shin, Kyle R Spinler, Avathamsa Athirasala, Rocky Diegmiller, P C Dave P Dingal, Irena L Ivanovska, and Dennis E Discher. Nuclear lamin stiffness is a barrier to 3D migration, but softness can limit survival. *JCB*, 204(5):669–682, 2014.

[47] Jamil El-ali, Peter K Sorger, and Klavs F Jensen. Cells on chips. *Nature*, 442(July):403–411, 2006.

[48] Valerie Liu Tsang and Sangeeta N Bhatia. Three-dimensional tissue fabrication. *Advanced Drug Delivery Reviews*, 56:1635–1647, 2004.

[49] Sharona Even-Ram, Vira Artym, and Kenneth M. Yamada. Matrix Control of Stem Cell Fate. *Cell*, 126(4):645–647, 2006.

[50] Christopher S Chen, Milan Mrksich, Sui Huang, George M Whitesides, and Donald E Ingber. Geometric Control of Cell Life and Death. *Science*, 1425(1997), 2009.

[51] John L Tan, Joe Tien, Dana M Pirone, Darren S Gray, Kiran Bhadriraju, and Christopher S Chen. Cells lying on a bed of microneedles: an approach to isolate mechanical

force. *Proceedings of the National Academy of Sciences of the United States of America*, 100(4):1484–9, 2003.

[52] Daniel T Chiu, Noo Li Jeon, Sui Huang, Ravi S Kane, Christopher J Wargo, Insung S Choi, Donald E Ingber, and George M Whitesides. Patterned deposition of cells and proteins onto surfaces by using three-dimensional microfluidic systems. *PNAS*, 97(6):2408–2413, 1999.

[53] By Bo Yuan, Yong Li, Dong Wang, Yunyan Xie, Yingyi Liu, Li Cui, Fuquan Tu, and Hao Li. A General Approach for Patterning Multiple Types of Cells Using Holey PDMS Membranes and Microfl uidic Channels. *Advanced Functional Meterials*, 20:3715–3720, 2010.

[54] Charlotte Aumeier, Laura Schaedel, Jérémie Gaillard, Karin John, Laurent Blanchoin, and Manuel Théry. Self-repair promotes microtubule rescue. *Nature Cell Biology*, 18(10):1054–1064, 2016.

[55] Laura Schaedel, Karin John, Jérémie Gaillard, Maxence V. Nachury, Laurent Blanchoin, and Manuel Théry. Microtubules self-repair in response to mechanical stress. *Nature Materials*, 14(11):1156–1163, 2015.

[56] Stefano Giulitti, Enrico Magrofuoco, and J. Voldman. Optimal periodic perfusion strategy for robust long-term microfluidic cell culture. *Lab on a Chip*, 13(22):4430, 2013.

[57] Skarphedinn Halldorsson, Edinson Lucumi, Rafael Gómez-Sjöberg, and Ronan M T Fleming. Advantages and challenges of microfluidic cell culture in polydimethylsiloxane devices. *Biosensors and Bioelectronics*, 63:218–231, 2015.

[58] V Lecault, M VanInsberghe, S Sekulovic, Djhf Knapp, S Wohrer, W Bowden, F Viel, T McLaughlin, A Jarandehei, M Miller, D Falconnet, A K White, D G Kent, M R Copley, F Taghipour, C J Eaves, R K Humphries, J M Piret, and C L Hansen. High-throughput analysis of single hematopoietic stem cell proliferation in microfluidic cell culture arrays. *Nature Methods*, 8(7):581–U93, 2011.

[59] Yolanda Schaerli and Florian Hollfelder. The potential of microfluidic water-in-oil droplets in experimental biology. *Molecular BioSystems*, 5:1392–1404, 2009.

[60] Jenifer Clausell-Tormos, Diana Lieber, Jean Christophe Baret, Abdeslam El-Harrak, Oliver J. Miller, Lucas Frenz, Joshua Blouwolff, Katherine J. Humphry, Sarah Köster,

Honey Duan, Christian Holtze, David A. Weitz, Andrew D. Griffiths, and Christoph A. Merten. Droplet-Based Microfluidic Platforms for the Encapsulation and Screening of Mammalian Cells and Multicellular Organisms. *Chemistry and Biology*, 15(5):427–437, 2008.

[61] Pingan Zhu and Liqiu Wang. Passive and active droplet generation with microfluidics: a review. *Lab on a Chip*, 17(online):34–75, 2017.

[62] Jon F Edd, Di Carlo, Katherine J Humphry, K Sarah, Daniel Irimia, and A Weitz. Controlled encapsulation of single-cells into monodisperse picolitre drops †‡. *Lab on a Chip*, 8:1262–1264, 2008.

[63] C. H. J. Schmitz, A. C. Rowat, S. Köster, and D. Weitz. Dropspots: a picoliter array in a microfluidic device. *Lab on a chip*, 9(1):44–49, 2009.

[64] Mohammad Ali Khorshidi, Prem Kumar Periyannan Rajeswari, Carolina Wählby, Haakan N. Joensson, and Helene Andersson Svahn. Automated analysis of dynamic behavior of single cells in picoliter droplets. *Lab on a Chip*, 14(5):931–937, 2014.

[65] Kwanghun Chung, Catherine A. Rivet, Melissa L. Kemp, and Hang Lu. Imaging single-cell signaling dynamics with a deterministic high-density single-cell trap array. *Analytical Chemistry*, 83(18):7044–7052, 2011.

[66] J Cooper Mcdonald, David C Duffy, Janelle R Anderson, and Daniel T Chiu. Review General Fabrication of microfluidic systems in poly (dimethylsiloxane). *Electrophoresis*, 21:27–40, 2000.

[67] Marina Krause, Joost te Riet, and Katarina Wolf. Probing the compressibility of tumor cell nuclei by combined atomic force–confocal microscopy. *Physical Biology*, 10(6):065002, 2013.

[68] Shefali Talwar, Nikhil Jain, and G. V. Shivashankar. The regulation of gene expression during onset of differentiation by nuclear mechanical heterogeneity. *Biomaterials*, 35(8):2411–2419, 2014.

[69] Guilhem Velve-Casquillas, Maël Le Berre, Matthieu Piel, and Phong T. Tran. Microfluidic tools for cell biological research. *Nano Today*, 5(1):28–47, 2010.

[70] M P Lutolf and J a Hubbell. Synthetic biomaterials as instructive extracellular microenvironments for morphogenesis in tissue engineering. *Nature biotechnology*, 23(1):47–55, 2005.

[71] Matthew J Dalby, Nikolaj Gadegaard, and Richard O C Oreffo. Harnessing nanotopography and integrin-matrix interactions to influence stem cell fate. *Nature materials*, 13(6):558–69, 2014.

[72] F Chowdhury, S Na, D Li, Y C Poh, T S Tanaka, F Wang, and N Wang. Material properties of the cell dictate stress-induced spreading and differentiation in embryonic stem cells. *Nat Mater*, 9(1):82–88, 2010.

[73] J David Pajerowski, Kris Noel Dahl, Franklin L Zhong, Paul J Sammak, and Dennis E Discher. Physical plasticity of the nucleus in stem cell differentiation. *Proceedings of the National Academy of Sciences of the United States of America*, 104(40):15619–15624, 2007.

[74] Peter Cartwright, Cameron McLean, Allan Sheppard, Duane Rivett, Karen Jones, and Stephen Dalton. LIF/STAT3 controls ES cell self-renewal and pluripotency by a Myc-dependent mechanism. *Development (Cambridge, England)*, 132(5):885–96, 2005.

[75] Tianshu Feng, Eva Szabo, Ewa Dziak, and Michal Opas. Cytoskeletal disassembly and cell rounding promotes adipogenesis from ES cells. *Stem Cell Reviews and Reports*, 6(1):74–85, 2010.

[76] T Wakayama, I Rodriguez, A C Perry, R Yanagimachi, and P Mombaerts. Mice cloned from embryonic stem cells. *Proceedings of the National Academy of Sciences of the United States of America*, 96(26):14984–14989, 1999.

[77] Marc A M J Van Zandvoort, Cees J. De Grauw, Hans C. Gerritsen, Jos L V Broers, Mirjam G A Oude Egbrink, Frans C S Ramaekers, and Dick W. Slaaf. Discrimination of DNA and RNA in cells by a vital fluorescent probe: Lifetime imaging of SYTO13 in healthy and apoptotic cells. *Cytometry*, 47(4):226–235, 2002.

[78] M. Schliwa. Action of cytochalasin D on cytoskeletal networks. *Journal of Cell Biology*, 92(1):79–91, 1982.

[79] Tüzer Kalkan, Nelly Olova, Mila Roode, Carla Mulas, Heather J Lee, Isabelle Nett, Wolf Reik, Paul Bertone, and Austin Smith. Tracking the embryonic stem cell transition from ground state pluripotency. *BioRxiv*, 2016.

[80] Carla Mulas, Tüzer Kalkan, and Austin Smith. Nodal secures pluripotency upon embryonic stem cell progression from the ground state. *bioRxiv*, (July), 2016.

[81] Adam Filipczyk, Carsten Marr, Simon Hastreiter, Justin Feigelman, Michael Schwarzfischer, Philipp S. Hoppe, Dirk Loeffler, Konstantinos D. Kokkaliaris, Max Endele, Bernhard Schauberger, Oliver Hilsenbeck, Stavroula Skylaki, Jan Hasenauer, Konstantinos Anastassiadis, Fabian J. Theis, and Timm Schroeder. Network plasticity of pluripotency transcription factors in embryonic stem cells. *Nature Cell Biology*, 17(10):1235–1246, 2015.

[82] Allon M. Klein, Linas Mazutis, Ilke Akartuna, Naren Tallapragada, Adrian Veres, Victor Li, Leonid Peshkin, David A. Weitz, and Marc W. Kirschner. Droplet barcoding for single-cell transcriptomics applied to embryonic stem cells. *Cell*, 161(5):1187–1201, 2015.